INAUGURAL-DISSERTATION

zur Erlangung der Doktorwürde
der Naturwissenschaftlich-Mathematischen Gesamtfakultät
der Ruprecht-Karls-Universität Heidelberg

vorgelegt von:

Thomas Mrowiec
aus Kattowitz

Tag der mündlichen Prüfung: 14.05.2009

Thema:

Isoform specificity of 14-3-3 proteins in COPII dependent ER export of membrane proteins

Gutachter:

Prof. Dr. Blanche Schwappach

PD Dr. Matthias Mayer

Meiner Familie

AATBK

Acknowledgements

First of all, I would like to express my greatest gratitude to my supervisor Prof. Dr. Blanche Schwappach. Her patience, her tireless helpfulness and the ability to spread her enormous enthusiasm for science made my time in her group a time full of experiences.
I would also like to thank PD Dr. Matthias Mayer for his great help and support as second supervisor during my thesis.

Very special thanks go to Prof. Dr. Anne Spang. Her help and her advices led to some of the most important results obtained in my study.

My thanks are due to all members in the Schwappach lab. A warm thank you goes to Anne, Bastian, Camille, Eric, Julia, Jutta, Katja, Kai, Nikolai, Sebastian and Volker. You all made work in the lab much more fun.

I would like to thank Jutta Rami for her help concerning many important organizational issues. I want to thank my football pals from the ZMBH for great fun and wonderful goals.

The thesis was carried out at the Zentrum für Molekulare Biologie der Universität Heidelberg (ZMBH) and at the Faculty of Life Sciences (University of Manchester).
I would like to thank the GK1188 and the Welcome Trust for funding.

Table of contents

1. Summary

1.1 Abstract

The two 14-3-3 proteins Bmh1 and Bmh2 belong to a large family of dimeric proteins, which are conserved in all eukaryotic cells. They have been described as abundant modulators and linked to a broad range of essential cellular processes. 14-3-3 isoforms are highly similar in their structure and thought to have a least partially overlapping functions.

One role of 14-3-3 proteins is to facilitate forward transport of multimeric membrane proteins. Recent work in our group has revealed an isoform specific function for the yeast 14-3-3 isoform Bmh1. However, the mechanism by which only 14-3-3 Bmh1, but not Bmh2, promotes forward transport is not known.

In this work, I focus on the investigation of the mechanism that causes isoform specificity of 14-3-3 proteins in the forward transport of multimeric membranes proteins. I chose a well defined reporter system in *Saccharomyces cerevisiae*, that allowed me to combine qualitative and quantitative methods.

My results show that different steady-state localizations of the reporter are due to differences in ER export efficiency, because formation of COPII coated vesicles is less efficient in a Δ*bmh1* background.

Both yeast 14-3-3 proteins were shown to interact with the COPII component Sec23. Mutating a putative 14-3-3 binding site in Sec23 resulted in mislocalization of cycling proteins *in vivo*. Furthermore, 14-3-3 Bmh1 was found to fulfill its stimulatory role through its distal C-terminal region. Pulldown studies with Bmh1 and Bmh2 C-termini identified a nucleoside diphosphate kinase (Ndk1) as a new interaction partner of yeast 14-3-3 proteins. *In vitro* packaging assays were used to demonstrate that Bmh1 and Ndk1 act at the level of vesicle formation from ER membranes. In contrast, a dominant negative role of Bmh2 in complex with Ndk1 was discovered.

I speculate, that 14-3-3 proteins in combination with Ndk1 might influence transport kinetics of cycling proteins by structural regulation of COPII vesicles.

1.2 Zusammenfassung

Die beiden Proteine Bmh1 und Bmh2 aus der Bäckerhefe gehören der grossen 14-3-3 Proteinfamilie an. 14-3-3 Proteine sind konserviert in allen eukaryotischen Zellen und haben die Eigenschaft als Dimere aufzutreten. Sie wurden als weiterverbreite Modulatorproteine beschrieben und mit einer Vielzahl verschiedener, essenzieller Zellvorgänge in Verbindung gebracht. Die verschiedenen Isoformen der 14-3-3 Familie weisen eine sehr ähnliche Struktur auf und man nimmt an, dass sie zumindest teilweise überlappende Funktionen haben und oftmals eine Isoform durch eine andere ersetzt werden kann.

Eine der vielen Rollen von 14-3-3 Proteinen liegt in der Unterstützung des Forwärtstransports von multimeren Membranproteinen. Neueste Erkenntnisse aus unserer Arbeitsgruppe zeigten eine isoformspezifische Funktion der 14-3-3 Bmh1 Isoform auf. Der isoformspezifische Funktionsmechanismus jedoch blieb bisher unerklärt.

Der Fokus meiner Arbeit liegt in der Aufklärung des isoformspezifischen Funktionsmechanismus, der verantwortlich ist dafür, dass die Bmh1 Isoform, nicht aber Bmh2, den Vorwärtstransport von multimeren Membranproteinen fördert.

Mit Hilfe eines gut charakterisierten Reportersystems in *Saccharomyces cerevisiae* war es mir möglich, qualitative und quantitative Methoden zu kombinieren.

Meine Ergebnisse zeigen, dass die Gleichgewichts-Lokalisation des gewählten Reporterproteins durch Regulation des Austritts aus dem ER (Endoplasmatisches Retikulum) zustande kommt. Die Bildung von COPII Vesikeln am ER war weniger effizient in einem Δ*bmh1* Stamm, als im Wildtyp-Stamm.

Die Interaktion zwischen der COPII Komponente Sec23 und beiden 14-3-3 Proteinen wurde nachgewiesen. Mutationen in einem putativen 14-3-3 Bindungsmotif in Sec23 führten zur fehlerhaften Lokalisation von zirkulierenden Membranproteinen *in vivo*.

Desweiteren wurde der C-Terminus von Bmh1 als die Region identifiziert, die für den isoformspezifischen Effekt verantwortlich ist. Pulldown-Versuche mit den C-Termini von Bmh1 und Bmh2 führten zur Identifizierung von Ndk1, einer Nukleosid-Diphosphat-Kinase, als neuen Interaktionspartner für die 14-3-3 Isoformen in Hefe. Mit Hilfe von *in vitro* COPII-budding-assays konnte ich zeigen, dass Bmh1 und Ndk1 zusammen die Bildung von COPII-Vesikeln an der ER Membran fördern. Im Gegensatz dazu wurde ein dominant negativer Effekt für Bmh2 im Komplex mit Ndk1 entdeckt.

Ich spekuliere, dass 14-3-3 Proteine in Kombination mit Ndk1 den Transport von zirkulierenden Proteinen über strukturelle Regulation der COPII-Vesikelbildung regulieren.

2. Introduction

Proteins are involved in all cellular processes. The variety of protein functions is made possible by their amino acid composition and their three-dimensional shape. Proteins often function through binding to other molecules. Specificity in ligand binding and binding kinetics define all cell functions. Whilst many protein-protein interactions use surfaces unique to the interacting molecules, other interactions rely on adaptor proteins that recognize domains or motifs found in a large group of otherwise unrelated proteins. Adaptor proteins can facilitate protein-protein interactions by bringing two interaction partners into close proximity. They can exert regulatory functions by favoring certain conformations or by masking binding sites for other proteins. 14-3-3 proteins are a good example of a class of adaptor proteins with a stunning variety of more than 200 interaction partners for which they act as scaffolding, regulatory or masking proteins.

In this study two members of the large family of 14-3-3 proteins were investigated with respect to their specific function in promoting the forward trafficking of multimeric membrane proteins.

2.1 14-3-3 proteins

14-3-3 were first discovered in a systematic classification of brain proteins (Moore et al., 1967). The family of 14-3-3 proteins contains a large number of isoforms in mammalian cells (beta, eta, epsilon, gamma, sigma, tau and zeta), two in yeast (Bmh1 and Bmh2), 15 isoforms in plant cells and two in *D. mellanogaster* and *C. elegans*. All isoforms are highly similar in their sequence. Similarity ranges from 60% between 14-3-3 sigma and epsilon and 81% similarity between the two yeast isoforms to over 90% for *C. elegans* isoforms. All 14-3-3 proteins share the common structure of nine alpha-helices which are arranged into groups of two, two, two and three (Rittinger et al., 1999). One striking feature of all 14-3-3 isoforms is their ability to form homo- and heterodimers through interactions of helices αA to αD (see Figure 1; Xiao et al., 1995, Liu et al., 1995). Helices αC, αE, αG and αI form a peptide binding groove that is positively charged due to the presence of two arginine residues. The best described interactions involve 14-3-3 binding to phosphorylated binding motifs on a

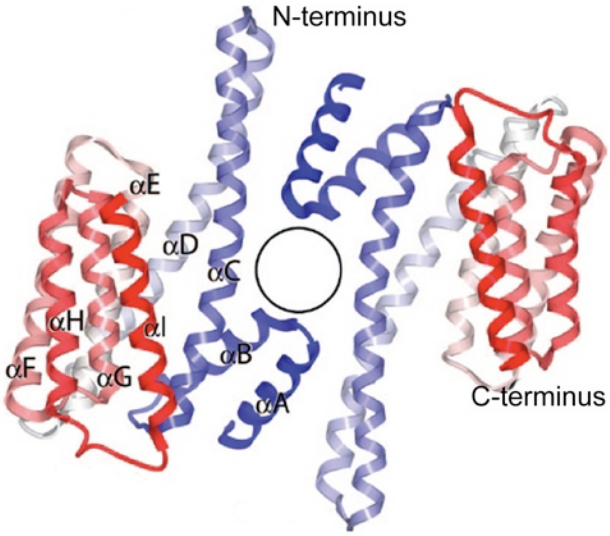

Figure 1: 14-3-3 dimer formation

Two 14-3-3 monomers form a homodimer through interactions of their N-terminal regions (blue alpha-helices αA to αD). Dimerization creates a aperture ring in the central interaction area (marked by circle).
(Yang et al., 2006)

large variety of target proteins. Three motifs of different consensus were classified as mode-I, mode-II and mode-III (see Fig. 24, page 68 for overview). Besides phosphorylation-dependent binding, 14-3-3 were shown to bind non-phosphorylated motifs as well (van Zeijl et al., 2000; Wilker und Yaffe, 2004; Yuan et al., 2003). Hence 14-3-3s are extremely versatile proteins that were found to be involved in various different cellular processes like signal transduction, metabolism, DNA damage response and many more (Mackintosh, 2004; Yaffe, 2002; Tzivion und Avruch, 2002; van Hemert et al., 2001). In total, over 200 interaction partners have been identified for 14-3-3 proteins (Pozuelo Rubio et al., 2004). However, the molecular mechanisms of how 14-3-3 proteins participate in these reactions are mostly not understood. Especially the question of isoform specificity has not been addressed in detail in most cases.

The large number of isoforms provokes several open questions: Is heterodimerisation controlled? And if, how? Where are individual isoforms expressed? Do 14-3-3 isoforms have overlapping or specific functions (see Yaffe et al., 2002 for review) ?

2.2 The role of 14-3-3s in protein transport

14-3-3 proteins have been demonstrated to influence protein localization by sequestering the protein in a subcellular compartment until 14-3-3 binding is abolished (see Fig. 2; Dougherty and Morrison, 2004). The common mechanism seems to be masking of localization motifs. This includes proteins that are involved in Ras and heterotrimeric G-protein signaling. Here, cytosolic 14-3-3 binding masks interaction regions, that are required for localization of the proteins to the plasma membrane (Dhillon et al., 2002; Ory et al., 2003; Niu et al., 2002). In the case of mitochondrial and nuclear localized proteins, 14-3-3 binding masks subcellular targeting sequences. However, 14-3-3 proteins were also shown to influence targeting of proteins which traffic along the secretory pathway. After co-translational integration into the ER membrane, most of these proteins are processed at ER exit sites and packaged into COPII vesicles. 14-3-3 proteins have been found to contribute to the cell surface expression of several multimeric membrane proteins (see Table 1 for detailed overview). These proteins share the commonality to expose a coatomer protein complex I- (COPI-) interacting motif in addition to a 14-3-3-binding motif. The two interaction sites can overlap, or be very close to each other, so that the simplest model proposes masking of the COPI signal to prevent retrograde transport of the protein back to the ER, thereby allowing efficient forward transport. However, export of multimeric membrane proteins seems to be very well controlled and direct confirmation of the masking hypothesis is lacking so far. Recent work on K^+ channels TASK-1 and TASK-3 has revealed a new C-terminal tri-basic motif just next to a previously described 14-3-3 mode-III binding site, that when masked by 14-3-3, leads to ER exit (O'Kelly and Goldstein, 2008; Zuzarte et al., 2009). Although the masking hypothesis seems very logical and simple, O'Kelly and Goldstein in contrast suggested that masking

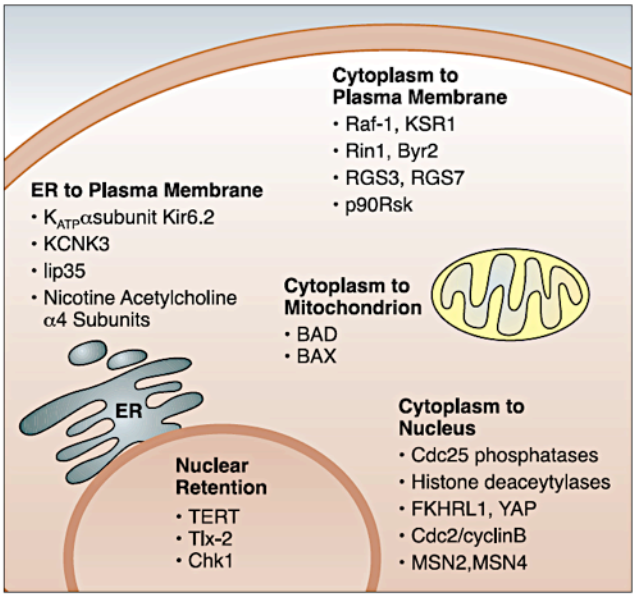

Figure 2: 14-3-3s regulate protein localization.

Overview of proteins, whose localization is influenced by 14-3-3 protein binding.
(Dougherty and Morrison, 2004)

a COPI binding motif at the N-terminus of TASK-1 and a regulatory role of 14-3-3 at the C-terminal mode-III binding site are required for TASK-1 export (see discussion for additional detail).

Membrane protein	Interaction motif	14-3-3 isoform	Consequence of interaction	References
α_2-adrenergic receptor (α_2AR)	Not precisely described: 3i loop region of α_2AR	ζ	Not investigated	Prezeau et al., 1999
CD81	Not investigated (candidate -RNSSVY-)	ε	Not investigated	Clark et al., 2004
$GABA_B$ receptor	C-terminal region containing -LRSRR-	η, ζ	None for ζ isoform	Couve et al., 2001; Brock et al., 2005
GPR15	C-terminal region containing -RSV^{P}SL-	ε, η, γ, τ, ζ	Cell surface expression	Shikano et al., 2005
HERG K^+ channel	N- and C-terminal -S^P-	ε, η	Stimulation of channel activity	Kagan et al., 2002
IGFIR (insulin-like growth factor I receptor)	C-terminal -^{1272}S^{P}XP- and -^{1283}S^{P}XP-	ε	Unknown as yet	Craparo et al., 1997
Interleukin 9 receptor (IL-9R) α-chain	-^{518}RS^{P}WT^{P}F^{522}-	ζ	Not investigated	Sliva et al., 2000
Invariant chain of MHC II	-RRSRS^P-	Not specified	Cell surface expression and transport to lysosomal Ag-processing compartments	Kuwana et al., 1998; Anderson et al., 1999
Kainate receptor subunit KA2	-RKTSRSRRRRR-	γ, β, ζ	Correlates with cell surface expression	Vivithanaporn et al., 2006
KCNK3 rTASK-1	-RRSS^{P}V-	ε, γ, β, σ, ϑ(τ), ζ, η, θ	Required for cell surface expression	O'Kelly et al., 2002; Rajan et al., 2002; Shikano et al., 2005
KCNK9 rTASK-3	-RRKSV- -RRKSI-	γ, β, σ, ε, ζ, η, θ	Required for cell surface expression	Rajan et al., 2002
KCNK15	-RWKSI-	γ, β, σ, ε, ζ, η, θ	Required for cell surface expression	Rajan et al., 2002
Kir2.1-LRKR-SWTY	-SWT^{P}Y-	ε, η, γ, τ, ζ	Cell surface expression	Shikano et al., 2005
K_{ATP}-channel Kir6.2 subunit	-LRKR-	ε, ζ	Cell surface expression of multimeric reporter constructs	Yuan et al., 2003
NAchR α4 subunit	-RSLS^{P}VQ-	η	Cell surface expression	Jeanclos et al., 2001
Na^+, K^+-ATPase	-KKS^{P}KK-	Not specified	Increased endocytosis	Efendiev et al., 2005
Norepinephrine transporter (hNET)	Not investigated	α/β, η, ε, δ/ζ	Not investigated	Sung et al., 2005
Plasma membrane Ca^{2+}-ATPase	Not described	ε	Inhibition of calcium pump activity	Rimessi et al., 2005
Plant plasma membrane H^+-ATPase	-QSYT^{P}V- and non-phosphorylated upstream region	Not specified	Activation of proton pump	Wurtele et al., 2003; Fuglsang et al., 2003
Pmp2p-LRKR	-LRKR-	Bmh1p, Bmh2p	Forward transport only in the presence of Bmh1p	Michelsen et al., 2006
Slowpoke (dSlo) K_{Ca}-channel via Slob	-^{50}RSNS$^{54\,P}$- and -^{76}RSAS$^{79\,P}$- of Slob	ζ	Complex with dSlo and Slob-downregulation of channel activity	Zhou et al., 1999

Table 1: Membrane proteins that interact with 14-3-3 proteins.
(from Mrowiec and Schwappach, 2006)

For other multimeric membrane proteins, like the K_{ATP}-forming subunits SUR1 and Kir6.2, binding of 14-3-3 depends on the multimeric presentation of an Arg-based motif (LRKR). Yuan and colleagues showed that tetrameric exposure of the last 36 amino acids of the Kir6.2 subunit, containing the Arg-based motif increases the preference for 14-3-3 binding, whereas the monomeric tail bound COPI instead (Yuan et al., 2003). In their studies with the

K_{ATP}-channel complex, Heusser and colleagues demonstrated that 14-3-3 binding promotes surface expression of only correctly assembled membrane protein complexes. This result underlines the role of 14-3-3 proteins as an important factor in the quality-control mechanism (Heusser et al., 2006; see Ellgard and Helenius, 2003 for review). To understand the interaction between Arg-based motifs in the K_{ATP} subunits and 14-3-3 proteins in more detail, Michelsen et al moved from mammalian cells to the yeast system. Using the last 36 amino acids of Kir6.2 fused to a multimeric Pmp2 reporter protein (ccPmp2-LRKR), Michelsen and colleagues could show that knockout of one isoform (Bmh1), but not the other, lead to accumulation of the multimerised reporter protein in the ER (see Fig. 3). In contrast, presence of Bmh1 alone was sufficient for very effective export of the reporter protein from the ER.

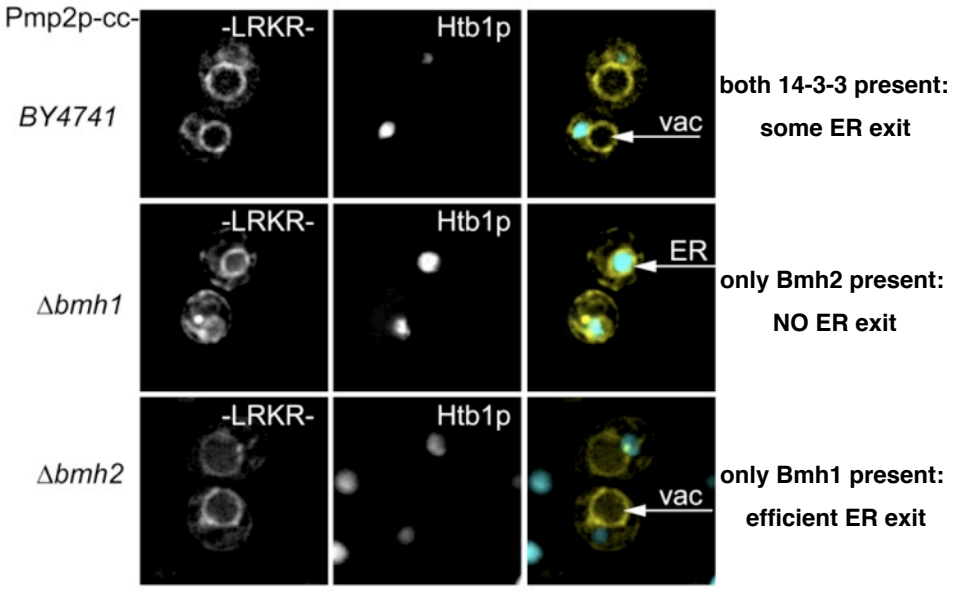

Figure 3: Trafficking of ccPmp2-LRKR reveals 14-3-3 isoform specificity.

Life cell imaging of the ccPmp2-LRKR-YFP fusion protein. The reporter protein localizes mostly in vaculole in wildtype cells, indicating ER exit. Knockout of Bmh1 (*Δbmh1*), meaning only Bmh2 is present, leads to accumulation of ccPmp2-LRKR-YFP protein in the ER. In contrast, the reporter leaves the ER very efficiently in the *Δbmh2* strain, demonstrating the stimulatory role of Bmh1 in forward transport.
(Michelsen et al., 2006)

Different models for the mechanism by which 14-3-3 proteins can modulate forward transport of multimeric membrane proteins have been discussed (see Fig. 4; Shikano et al., 2006; Mrowiec and Schwappach, 2006 for review).

Yuan and colleagues proposed a simple masking mechanism by which 14-3-3 proteins interact with Arg-based motifs only when exposed in a multimeric fashion. This links 14-3-3 to channel assembly, but the details of this interaction and its mechanistic consequences for channel trafficking have not been described yet.

A major aim of my work was to investigate by which mechanism 14-3-3 binding to the Arg-based motif leads to forward transport.

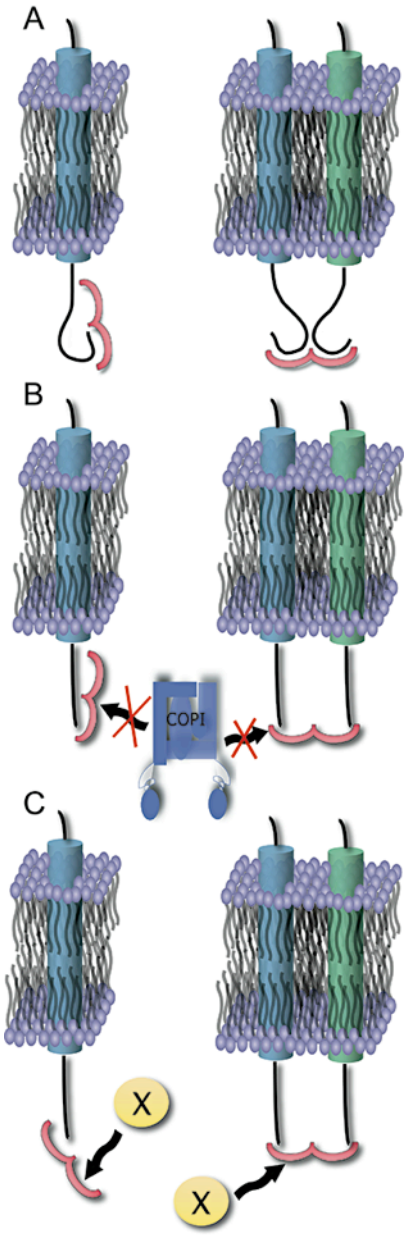

Fig 4: Hypothetical mechanisms for 14-3-3-dependent trafficking to the cell surface.

(A) Clamping: 14-3-3-binding alters the conformation of the cytosolic domain of the membrane protein resulting in the removal of a peptide sorting motif from its active zone.
Shikano and Li (2003) showed that functionality of C-terminal di-lysine (-KKXX) and Arg-based ER localization signals depends on different zones of membrane proximity. Thus, conformational changes introduced by 14-3-3 binding could switch the signal between the active and inactive state.

(B) Masking: 14-3-3 proteins sterically block access of the COPI coat complex to the cytosolic regions of the membrane protein that are in contact with 14-3-3.
Although masking is the most elegant explanation, recent work on the TASK-1 K^+ channel by Zuzarte and colleagues and O'Kelly and Goldstein raised a controversy whether masking is sufficient to explain the role of 14-3-3 proteins in TASK potassium channel forward transport. O'Kelly and Goldstein suggest an additional, regulatory role for 14-3-3 proteins instead of simple masking. This demonstrates that the understanding of the role of 14-3-3 proteins in K^+ channel trafficking is far from complete.

(C) Scaffolding: 14-3-3 proteins recruit additional machinery to the membrane protein. Protein X could functionally inactivate the COPI coat or recruit components required for forward transport.
O'Kelly and Goldstein (2008) described the requirement for 14-3-3 as scaffold proteins to recruit p11 to the C-terminal tail of TASK-1 K^+ channels. Both proteins were necessary to form a ternary complex with the channel. p11 then acts as a modulator protein to enhance surface expression.

(adapted from Mrowiec and Schwappach, 2006)

2.3 The secretory pathway

The secretory pathway is a network of functionally and structurally different compartments in eukaryotic cells. It allows the cell to process and modify proteins and to communicate with its environment through sequential secretion of proteins. Entry point of the secretory pathway is the ER (endoplasmatic reticulum). The ER surrounds the nucleus and spreads out widely into the cell. It is present as smooth and rough ER. Latter being ER that is covered with ribosomes which facilitate protein synthesis and protein entrance through the translocon complex (Gorlich and Rapoport, 1993). Inserted proteins undergo a number of modifications in the lumen of the ER: asparagine-linked glycosylation (N-glycosylation), disulfide bond formation and protein folding. Chaperones, like the Hsp70 family, control protein folding and stabilize unfolded proteins (see Bukau et al., 2006 for review). ER associated degradation (ERAD) of

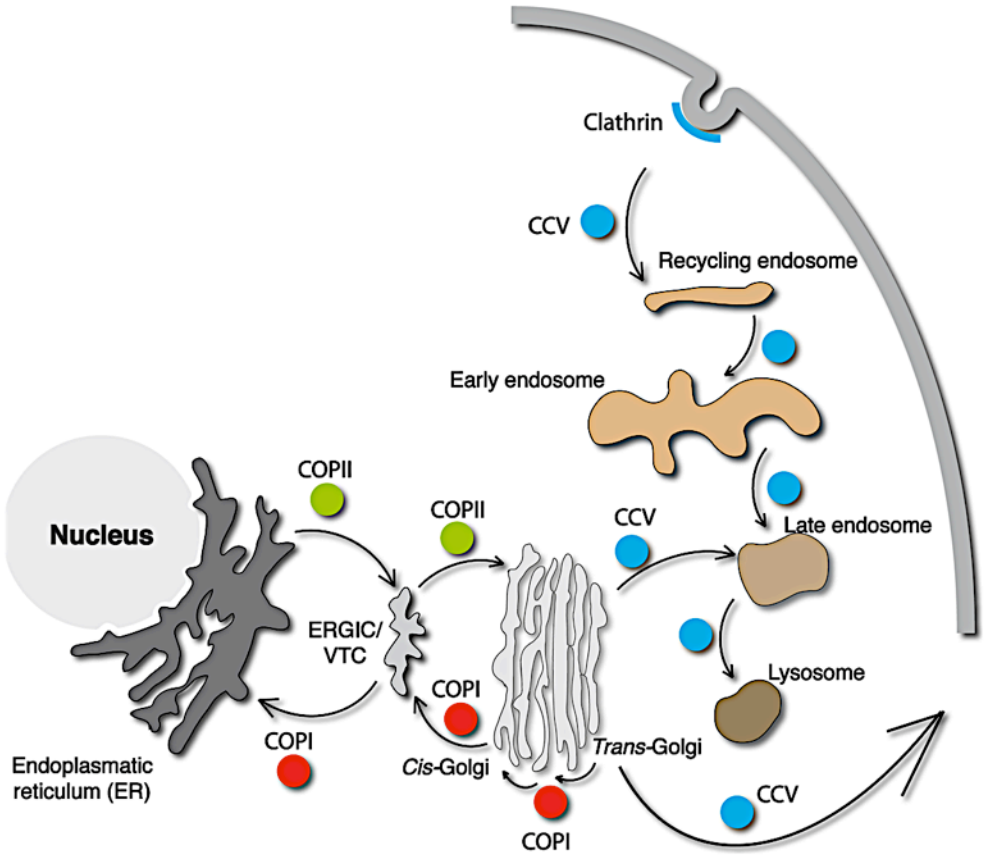

Figure 5: Overview of the secretory pathway.

Proteins enter the secretory pathway at the ER. They are transported by COPII to the ERGIC/VTC where proteins are concentrated and further transported to the *cis*-Golgi network. Retrograde transport back to the ER is carried out by COPI vesicles, that can also facilitate protein trafficking between Golgi stacks. Clathrin-coated vesicles (CCVs) take over from the *trans*-Golgi network and deliver the protein to its final destination. In addition, CCVs are responsible for endocytosis at the plasma membrane. (adapted from Kirchhausen et al., 2000)

missfolded proteins can be modulated by chaperones as well, to control folding capacity of the ER lumen and to prevent protein aggregation. Correctly folded proteins leave the ER through so called ER-exit-sites (ERES), or transitional ER (tER), where cargo is concentrated and packaged into COPII (Coat-protein-complex II) vesicles (Orci et al., 1986; Hughes and Stephans, 2007 for review). Quality control mechanisms are applied at ER exit sites to guarantee proper assembly of proteins (Mezzacasa and Helenius 2002). This includes multimeric membrane proteins as well: The ER export of K_{ATP} channel subunits is coupled to proper assembly of the heterooctamer. Furthermore, 14-3-3 proteins have been proposed to monitor assembly of multimeric membrane protein subunits (Zerangue et al., 1999; Yuan et al., 2003). Recent studies suggest that ER exit sites are dynamically regulated to accommodate different cargo and to respond to changing demands on cargo flux (Aridor et al., 1999; Aridor and Balch, 2000; Guo and Linstedt, 2006; Farhan et al., 2008; Higashio et al., 2008).

Formed COPII vesicles transport the cargo via the ERGIC (ER-golgi-intermediate-compartment; Saraste und Kuismanen, 1984), also described as VTC (vesicular-tubular-clusters; Balch et al., 1994), to the *cis*-Golgi network. This compartment is formed of flexible, connected membrane stacks. On its way from *cis*- to *trans*-Golgi the protein undergoes additional modifications like O-glycosylation. Sorting from the *trans*-Golgi membrane is very versatile and delivers cargo to endomembrane compartments like the lysosome/vacuole or to the plasma membrane.

Three different vesicles transport cargo along the secretory pathway: COPI, COPII and Clathrin-coated vesicles (CCVs; see Table 2 for general comparison). The formation of these vesicles has in common that small GTP-binding proteins (Sar1 for COPII, Arf1 for COPI and Arf1/6 for Clathrin-coated vesicles) initiate recruitment of coat components to the donor membrane. These coat proteins then capture and concentrate cargo and generate local membrane curvature, leading to vesicle fission (see Lee et al., 2004 for review). GTP hydrolysis stimulates fission of the vesicle from the donor membrane. When the target membrane is reached, vesicle tethering and fusion is promoted by SNARE proteins.

The COPI coatomer complex is primarily responsible for retrograde transport of proteins from the *cis*-Golgi back to the ER (Letourneur et al., 1994). Recognition of ER-sorting motifs like the C-terminal dilysine motif -KKXX (Nilsson et al., 1989), -WXXW (Cosson et al., 1998) and Arg-based -LRKR-motifs by the coat, sorts membrane proteins into COPI-coated vesicles

(Zerengue et al., 1999). It was shown, that the COPI complex can act in quality control to bring improperly assembled K_{ATP} channel subunits back to the ER to allow a new round of assembly (Yuan et al., 2003; Michelsen et al., 2005; Mrowiec and Schwappach, 2006 for review).

Clathrin-coated vesicles (CCVs) are the best studied class of vesicles and can bud from plasma membrane as well as the *trans*-Golgi network and facilitate endocytosis and transport between lysosomes, endosomes and the *trans*-Golgi network (Kirchhausen, 2000 for review). The variety of transport routes is achieved by interactions with different adaptor proteins (Hirst et al., 1999). The major component of CCVs is clathrin: Three heavy chains (CHC) and three light chains (CLC) form a so called triskelion that defines the outer coat of CCVs (Ungewickell und Branton, 1981).

COPII vesicles form at ER membranes and transport cargo proteins to the *cis*-Golgi network. Since these vesicles are of major interest in this study, they will be discussed in the following section in more detail.

Transport/ Component	**COPII**	**COPI**	**Clathrin**
Transport	ER to *cis*-Golgi	- *cis*-Golgi to ER - between Golgi stacks	- trans-Golgi to plasma membrane and to late endosome - between endosome and lysosome - endocytosis
GTPase	Sar1	Arf1	Arf1 (AP1/3/4), Arf6 (AP2)
Guanine-exchange factor (GEF)	Sec12	Sec7-like proteins, GBF1	Sec7-like proteins
GTPase-activating protein (GAP)	Sec13/31, Sec23/24	Coatomer	?
Inner-coat complex	Sec23/24	beta/delta/gamma/ zeta-Coatomer subunits	AP1-4
Outer-coat complex	Sec13/31	alpha/beta'/epsilon-Coatomer subunits	Clathrin

Table 2: Comparison of general aspects of COPII, COPI and CCVs.

2.4 COPII transport in the secretory pathway

Barlowe and colleagues discovered COPII-coated vesicles in genetic studies of temperature sensitive *Saccharomyces cerevisiae* strains defective in ER export (Barlowe et al., 1994). Since then, enormous progress has been achieved to understand the mechanisms that underlie COPII formation. Budding of a COPII vesicle at the ER membrane is initiated by the small GTPase Sar1. The cyctosolic GDP-bound form of Sar1 first binds its membrame bound interaction partner Sec12. Sec12 is a guanine exchange factor (GEF) that catalyses GDP to GTP exchange on Sar1 (Barlowe et al., 1993; Barlowe and Schekman, 1993). GTP binding leads to exposure of an N-terminal amphipathic α-helix into the ER membrane (Goldberg, 1998 ; Bi et al., 2002) that anchors Sar1 in the membrane. Membrane bound Sar1 then recruits coat components in two steps: First, the inner coat components Sec23 and Sec24 are recruited. Cargo selection and binding occurs most likely by Sec24. Multiple cargo binding domains have been identified in Sec24 that suggest specific cargo selection by inner coat components (Miller et al., 2003; see Mancias and Goldberg, 2005 for review). Recent studies of the X-ray structures of the four human Sec24 proteins revealed specific sites in Sec24a and Sec24b that were absent in Sec24c and Sec24d and allowed selective cargo binding (Mancias and Goldberg, 2008). Binding of correctly assembled cargo proteins can enhance affinity to Sec24, thus stabilizing the inner coat formation and allowing more time for recruitment of outer coat components Sec13 and Sec31. This could be one mechanism of cargo concentration and could function as a proofreading mechanism (Sato and Nakano, 2007). Insertion of Sar1-GTP into the membrane and binding of the bowtie-shaped Sec23/24 complex introduces membrane curvature that is absolutely required for vesicle formation (Farsad and De Camilli, 2003; Lee et al., 2005). Recent work by Stagg and colleagues suggests a Sec23/24-cargo ternary prebudding complex that needs to be formed first to allow recruitment of Sec13/31 (Stagg et al., 2008). Sec13/31 are thought to function as structural scaffold, that stabilizes the Sar1-Sec23/24-prebudding complex and enhances membrane curvature (Stagg et al., 2006). New structural insights have revealed that the outer coat is capable of forming COPII vesicles of different shape and size. This strongly enhances the flexibility of coat geometry and allows even very large vesicles to be packaged (Stagg et al., 2006; Stagg et al., 2008). Still, the observed maximum angle for the flexible hinge region between Sec13 and Sec31 is sufficient for vesicles up to 1000 Å. However for very large cargoes such as procollagen, even vesicles of this size are not sufficient.

Sequential addition of COPII coat components suggests a stepwise increasing GAP (GTPase-activating protein) activity that stimulates GTP hydrolysis on membrane bound Sar1-GTP and facilitates the release of a formed COPII vesicle (Lee et al., 2004). Thus, binding of the Sec13/31 complex was shown to accelerate the Sec23-mediated GAP activity (Antonny et al. 2001). However, as shown by Antonny and Schekman, GTP hydrolysis is not required for vesicle fission, since budded vesicles could be observed by using the nonhydrolysable GTP analogue (GTPγS) (Antonny and Schekman, 2001).

Figure 6 summarizes the steps required to form a COPII vesicle.

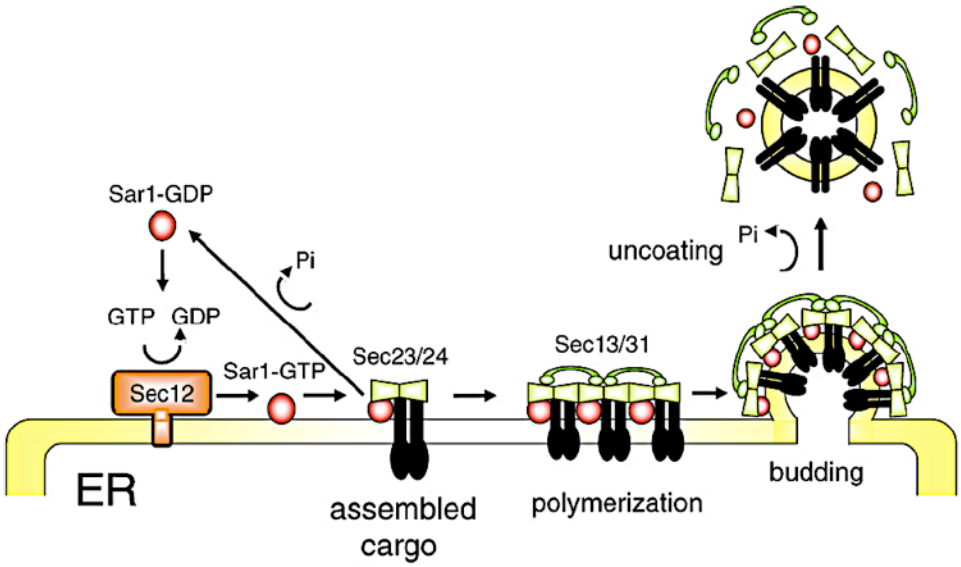

Figure 6: Cartoon of COPII vesicle formation.

The guanine exchange factor (GEF) Sec12 catalyses the exchange of GTP for GDP on the cytosolic Sar1 protein. This leads to binding of Sar1-GTP to the ER membrane and recruitment of the Sec23/24 complex. Cargo selection by Sec24 keeps the inner coat (Sar1-Sec23/24) stable and allows binding of the outer coat components Sec13/31. Sec13/31 is able to form flexible vesicle cages around the inner coat which in combination with Sar1 membrane insertion and the Sec23/24 bowtie-shaped structure leads to vesicle formation. GTPase-activating protein activity by Sec23 and Sar1 itself finally leads to release of the COPII vesicle.
(Figure from Sato and Nakano, 2007)

Multimerisation of the Sar1/Sec23/24-cargo complex, the flexible hinge region in Sec13/31 and its contact with the inner membrane coat are highly plausible putative interaction targets for regulatory factors. 14-3-3 proteins have been previously reported to interact with Sec23 (Pozuelo Rubio et al., 2004). One aspect of my thesis was the investigation of a putative role of yeast 14-3-3s as regulatory factors of COPII budding.

2.5 Trafficking of K_{ATP} channels

ATP sensitive potassium channels (K_{ATP} channels) were first identified in 1983 by Noma and found to be present in many tissues, such as the pancreas (Ashcroft et al., 1984). They function as inwardly rectifying potassium channels and play crucial roles in important cellular processes like the insulin secretion from pancreatic β-cells (Cook et al., 1988; Ashcroft and Rorsman, 1989). Increasing glucose concentration in the cell leads to production of ATP in the cytosol. ATP inhibits the K_{ATP} channel (Babenko et al., 1998) and leads to membrane depolarization through altered membrane potential. Influx of calcium through the now activated Ca^{2+} channels facilitates exocytosis of insulin containing granules that once fused to the plasma membrane, release insulin to lower glucose levels in the blood stream (Miki et al., 1999).

K_{ATP} channels are present as an octamer formed by two groups of four subunits each. The first group is built by four units of the sulphonylurea receptor 1 (SUR1) which is a member of the ATP-binding cassette (ABC) membrane transporter superfamily. Four SUR1 form the regulatory part of the channel. The pore-forming domain of K_{ATP} channels is composed of four units of inwardly rectifying potassium channels (Kir6.x). The composition of K_{ATP} channels in pancreatic β-cells is shown in Figure 7.

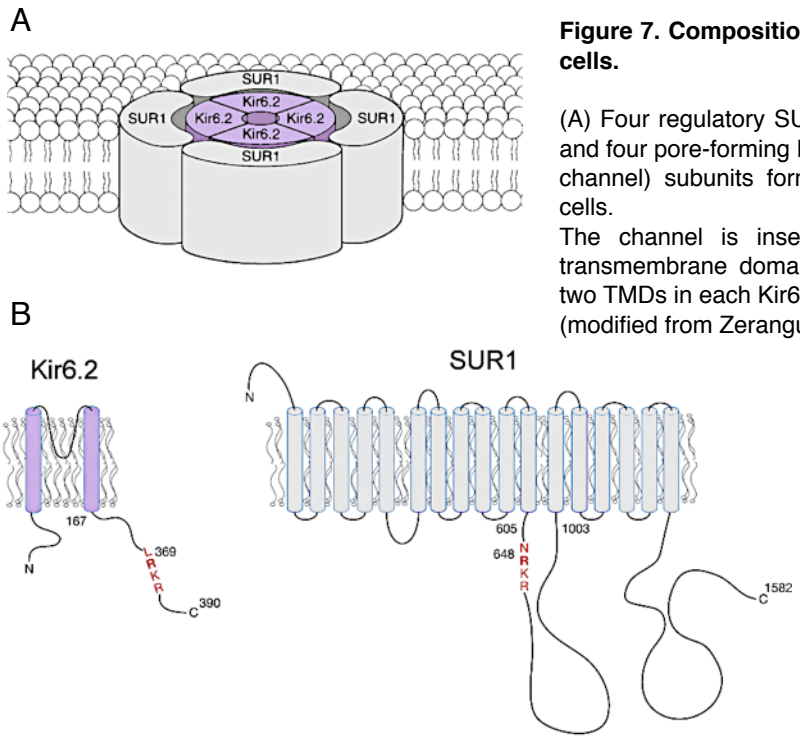

Figure 7. Composition of a K_{ATP} channel in pancreatic β-cells.

(A) Four regulatory SUR1 (sulphonylurea receptor) subunits and four pore-forming Kir6.2 (inwardly rectifying potassium channel) subunits form the K_{ATP} channel in pancreatic β-cells.
The channel is inserted in the membrane through 17 transmembrane domains (TMD) in each SUR subunit and two TMDs in each Kir6.2 subunit.
(modified from Zerangue et al., 1999).

(B) Topology of Kir6.2 and SUR1.
C-terminal loops are exposed into the cytoplasm in both subunits. These regions contain the Arg-based motif (highlighted in red), which was identified to be a binding motif for COPI and 14-3-3 proteins (Yuan et al., 2003).
(modified from Michelsen et al., 2005)

A distinct feature of the K_{ATP} channel formed by SUR1 and Kir6.2 is that both subunits expose a Arg-based motif (LRKR-motif) in the cytosolic regions (see Fig. 7 B). Schwappach and colleagues could show that these signals retain single subunits in the ER until correct assembly of the octameric channel occurs (Schwappach et al., 2000; Zerengue et al., 1999). Further investigations by Yuan and colleagues identified binding of 14-3-3 proteins to the LRKR-motif. Using the last 36 amino acids of the Kir6.2 subunit they demonstrated that 14-3-3 proteins bind preferentially to multimeric versions of the tail containing the LRKR-motif. On the other hand, monomeric presentation, mimicking unassembled channel subunits, lead to strong binding and retrieval by the COPI machinery (Yuan et al., 2003; Michelsen et al., 2007). The resulting model is shown in Figure 8.

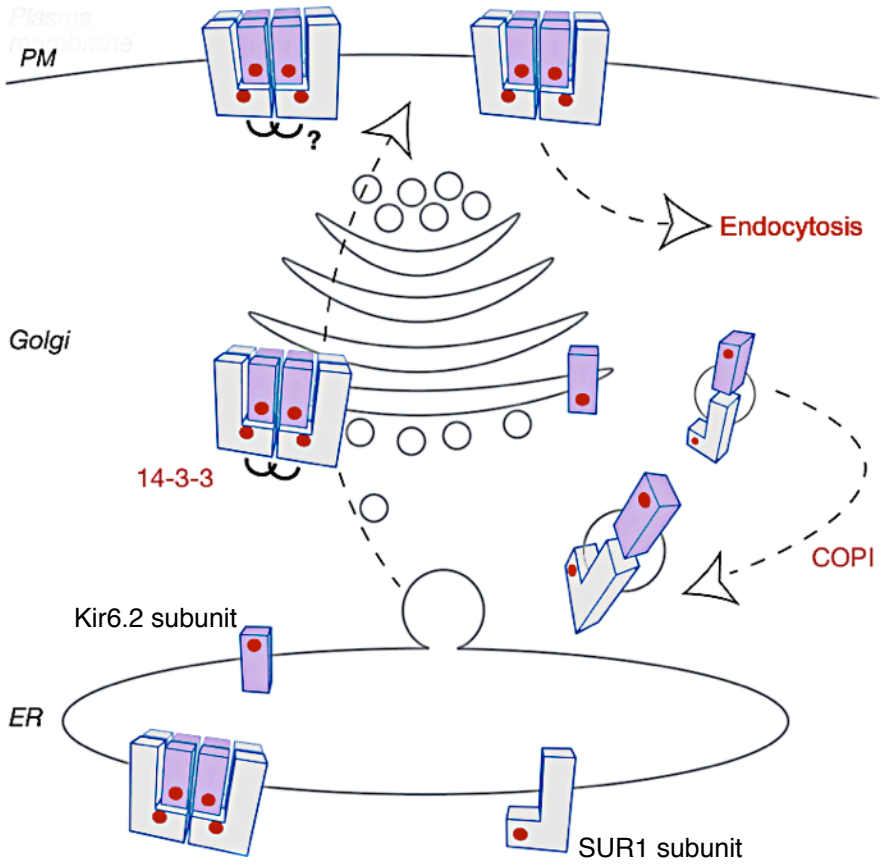

Figure 8. Model of the K_{ATP} channel transport.

SUR1 subunits are displayed as L-shaped structure. Kir6.2 subunits as rectangular structures. Red dots symbolize the Arg-based LRKR-motif exposed by both subunits.
14-3-3 proteins bind to multimeric presentation of the LRKR motif and mask the motif, so that COPI retrieval can not occur. Monomeric presentation leads to retrograde trafficking back to the ER by the COPI machinery.
According to this model 14-3-3 and COPI create a quality control mechanism since only properly assembled channels (octamers of four SUR1 and four Kir6.2) reach the plasma membrane (Yuan et al., 2003).
Presence of a di-leucine signal is involved in endocytosis of the channel from the plasma membrane.
(modified from Michelsen et al., 2005)

2.6 Aims of the thesis

Yuan et al identified two mammalian 14-3-3 isoforms to interact with a multimeric version of the last 36 amino acids of the C-terminal Kir6.2 tail. Using mammalian cells, a general regulatory function of 14-3-3 proteins could be defined. However, to gain mechanistic insights into isoform specific binding and regulation of K_{ATP} channel trafficking by 14-3-3 proteins the yeast system offers key benefits: (1) Only two 14-3-3 isoforms (Bmh1 and Bmh2) are present in yeast, in comparison to seven in mammalian cells. (2) Knockouts are available in the form of a Δ*bmh*1, a Δ*bmh2* and a viable Δ*bmh1*Δ*bmh2* strain.

For these reasons, Michelsen and colleagues made use of a Pmp2 reporter protein that was fused to the last 36 amino acids of Kir6.2 containing the Arg-based motif and a fluorescence reporter (see Fig. 9). K_{ATP} channel assembly was simulated by multimerization of the tail through addition of an GCN4 leucine zipper variant pLI (Harbury et al., 1993). Monitoring the localization of the Pmp2 reporter, Michelsen et al demonstrated an isoform specific role of Bmh1 in forward trafficking (see Fig. 3).

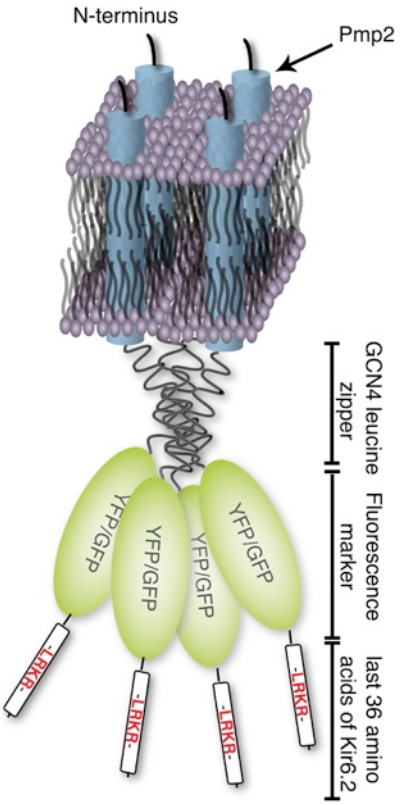

Figure 9: Cartoon of the tetrameric Pmp2 fusion protein.

The 38 amino acids long isoproteolipid Pmp2 is a yeast membrane-bound regulator of the plasma membrane proton pump (Navarre et al., 1994). The protein was fused to a GCN4 leucine zipper, a fluorescence marker like YFP or GFP and the last 36 amino acids of Kir6.2 containing the Arg-based LRLR motif (highlighted in red). Tetramerization of four fusion proteins is caused by the GCN4 leucine zipper and mimics the assembly of K_{ATP} channels.

I made use of yeast as a model to test several hypotheses for the mechanism of 14-3-3 dependent sorting in eukaryotic cells.

The following questions were the main focus of my thesis. To tackle them I combined yeast live cell imaging, site-directed mutagenesis of the 14-3-3 proteins and an *in vitro* COPII budding assay with biochemical methods.

- How can two 14-3-3 isoforms that share 81% similarity show isoform specific behavior? What are the mechanistic details that create isoform specificity?

- At which step(s) of the forward trafficking process do 14-3-3 proteins act?

- Can simple masking of the Arg-based COPI recognition motif by 14-3-3 proteins explain that Bmh1 but not Bmh2 promotes forward transport?

3. Materials and methods

3.1 Materials

3.1.1 Reagents and kits

Reagent / Kit	Company
Agar	Melford
Amino acid mix (CSM)	BIO 101
Amino acids: L-Arginine, L-Histidine, L-Leucine, L-Tryptophan	BIOMOL
Amino acids: L-Methionine, Uracil	Sigma
Biomate 5 (UV-Vis spectrophotometer)	Thermo scientific
Bradford Reagenz Protein Assay	BioRad
Complete® Protease Inhibitor (+/- EDTA)	Roche
CSM amino acid powder (lacking Ade, His, Leu, Met, Trp, Ura)	Q-BIOgene
Drop-out mix synthetic	US Biological
ECL™ Western Blotting Detection Reagents	Amersham Biosience
ER-Tracker	Molecular Probes
Factor Xa	Amersham
GSH-Agarose	Sigma
High Pure PCR Product Purification Kit	Roche
Hybond™-ECL™ Nitrocellulose membrane	Amersham Bioscience
IgG Sepharose 6 Fast Flow	GE Healthcare
ImmunoPure® Immobilized Protein A/G	Pierce
MobiCols Filtertubes 35µm pore size	MoBiTec
Peptone	Melford
Protino Ni-NTA 2000	Macherey-Nagel
QIAprep Spin Miniprep Kit	QIAGEN
Tryptone	Melford
UVI doc	UVITEC
Yeast extract	Melford
Yeast nitrogen base w/o amino acids	BD
YeaStar Genomic DNA Kit	Zymo Research

Other chemicals used in this study were purchased from Sigma, Roth, Roche, Serva, Merck, USB, AppliChem, J.T.Baker, Boehringer, Biomol, Amersham, Molecular Probes, Bio-Rad.

3.1.2 Enzymes

Restriction enzymes	Company
AatII; AgeI; ApaI	Fermentas und New England Biolabs
BamHI; BglI; BglII; Bsp120I	
EcoR I; EcoR V	
Hind III; HpaI; KpnI;	
NcoI; NdeI; NheI; MluI; NotI; NsiI	
PmeI; PstI	
SacI; SalI; SmaI; SphI	
XbaI; XhoI	

Enzymes used for manipulation of DNA	Company
CIAP (Calf Intestine Alkaline Phosphatase)	Fermentas
Expand High Fidelity DNA polymerase thermo stabile	Roche
Pfu DNA polymerase thermo stabile	Fermentas
Taq DNA polymerase thermo stabile	Schwappach lab
T4-DNA ligase	Fermentas
T4-DNA polymerase	Fermentas

Other enzymes	Company
ImmunO Zymolyase	MP Biomedicals

3.1.3 Media and antibiotics for bacterial cultures

Medium / antibiotic	Preparation
SOC medium	Add 1 ml 40% glucose and 1 ml $MgCl_2$ to 100 ml of the following medium: Per liter: 20 g tryptone, 5 g yeast extract, 0.5 g NaCl, 2.5 ml 1 M KCl. Adjust pH to 7.0 with NaOH. Aliquot in 100-ml and sterilize by autoclaving.
Luria-Bertani (LB) medium	Per liter: 10 g tryptone, 5 g yeast extract, 10 g NaCl. Adjust pH to 7.0 with NaOH. Sterlize by autoclaving. Add antibiotics if necessary.
Luria-Bertani (LB) agar	Per liter: 10 g tryptone, 5 g yeast extract, 10 g NaCl. Adjust pH to 7.0 with NaOH. Add 15 g agar before autoclave. Add antibiotics if necessary.
2YT medium	Per liter: 15 g Trypton, 10 g yeast extract, 5 g NaCl, 2% (v/v) Glycerine, 30 mM Potassiumphosphate. Sterlize by autoclaving. Add antibiotics if necessary.
Ampicilin (Amp) stock	Prepare 100 mg/ml stock in MiliQ H_2O and sterilize by filtration through a 0.22 µm filter. Aliquot and store at –20 °C. Working concentration was 100 µg/ml.
Kanamycin (Kan) stock	Prepare 50 mg/ml stock in MiliQ H_2O and sterilize by filtration through a 0.22 µm filter. Aliquot and store at –20 °C.
Doxycycline stock	Dissolve doxycycline sulfate (Sigma) in MiliQ H_2O to a concentration of 1 mg/ml. Sterilize by filtration through a 0.22 µm filter and store at 4 °C in a light-tight container. Make fresh stock every 4 weeks.
Chloramphenicol stock	Dissolve chloramphenicol in ethanol to a concentration of 34 mg/ml. Sterilize by filtration through a 0.22 µm filter, aliquot and store at -20 °C.

3.1.4 Media, antibiotics and solutions for yeast cultures

Medium / antibiotic	Preparation
Nourseothricin (CloNat)	Prepare 100 mg/ml (1000x) stock solution. Sterilize by filtration through a 0.22 µm filter, aliquot and store at -20 °C.
G418 (Geneticin)	Prepare 200 mg/ml (1000x) stock solution. Sterilize by filtration through a 0.22 µm filter, aliquot and store at -20 °C.
Yeast full medium (YPAD)	Per liter: Dissolve 10 g yeast extract, 20 g Peptone in MiliQ H_2O. After autoclaving, add 40 mg Adenine and 40 ml of 40% Glucose through a 0.22 µm filter.
Selective yeast medium	Per liter: Mix 6.7 g yeast nitrogen base, 0.65 g CSM amino acid powder, 20 g glucose, 20 mg of each necessary amino acid in MiliQ H_2O and sterilize by filtration through a 0.22 µm filter.
Yeast plates	Dissolve 40 g/l agar in MiliQ H_2O and autoclave. Combine 50% (v/v) of yeast medium (doubled concentration of ingredients) and 50% agar (v/v), mix and pour plates.
Lithium acetate solution	Prepare a 1 M lithium acetate stock solution, (10x) pH 7.5 in MiliQ H_2O.
Polyethylene glycol (PEG) solution	Prepare a 50% PEG stock solution with PEG 4000 in MiliQ H_2O.

3.1.5 General solutions used in the study

Solution	Preparation
Annealing buffer	For a 2x solution: 40 mM Tris/HCl, pH 7.6, 60 mM NaCl.
Western blot blocking solution	Dissolve 5% (w/v) milk powder, 0.02% NP-40 in 1x TBS solution.

Coomassie staining solution	Per 1 liter: Dissolve 2 g Coomassie Brilliant Blue in 300 ml ethanol (absolut) and 100 ml acidic acid.
Coomassie fixation and destain solution	Per 1 liter: Mix 300 ml ethanol (absolut), 100 ml acidic acid and 600 ml MiliQ H_2O.
DNA loading buffer	Dissolve 30% (w/v) Ficoll 400, 0.25% (w/v) bromophenol blue and 0.25% xylene cyanol in MiliQ H_2O.
Phosphate buffered saline (PBS)	Combine 140 mM NaCl, 3 mM KCl, 8 mM Na_2HPO_4, 1.5 mM KH_2HPO_4, pH 7.4, ad 1l MiliQ H_2O.
Ponceau-S	Per liter: 20 g Ponceau-S, 300 g trichloroacetic acid, 300 g sulfosalicylic acid in MiliQ H_2O.
SDS PAGE running buffer	Prepare 250 mM glycerin, pH 8.3, 125 mM Tris and 0.1% (v/v) of 10% SDS solution, in MiliQ H_2O for 5x solution.
SDS PAGE sample buffer	Prepare 250 mM Tris-HCl, ph 6.8, 50% (v/v) glycerin, 5% (v/v) of 10% SDS solution, 0.5% (w/v) bromophenol blue and 250 mM dithiothreitol (DTT) in MiliQ H_2O for 5x solution.
10 % SDS	Per liter: Dissolve 100 g sodium dodecyl sulphate in MiliQ H_2O.
T4-ligase buffer	Prepare 50 mM Tris-HCl, pH 7.6, 10 mM $MgCl_2$, 1 mM ATP, 1 mM DTT, 50 mg/ml PEG-8000 in MiliQ H_2O for 10x stock solution. Aliquot and store at -20 ºC.
TAE - DNA running buffer	Prepare 800 mM Tris-HCl, pH 7.5, 200 mM Na-acetate, 20 mM EDTA, pH 8 in MiliQ H_2O for 20x stock solution.
Tris buffer for SDS PAGE stacking gel	1 M Tris-HCl, pH 6.8 for 8x stock solution.
Tris buffer for SDS PAGE seperation gel	1.5 M Tris-HCl, pH 8.8 for 4x stock solution.
TBS	Prepare 240 mM Tris-HCl, ph 7.4, 1.36 M NaCl, 30 mM KCl in MiliQ H_2O for 10x stock solution.

Western blot (semi-dry) transfer buffer	Prepare 390 mM glycine, 480 mM Tris, pH 8.3, 3.7 g/l SDS in MiliQ H_2O for 10x stock solution. Add 20% (v/v) methanol in 1x transfer buffer solution.
Western blot (wet) transfer buffer 10x	For a 10x stock solution prepare a solution of 250 mM Tris, 1.92 M glycine, pH 8.3. Do not use HCl for pH adjustment.
Ammonium persulfate (APS)	Dissolve 1 g ammonium persulfate in 10 ml MiliQ H_2O for a 10% stock solution. Store at 4 °C.
Phenylmethylsulfonyl fluoride (PMSF)	Dissolve PMSF in isopropanol, 17.4 mg/ml for a 100 mM stock solution. Aliquot and stored at -20 ºC.
Isopropylthio-β-D-galactoside stock (IPTG)	Dissolve IPTG in MiliQ H_2O, 238.3 mg/ml for 1 M stock solution. Sterilize the solution through a 0.22 μm filter. Make 1 ml aliquots and store at –20 ºC.
BN-PAGE solubilization buffer A	50 mM NaCl, 50 mM imidazole, 2 mM EDTA, 2 mM 6-amino-hexanoic acid, pH 7.0
BN-PAGE solubilization buffer B	50 mM imidazole, pH 7.0, 2 mM EDTA, 750 mM 6-amino-hexanoic acid

3.1.6 Technical equipment used in the study

Equipment	**Company**
Electroporator	BioRad
PTC-200, Peltier Thermal Cycler	MJ Reaearch
Electrophoresis unit Mighty Small	Amersham Bioscience
Hoefer Mighty Small Gel System	Hoefer
Sonifier 450	Branson
Biofuge pico centrifuge	Heraeus
Ultra centrifuges	Beckman
High speed centrifuges	Sorvall and Heraeus

DeltaVision microscope (equipped with a 100×/0.35-1.5 Uplan Apo objective and a Sedat quadruple filter set (Chroma 86000v2))	Leica
Coolsnap HQ camera	Photometrics
Biacore 3000	BiaCore
Trans-Blot Cell	BioRad
Trans-Blot SD Cell	BioRad

3.1.7 Antibodies

Antibody (used concentration)	**Derived from**
Anti-GFP (1:1000)	D. Görlich lab
Anti-HA (1:1000 for WB)	Covance
Anti-Bmh (1:1000 for WB)	This study
Anti-Bmh1 (1:2000)	P. van Heusden lab
Anti-Sec61 (1:10000)	M. Seedorf lab
Anti-Kir6.2 (1:1000)	Schwappach lab
Anti-Sec22 (1:2000)	A. Spang lab
Anti-Bos1 (1:2000)	A. Spang lab
Anti-Bet1 (1:2000)	A. Spang lab
Anti-Sec24 (1:2000)	A. Spang lab
Anti-Emp47 (1:2000)	H. D. Schmitt lab
Anti-Ndk1 (1:1000)	Pain lab
Secondary antibodies: HRP conjugated (1:5000)	Jackson Immunoresearch

3.1.8 Bacterial strains used in this study

Strain	**Genotype**
DH5α	*hdsR*17 *supE*44 Δ*lac*U169 (F80 *lacZ*ΔM15) *recA*1 *endA*1 *gyrA*96 *thi* 1 *rel*A1Δ

BL21 DE3 Star pRosetta	Δ(*mcr*A)183 Δ(*mcr*CB-*hsd*SMR-*mrr*)173 *end*A1 *sup*E44 thi-1 *rec*A1 *gyr*A96 *rel*A1 *lac*[F' *pro*AB *lac*q ZΔ M15 Tn10 (Tetr)]; RNAseE-; pRosetta

3.1.9 Yeast strains used in this study

Strain	Genotype	Derived from
Euroscarf knockout library	COMP-SET 1-A	EUROSCARF
TetO7 library	Yeast Tet-promoters Hughes Collection (yTHC)	Open Biosystems
Y00000	BY4741*, MATa, his3Δ1, leu2Δ0, met15Δ0, ura3Δ0*	EUROSCARF
Y06173 Δ*bmh1*	BY4741*, MATa, his3Δ1, leu2Δ0, met15Δ0, ura3Δ0, yer177w::kanMX4*	EUROSCARF
Y04034 Δ*bmh2*	BY4741*, MATa, his3Δ1, leu2Δ0, met15Δ0, ura3Δ0, ydr099w::kanMX4*	EUROSCARF
RRY1249 Δ*bmh1*Δ*bmh2*	Sigma1278b*, MATalpha, ura3-52, leu2::hisG, his3::hisG, bmh2::His3+, bmh1::His3+*	Fink lab
RRY1257 WT zu RRY1249	Sigma1278b*, MATa/alpha, ura3-52, his3::hisG, RED1+, Trp1+/trp1::hisG, Leu2+/leu2::hisG*	Fink lab
YKL067W Δ*ndk1*	BY4741*, MATa, his3Δ1, leu2Δ0, met15Δ0, ura3Δ0,* ykl067w*::kanMX4*	EUROSCARF
Δ*ndk1* Δ*bmh1*	BY4741*, MATa, his3Δ1, leu2Δ0, met15Δ0, ura3Δ0,* ykl067w*::kanMX4, yer177w::natMX4*	This study
Δ*ndk1* Δ*bmh2*	BY4741*, MATa, his3Δ1, leu2Δ0, met15Δ0, ura3Δ0,* ykl067w*::kanMX4, ydr099w::natMX4*	This study

AH109	*Mat a, trp1-901, leu2-3, 112, ura3-52, his3-200, gal4Δ, gal80Δ, LYS2GAL1UAS-GAL1TATA-HIS3, GAL2UAS-GAL2TATA-ADE2, URA3::MEL1UASMEL1TATA-lacZ, MEL1*	Clontech

3.1.10 Plasmids

Plasmid	Description	Derived from
pJ478	ZZ-cc-LRKRS- in pQE60	Schwappach lab
pJ479	ZZ-cc-LKKKS- in pQE60	Schwappach lab
pJ486	*BMH1* in pQE80	D. Görlich lab
PJ487	*BMH2* in pQE80	D. Görlich lab
pL588	*PMP2*-GFP-LRERS- in p416	Schwappach lab
pM628	*PMP2*-cc-YFP-LRKRS- in p416	Schwappach lab
pM629	*PMP2*-cc-YFP-LKKKS- in p416	Schwappach lab
pM630	*PMP2*-cc-YFP-LRKRS- in p415	Schwappach lab
pM643	*PMP2*-YFP-LKKKS- in p416	Schwappach lab
pM650	*PMP2*-YFP-LRKRS- in p416	Schwappach lab
pN654	*PMP2*-YFP-KKXX in p416	Schwappach lab
pL571	PMP2-GFP-KKXX in p416	Schwappach lab
pM653	*PMP2*-cc-YFP-LKKKS- in p415	Schwappach lab
pG304	*GEF1*-GFP in p416	Schwappach lab
pT987	14-3-3 H1N2C in p416	This study
pT988	14-3-3 H2N1C in p416	This study
pT972	*SEC23*-S79N in BFGIII	This study
pT973	*SEC23*-S726N in BFGIII	This study
pT986	*SEC23*-S79N/S726N in BFGIII	This study
pT971	*SEC23* in BFGIII	This study
pJ480	proteinA (2x)-R18	This study
pN681	*BMH1* in p416	This study
pS911	PRC1(150bp)-pHluorin in p416	This study
	BMH1 C-terminus in pGEX6PI	This study
	BMH2 C-terminus in pGEX6PI	This study
	BMH1 C-terminus in pGBKT7	This study
	BMH2 C-terminus in pGBKT7	This study

YNK1 in p416	This study
YNK1-H6 in p416	This study
YNK1-HA3 in pRS416	Pain lab
YNK1-H6 in pET21b	Pain lab
SAR1-GST in pGEX-3x	A. Spang lab
pYM15	EUROSCARF

3.2 Methods

3.2.1 Working with DNA

3.2.1.1 Purification of plasmid DNA from bacteria

5 ml of bacterial culture was incubated over night (oN) in the appropriate LB medium with antibiotic(s) at 37 ºC. Plasmid DNA was purified using the QIAprep Spin Miniprep Kit (QIAGEN) according to the user manual. Cell lysis is based on alkaline lysis. After precipitation of proteins and cleaning from chromosomal DNA and cell trash, plasmid DNA is bound to a silica-gel membrane (anion-exchange matrix), washed and eluted using 50 µl of MiliQ water (for ligation) or 50 µl of elution buffer (QIAGEN). Plasmid DNA was checked by analytical test digestion and sequence analysis (GATC).

3.2.1.2 Purification of genomic DNA from yeast

5 ml of yeast culture were incubated oN in the appropriate selective yeast medium. Plasmid DNA was purified using the YeaStar Genomic DNA Kit (Zymo Research) according to the manufacturer's instructions. Cell lysis is based on digestion of the cell wall using R-Zymolyase (Zymo Research). DNA was purified on a affinity column.

3.2.1.3 Determination of DNA concentration

DNA concentration was determined by spectrophotometric analysis at a wavelength of 260 nm. DNA absorbs UV light at this wavelength and DNA concentration is a direct function of the absorbed light. The linear relationship between absorbance and DNA concentration makes it possible to calculate the total DNA concentration as follows:
Unknown mg/ml = 50 µg/ml * Measured A260 value * dilution factor.

3.2.1.4 Restriction digest

Restriction digest was performed according to the standard method described by Sambrook et al., 1998.

1 Unit of restriction enzyme, 2 µg of DNA for plasmid digestion and 2-10 µg of DNA for smaller insert fragments were used in a reaction mix of a total volume of 30 µl. Incubation time was 1.5 h, incubation temperature and reaction buffer were chosen according to the used enzyme(s). To prevent self-circularization of the digested plasmid, 1 Unit of alkaline phosphatase (CIAP, Roche) was added for 20 min at 37 ºC to the plasmid DNA reation mix after digestion.
Blunt ends were created using 5 units of T4 DNA polymerase and 3-5 µg of DNA fragment in the presence of 1.2 mM dNTPs (300 µM for each dNTP) at 37 °C for 30 min.

3.2.1.5 DNA gel electrophoresis

DNA fragments were diluted in a 6x DNA loading buffer and separated by agarose gel electrophoresis at 50-200 V using 0.8-1.5% agarose gels. DNA was stained using ethidium bromide in a concentration of 100 mg/ml in the gel. Visualization was performed using ultraviolet (UV) light. A UVIdoc system (UVITEC) was used for documentation.

3.2.1.6 DNA purification from agarose gels

DNA fragments were purified after seperation on a agarose gel by using the High Pure PCR Product Purification Kit (Roche). Purification was performed according to the manufacturer's instructions.
Since DNA fragments smaller than 100 bp are removed in the washing steps of the High Pure PCR Product Purification Kit, those small fragments were purified by using the Ultrafree-MC Centrifugal Filter Units with Microporous Membrane (0.45 µM, Millipore).

3.2.1.7 Ligation of DNA fragments

Ligation of DNA fragments was performed using the enzym T4-DNA ligase, which catalyses the building of phosphodiester bond between two DNA molecules.
In a typical ligation reaction 1-2 units of T4-DNA ligase, 50-100 ng of digested vector and insert DNA (in a molar ratio of 3-10 times the vector DNA) were incubated for 16 h at 18 ºC

in a ligase specific buffer. T4-DNA ligase was inactivated by incubating the reaction mix for 10 min at 65 ºC. The ligation product was than ready for transformation.

3.2.1.8 Preparation of competent bacterial cells

One single bacterial colony was picked and inoculated in 20 ml LB medium over night (oN) at 37 ºC. 10 ml of the oN culture were diluted in 900 ml LB medium and grown at 37 ºC until an OD_{600} of 0.5-0.7 has been reached. The culture was cooled down on ice and pelleted in 50 ml tubes (3000 rpm, 5 min at 4 ºC). The bacterial pellet was washed extensively with sterile and ice cold MiliQ H_2O. In addition, a last washing step with sterile, ice cold 10 % glycerol solution was performed to remove all remaining salt in the pellet. Finally, the pellet was resuspended in 3 ml of sterile, ice cold 10 % glycerol solution, distributed in 50 µl aliquots, immediately frozen in liquid nitrogen and stored at -80 ºC.

3.2.1.9 Transformation of bacteria

Transformation of bacteria was performed by electroporation with a Gene Pulser II electroporator (BioRad).
50 µl of competent bacteria cells (DH5α or BL21) were mixed on ice with 1-2 µl of ligation product, or 1 µl of diluted plasmid DNA (for retransformation) and electroporation was performed at a voltage of 2.5 mV, a resistance of 400 Ω and a capacity of 25 µF. Bacterial cells were diluted in SOC medium and incubated for 45 min at 37 ºC for regeneration. Recovered cells were streaked out on LB agar plate supplemented with appropriate antibiotic(s) and further incubated at 37 °C until single colonies appeared.

3.2.1.10 Polymerase chain reaction (PCR)

Polymerase chain reaction was performed according to standard protocols as described in Lawyer et al., 1989 and Saiki et al., 1988. A typical reaction mix was setup as following:

100 ng	DNA template
0.4 µM	forward primer

0.4 µM reverse primer

600 µM dNTPs (GTP, ATP, TTP and CTP)

5 µl 10x PCR reaction buffer

2.5 units pfu, Taq, or High fidelity Expand Polymerase

ad 50 µl with MiliQ H_2O

A Peltier Thermo Cycler (MJ Research) was used for amplification with a typical PCR program as follows:

step	description	duration	temperature
1	initial DNA denaturizing	2 min	94 °C
2	DNA denaturizing	20 sec	94 ºC
3	annealing	30 sec	calculated temperature (see below)
4	elongation	calculated time (see below)	72 ºC
5	repeat steps 2 - 4	25 – 30 cycles	
6	final elongation	2 min	72 ºC
7	store PCR product	∞	4 ºC

The primer specific annealing temperature was calculated using the formula:

Tm -2 °C (Tm =4x(G+C)+2x(A+T)

Elongation temperature was calculated with 1 min per kB of the amplified DNA fragment.

The PCR product was processed as described in 3.2.1.5 and 3.2.1.6.

3.2.1.11 DNA sequencing

To confirm correctness of manipulated DNA molecules, samples were sent out to GATC GmbH for sequencing and verified.

3.2.2 Biochemical methods

3.2.2.1 Protein expression in bacteria

3.2.2.1.1 Expression of untagged 14-3-3 proteins

14-3-3 isoforms were cloned into pQE80 expression vector (QIAGEN) and transformed in DH5α cells.

25 ml of 2YT medium and the appropriate antibiotic (here: ampicillin) were inoculated with one colony for over night (oN) uncubation at 37 ºC. 20 ml of the oN culture were used to inoculate a one liter 2YT culture, growth at 37 ºC was monitored and stopped at a OD_{600} = 0.6-0.8. Isopropylthio-β-D-galactoside (IPTG) was used in a concentration of 0.3 mM for induction. After induction for 2 h at 37 ºC, 10 ml of 100 mM PMSF were added and the culture was transferred on ice for 15 min. Bacterial cells were collected in a low speed spin (3000 rpm, 10 min, 4°C, Sorvall RC5C, GS3 rotor), washed and again collected at 5500 rpm, 15 min at 4 ºC using a Heraeus Megafuge 1.0. The resulting pellet was resuspended in 30 mL of the appropriate breaking buffer (Tris buffer + Roche Complete® Protease Inhibitor + EDTA) and sonified (2x2 min full power, 30% DutyCycle), or frozen in liquid nitrogen and stored at -80 ºC. Whole cell lysate was cleared from cell trash by low speed spinning (10 min at 2,000x g). To eliminate insoluble proteins and lipids, the supernatant was ultra centrifuged for 1 h at 100,000x g. Protein concentration was determined and Coomassie stained SDS PAGE gel electrophoresis was used to verify that the protein is not degraded.

3.2.2.1.2 Expression of GST tagged 14-3-3 Bmh1 and Bmh2 C-termini

14-3-3 Bmh1-/Bmh2-C termini were cloned into pGEX6PI expression vector and transformed in BL21 DE Star pRosetta cells.

20 ml of the oN culture (2YT medium + ampicillin and chloramphenicol) were used to inoculate a one liter 2YT culture, growth at 37 ºC was monitored and stopped at a OD_{600} = 0.6-0.8. Isopropylthio-β-D-galactoside (IPTG) in a concentration of 0.2 mM and 1 ml of benzylalcohol (induces chaperon expression, see de Marco et al., 2005) were used for induction. After 2 h at 37 ºC, 10 ml of 100 mM PMSF were added and the culture was transferred on ice for 10 min. Bacterial cells were collected in a low speed spin (10 min, 2,000x g at 4 ºC), resuspended in breaking buffer (20 mM HEPES, pH 6,8, 2% glycerol,

150 mM KAc, 5 mM $Mg(Ac)_2$, 1 mM EDTA, 1 mM DTT, 1 mM PMSF, 1x Roche Complete® Protease Inhibitor + EDTA) and sonified. Whole cell lysate was processed further as described in 3.2.2.1.1.

3.2.2.1.3 Expression of His tagged Ndk1 protein

6xHis-tagged Ndk1 was cloned into pET21b expression vector (Pain lab) and transformed into BL21 DE Star pRosetta cells.
Culture was grown and processed as described in 3.2.2.1.1.
Sonication was performed in 1x LEW buffer from Protino Ni-NTA 2000 kit (Macherey-Nagel).

3.2.2.1.4 Expression of GST tagged Sar1 protein

GST tagged Sar1 was cloned into pGEX-3x expression vector (A. Spang lab) and transformed in DH5α cells.
Culture was grown and processed as described in 3.2.2.1.1, except for the induction time, which was increased to 4 h with an IPTG concentration of 1 mM. The collected pellet was washed in TBS buffer (50 mM Tris, pH 7.4, 150 mm NaCl) and sonified in TBS buffer + 1% Triton X-100.

3.2.2.2 Protein purification and immobilization

3.2.2.2.1 Purification of of untagged 14-3-3 proteins

The last 36 amino acids of the distal C-terminus of the K_{ATP} channel subunit Kir6.2 (ccKir6.2) were fused to a mutated version of the GCN4 leucine zipper, pLI (see Harbury et al., 1993) and the affinity tag protein A (see Yuan et al., 2003). 5 ml of Sepharose 6 Fastflow beads (Amersham Biosciences) were diluted and sequentially washed with binding buffer (50 mM Tris-HCl, 50 mM NaCl, 5 mM magnesium acetate, pH 7.5). 600 µl of purified tetrameric Kir6.2 (Yuan et al., 2003) were incubated with the beads for 3 h at 4 ºC. Unbound protein was removed by washing with binding buffer. Beads with immobilized ccKir6.2 were transferred

to liquid chromatography columns (Sigma-Aldrich) and incubated with bacterial cell lysate with over expressed 14-3-3 isoform (see 3.2.2.1.1). 20 ml of binding buffer were used for washing. Fractions of 1 ml of purified, untagged 14-3-3 protein were collected by eluting with high salt buffer (0.5 M $MgCl_2$, 50 mM Tris-HCl, pH 7.5). Protein concentration was determined and Coomassie stained SDS PAGE gel electrophoresis was used to verify that the protein is not degraded. Purified 14-3-3 protein solutions were dialyzed over night in the appropriate buffer.

3.2.2.2.2 Immobilization of GST tagged 14-3-3 Bmh1 and Bmh2 C-termini

GSH-agarose (Sigma) was incubated with MiliQ H_2O over night at 4 ºC, washed twice with breaking buffer (see 3.2.2.1.2) and moved to a liquid chromatography column (Sigma-Aldrich). The ultra-centrifuged supernatant from 3.2.2.1.2 was added. Increased amounts of bound GST-tagged protein could be achieved by repeated loading of GST-protein solution. Immobilized GST-tagged Bmh1-/Bmh2 C-terminus was used for interaction studies with Ndk1 protein and for pull-down experiments.
Increasing concentrations of $MgCl_2$ in elution buffer (20 mM HEPES, pH 9.5, 10 mM GSH, 5% glycerol, 150 mM KAc, 5 mM $Mg(Ac)_2$, 1 mM EDTA, 1 mM DTT) were used for collecting 1 ml fractions.

3.2.2.2.3 Purification of His tagged Ndk1 protein

The supernatant from 3.2.2.1.3 was processed following the instructions of the Protino Ni-NTA 2000 kit (Macherey-Nagel).
Protein concentration was determined and Coomassie stained SDS PAGE gel electrophoresis was used to verify that the protein is not degraded. Purified Ndk1 protein was dialyzed over night in the appropriate buffer.

3.2.2.2.4 Purification of GST tagged Sar1 protein

Purification of GST tagged Sar1 protein occurred according to protocol from the Spang lab. GSH-agarose (Sigma) was incubated with MiliQ H_2O over night at 4 ºC, washed twice with TBST buffer (TBS buffer + 0.1% Tween 20) and the ultra-centrifuged supernatant from . 2.2.1.4 was added for 1 h at 4 ºC. Agarose was washed three time in TBST buffer, once in TBS buffer (see 3.2.2.1.4) and finally in TCN buffer (25 mM Tris, pH 8, 1 mM $CaCl_2$, 100 mM NaCl), resuspended in 5 ml TCN buffer and transferred to a liquid chromatography column (Sigma-Aldrich). 10 units of Factor Xa solution (Amersham) were added and the solution was incubated for 4 h at 25 ºC with occasional mixing. 5 ml (pool 1) were collected after uncapping the column. These fractions contain cleaved, untagged Sar1 protein in TCN buffer. 5 ml of B88 buffer (20 mM HEPES, pH 6.8, 150 mM KOAc, 250 mM sorbitol, 5 mM $Mg(OAc)_2$) were added three times and the elutions were saved as pools 2-5. Protein concentrations of pools 1-5 were determined and pools containing highest protein concentrations were chosen. PMSF was added to a final concentration of 2 mM to pools containing Sar1. Protein solutions were cleared by ultra centrifugation (10 min at 50,000x g) and supernatants were aliquoted, frozen in liquid nitrogen and stored at -80 ºC.

3.2.2.3 Determination of protein concentration

Determination of protein concentration occurred as described by Bradford (1976). The change in absorbtion of the Coomassie-G-250 reagent is monitored at a wavelength of 595 nM using a spectrophotometer. Protein concentrations can be calculated by using the information from a standard curve (derived from defined concentrations of bovine serum albumin). Determination was repeated at least once to confirm the measured concentration.

3.2.2.4 SDS polyacrylamide gel electrophoresis (SDS-PAGE)

SDS-PAGE (Tris-glycine SDS-polyacrylamide gel electrophoresis) is based on the binding of the anionic detergent SDS to proteins in a in a mass ratio of 1.4 g SDS :1 g protein. By doing so, SDS confers a negative charge to the polypeptide in proportion to its length. Therefore, protein migration in a gel matrix is determined not by intrinsic electrical charge of the

polypeptide, but by molecular weight. SDS loading buffer was prepared with denaturizing reagents 2-Mercaptoethanol and DTT. The Hoefer Mighty Small Gel System was used for separation of proteins.

SDS PAGE resolving gels in a range of 8-13.5% were prepared as follows (20 ml total volume = 4 gels):

Solution components	8% gel	10% gel	13.5% gel
H_20	9.3 ml	7.9 ml	5.6 ml
30% acrylamide mix	5.3 ml	6.7 ml	9.0 ml
1.5 M tris (pH 8.8)	5.0 ml	5.0 ml	5.0 ml
10% SDS	0.2 ml	0.2 ml	0.2 ml
10% ammonium persulfate	0.2 ml	0.2 ml	0.2 ml
TEMED	0.012 ml	0.008 ml	0.008 ml

The stacking gel was prepared as follows (15 ml total volume = 4 gels):

Solution components	Stacking gel
H_20	10.2 ml
30% acrylamide mix	2.6 ml
1.0 M tris (pH 6.8)	1.0 ml
10% SDS	0.15 ml
10% ammonium persulfate	0.15 ml
TEMED	0.015 ml

Proteins were separated by electrophoresis in a 1x Tris-glycine electrophoresis buffer using a PowerPac 300 power supply (Bio-Rad) at 15-30 mA for approx. 30 min.

The PageRuler Prestained Protein Ladder (Fermentas) has been used as protein marker.

3.2.2.5 Blue Native Polyacrylamide Gel Electrophoresis (BN-PAGE)

A 5-18% Blue Native Polyacrylamide gradient gel was used to separate proteins in their native state.

The gradient gel was poured by combining a 5% and a 18% separation gel mix in a gradient mixer using the following recipe:

Solution components	4% stacking gel	5% separation gel	18% separation gel
H_20	3.5 ml	5.0 ml	2.25 ml
AB (49.5%T, 3%C)	0.5 ml	0.9 ml	2.75 ml
3x gel buffer	2.0 ml	3.0 ml	2.5 ml
glycerol	-	-	1.5 g
10% ammonium persulfate	0.05 ml	0.05 ml	0.025 ml
TEMED	0.005 ml	0.005 ml	0.0025 ml

Samples were treated with 5x loading buffer (5% Coomassie, 50 mM BisTris, 750 mM ε-aminocaproic acid, 50% glycerol, pH 7.0). The gel was run at 4 ºC with 300 V / 15 mA. After 3 h the Coomassie containing cathode buffer was exchanged for a colorless cathode running buffer.

BSA and ferritin were used as protein markers.

3.2.2.6 Coomassie staining

SDS PAGE gels were incubated for 15 min in a fixation solution (40% ethanol, 10% glacial acetic acid in MiliQ H_2O) and than stained in Coomassie Brillant Blue containing solution for 30 min. The gel was washed and thereby destained in a destaining solution (20% ethanol, 10% glacial acetic acid in MiliQ H_2O). Additional destaining was achieved by incubating the gel in MiliQ H_20 over night.

3.2.2.7 Western blot detection

Proteins were separated by SDS PAGE. The separation gel was carefully removed and incubated in 1x transfer buffer for 20 min with gently shaking. For wet blotting the Hybond-P PVDF transfer membrane (Amersham) was incubated for 10 min in methanol. For semi-dry blotting the Hybound ECL nitrocellulose membrane (Amersham) was incubated in transfer buffer for 10 min. Proteins were transferred by semi-dry blotting, using a semi-dry transfer apparatus (Trans-Blot SD Cell, Bio-Rad) or by wet blotting using a Trans-Blot Cell (BioRad) according to the instructions given in the user manual. Successful transfer was verified by Ponceau staining and the dye was removed by extensive washes with MiliQ H_2O. The stained

membrane was incubated in blocking solution (5% (w/v) milk powder in 1x TBS and 0.01% Nonidet-P40) for at least 1 h at room temperature or over night at 4 ºC to minimize unspecific signals. Primary antibodies were diluted in an optimist concentration in blocking solution and incubated with the membrane for 1 h. After this, membrane was washed (4 times, 5 min each) with blocking solution and incubated with secondary antibody in blocking solution (1:7,000) for HRP detection (30 min at room temperature (RT)) or in Alexa Fluor secondary antibodies (1:5,000, in 1x PBS, 0.1% Tween-20, 0.01% SDS, 3% milk powder) for detection with the Licor Odyssey system (1 h on darkness at 4 ºC). Membranes for HRP detection were washed (4 times, 5 min each in blocking solution) at RT, membranes for Licor Odyssey detection were washed (4 times, 5 min each in 1x PBS, 0.1% Tween-20) in darkness. Washing was completed with a final washing step with 1x TBS and 0.01% Nonidet-P40 for HRP detection and 1x PBS, 5 min wash for Licor Odyssey detection.

HRP detection:

Membranes were rinsed in MiliQ H_2O once and incubated with prepared 1.5 ml ECL reagent (Amersham) for 2 min. The ECL-film was developed in the dark room. Exposure time varied from 2 sec to overnight depending on the requirement.

Licor Odyssey detection:

Membranes were transferred quickly (to prevent exposure to light) onto a Licor Odyssey scanning unit. A prescan was performed to determine optimal scanning intensity and to define the scanning region. Final scans were done with a resolution of 84 µm and medium quality settings. Membranes were always kept wet during the scanning procedure. Licor Odyssey software was used to obtain quantitative information of single protein bands.

3.2.3 Working with yeast

3.2.3.1 Preparation of yeast total cell extract

An over night yeast culture was grown to early- to mid-log phase and collected by centrifugation (3 min, 3000 rpm with table top centrifuge). The pellet was resuspended in 200 µl of 0.1 M NaOH, vortexed and incubated for 10 min at RT. During incubation, 10 µl of the cell suspension were diluted in 990 µl of H_2O and OD_{600} was determined. The resulting value defines the amount of SDS loading buffer, that was added to the pellet after the following spin (1 min, 12,500 rpm with table top centrifuge): 1 OD unit = 1,000 µl of added SDS loading buffer. The resuspended pellet in SDS loading buffer was heated up to 65 ºC for 10 min.

3.2.3.2 Preparation of yeast cytosol

1-3 l of yeast culture were grown to to early- to mid-log phase and collected by centrifugation (5 min, 3,000x g). Cells were washed once in MiliQ H_2O and the pellet was resuspended in 2 ml of appropriate buffer. The dense cell suspension was slowly dropped into liquid nitrogen. Cells were lysed using mortar and pestle until only a fine powder was left. The resulting cell powder was then thawed in an ice-water bath, diluted with ice cold buffer (up to 30 ml) and cleared in a first spin (10 min, 10,000x g). The supernatant was then ultracentrifuged (1 h, 100,000x g). Clean cytosol was removed, avoiding the lipid layer on top and pellet on the bottom of the tube. Protein concentration was determined and small aliquots were frozen in liquid nitrogen and stored at -80 ºC.

3.2.3.3 Preparation of ER enriched membranes from yeast cells

ER enriched membranes were prepared adopting the protocol as described by Wuestehube and Schekman.

Yeast cultures were grown to an OD_{600}=2 and harvested by centrifugation (7 min, 2,000x g). The pellet was resuspended in 10 ml Buffer A (see below for detailed description) per liter of yeast culture and incubated for 10 min at RT with gentle agitation. Cells were collected (7 min, 2,000x g) and resuspended in Resuspension buffer (see below for detailed description)

and 40 µl of zymolyase (dilution: 0.03 g powder /200 µl MiliQ H_2O) per liter of initial yeast culture. Cell suspension was incubated for up to 1.5 h at 30 ºC and digestion of yeast cell wall was monitored until OD_{600} value dropped to less than 5% of the initial value. The resulting spheroplasts were washed by collection through a sucrose cushion (see below for detailed description) at 5,500x g, 20 min at 4 ºC. Alternatively, spheroplasts can be washed twice in Buffer B (see below for detailed description) and collected at 1,000x g, 5 min at 4 ºC. In both cases the resulting pellet was slowly frozen at -80 ºC and stored on -80 ºC until further processing (usually the next day). All processing steps were performed at 4 ºC. Thawing of the frozen spheroplast pellet occurred in a water-ice bath. After this, cold Lysis buffer (see detailed description below) was added in a ratio pellet to buffer of 3:1. The pellet was resuspended by vortexing and transferred to a douncer. Cells were homogenized slowly on ice using a douncer (douncing: 30 times), centrifuged (10 min, 3,000x g), again resuspended in Lysis buffer in the same 3:1 ratio and douncing and centrifugation were repeated. The resulting supernatant was transferred into ultracentrifugation tubes and membranes were collected by spinning for 10 min at 27,000x g. The supernatant was removed carefully, discarded and the pellet was resuspended in 3 ml Lysis buffer per 1 l of initial yeast culture. A sucrose density gradient was prepared from 1.5 M and 1.2 M sucrose (in HEPES buffer) solutions. The membrane suspension was then loaded carefully onto the 1.2 M sucrose layer and ER enriched membranes (microsomes) were collected from the 1.5 M/1.2 M interphase after ultracentrifugation (1 h, 100,000x g). Microsomes were washed twice in B88 buffer (see below for detailed description) and collected by centrifugation (10 min, 27,000x g). Finally, microsomes were resuspended in B88 buffer by adding 300 µl buffer per 1 liter of initial yeast culture, aliquoted in 16 µl samples, frozen in liquid nitrogen and stored at -80 ºC. Protein concentration was determined as described in 3.2.2.3.

Buffer A:

Reagent	Volume: 1 l
100 mM Tris-HCl, pH 9.4	12.1 g
10 mM DTT	10 ml
MiliQ H_2O	ad to 1 l

Resuspension buffer:

Reagent	Volume: 250 ml
0.7 M sorbitol	31.88 g
1.5% (w/v) bacto peptone	3.75 g
0.75% (w/v) yeast extract	1.88 g
0.5% (w/v) glucose	3.1 ml of 40% Glc solution
10 mM Tris-HCl, pH 7.4	2.5 ml of 1 M Tris-HCl, pH 7.4
MiliQ H_2O	ad to 250 ml

Sucrose cushion:

Reagent	Volume: 500 ml
0.8 M sucrose	137 g
1.5% (w/v) Ficoll-400	7.5 g
20 mM HEPES, pH 7.4	10ml of 1 M HEPES, pH 7.4
MiliQ H_2O	ad to 500 ml

Wash buffer B:

Reagent	Volume: 1 l
0.7 M sorbitol	127.5 g
1.5% (w/v) Ficoll-400	7.5 g
20 mM HEPES, pH 7.4	20 ml of 1 M HEPES, pH 7.4
MiliQ H_2O	ad to 1 l

Lysis buffer:

Reagent	Volume: 500 ml
0.1 M sorbitol	9.1 g
20 mM HEPES, pH 7.4	10ml of 1 M HEPES, pH 7.4
50 mM KAc	2.45 g
2 mM EDTA	2.0 ml of 0.5 M EDTA solution
1 mM DTT	500 µl of 1 M DTT stock solution
1 mM PMSF	0.085 g
Complete® Protease Inhibitor (Roche)	add 1 tablet /50 ml buffer before use (if requested)
MiliQ H_2O	ad to 500 ml

Sucrose density step gradient:

Reagent	Volume: 100 ml	
1.5 M sucrose	53.3 g	1.5 M sucrose solution
1.2 M sucrose	41.1 g	1.2 M sucrose solution
20 mM HEPES, pH 7.4	2 ml of 1 M HEPES, pH 7.4	
MiliQ H_2O	ad to 100 ml	

Reaction buffer B88:

Reagent	Volume: 250 ml
20 mM HEPES, pH 6.8	5 ml of 1 M HEPES, pH 6.8
150 mM KAc	3.68 g
5 mM MgAc	0.40 g
250 mM sorbitol	11.4 g
MiliQ H_2O	ad to 250 ml

3.2.3.4 Preparation of Golgi enriched membranes from yeast cells

Golgi membranes were enriched using a protocol by the Spang lab.

3 l of yeast culture was grown to early- to mid-log phase and collected by centrifugation (5 min, 3,000x g). The pellet was washed once in MiliQ H_20 and resuspended in 2 ml B88 buffer. The dense cell suspension was slowly dropped into liquid nitrogen. Cells were lysed using mortar and pestle. The resulting cell powder was thawn in an ice-water bath and afterwards diluted with up to 30 ml of B88 buffer, 1 mM DTT and 1 mM PMSF. Supernatant from the spin (5 min, 5,000x g) was collected and ER membranes were removed by two additional spins (15 min, 15,000 rpm SW40 rotor). The ER free supernatant was than loaded on a 60% sucrose cushion and centrifuged (30 min, 100,000x g). Membranes, which sedimented on the cushion were collected, diluted to the volume prior to ultracentrifugation, loaded on the 60% sucrose cushion and the ultracentrifugation step was repeated. Finally, Golgi enriched membranes were collected from the interphase and 200 µl aliquots were frozen in liquid nitrogen and stored at -80 ºC after determination of the protein concentration.

3.2.3.5 Yeast transformation

Yeast cells were transformed using the lithium acetate method described by Ausubel et al., 1997. One yeast colony was picked and grown in appropiate medium (YPAD or selective medium) at the appropriate temperature (usually 30 ºC, 25 ºC for temperature sensitive starins). Yeast cells were then collected by low speed spin, washed in MiliQ H_2O and resuspended in 200 µl lithium acetate buffer (100 mM lithium acetate, pH 7.5, 50 mM TrisHCl, pH 7.5, 1 mM EDTA). 1-3 µg plasmid DNA, 18 µl boiled carrier DNA (10 mg/ml in TrisHCl, pH 8.0, 1 mM EDTA) and 1.2 ml polyethylenglycol (100 mM lithium acetate, pH 7.5, 50 mM TrisHCl, pH 7.5, 1 mM EDTA, 40% (w/v) polyethylenglycol 4000) were added and mixed by vortexing. Incubation occurred at 42 ºC and at RT for temperature sensitive strains. After this, yeast cells were collected by centrifugation (5 min, 2,000x g), resuspended in sterile MiliQ H_2O and plated onto appropriate agar plates.

3.2.3.6 Deletion of yeast genes

Deletion of 14-3-3 *BMH1* and *BMH2* genes in the background of a Δ*ndk1* strain was realized by homologues recombination. Therefore a natMX4 cassette (containing the resistance gene for the antibiotic nourseothricin) was amplified from pAG25 vector, by using long primers, which included flanking regions of either *BMH1* or *BMH2* genes. PCR products (10 µl, 30 µl and 50 µl) were transformed into the Δ*ndk1* strain and cells were streaked out on YPAD plates containing 100 µg/ml nourseothricin. After few days at 30 ºC, colonies were picked and incubated at 30 ºC in nourseothricin containing liquid medium. The new knockout was verfied by PCR and Western blotting.

3.2.3.7 Creation of a C-terminally 6xHA tagged Ndk1 fusion protein

To genomically tag the Ndk1 protein by 6xHA, a PCR-based tagging method was applied. Using the following primer pair, that include the C-terminal region of Ndk1 and the 3' region following the *NDK1* gene, the 6HA sequence and a HIS3 marker sequence were amplified by PCR and inserted into wildtype, Δ*bmh1* and Δ*bmh2* yeast strains by homologues

recombination. The insertion of a HIS3 marker sequence allowed screening for correctly inserted 6xHA-tagged NDK1 on yeast plates lacking the amino acid Histidine.

(1) NDK1_Ctag_For: GAG-TTA-GTT-GAT-TGG-GAA-TCT-AAT-CAA-GCT-AAG-TGG-ATT-TAT-GAA-CGT-ACG-CTG-CAG-GTC-GAC

(2) NDK1_Ctag_Rev: AGA-AAA-AAA-AGG-CGC-TCA-TAT-GTA-CCC-TCC-CAT-GCC-ATA-AGT-TAT-ATC-GAT-GAA-TTC-GAG-CTC-G

3.2.4 Microscopy techniques

3.2.4.1 Life cell imaging

Live cell imaging was done by fluorescence microscopy and performed at RT in SC medium employing a DeltaVision restoration microscope equipped with a 100×/0.35-1.5 Uplan Apo objective and a Sedat quadruple filter set (Chroma 86000v2). Images were collected with a Coolsnap HQ camera (Photometrics); the Z optical spacing was 0.3 µm. Raw images were deconvolved using the conservative additive algorithm of Softworx software.
Localization of proteins, coupled to fluorescence markers (YFP or GFP) was monitored.

3.2.4.2 Immunofluorescence

25 ml of yeast culture was grown to early logarithmic phase and 2.5 ml of commercial 37% formaldehyde solution (filtered through 0.45 µm filter) was added for 45 min. Cell were collected at 2,000x g, 5 min and washed with fresh 4% formaldehyde fixation solution (for 50 ml: 2 g paraformaldehyde, heat, add 350 µl of 6N NaOH until solution clears, add 0.68 g KH_2PO_4 and 50 µl 1 M $MgCl_2$ (pH 6.5), filter through 45 µm filter) twice and finally resuspended and incubated in 4% formaldehyde fixation solution for 12-16 h with gentle shaking. Yeast cells were then harvested and washed with 200 mM Tris, pH 8, 20 mM EDTA, 1% beta-mercaptoethanol buffer (filtered) for 10 min. After collecting the cells by a low-speed spin (2,000x g, 5 min) cells were resuspended in spheroblasting buffer (1.2 M sorbitol, 50 mM potassium phosphate, pH 7.3, 1 mM $MgCl_2$, filtered) and zymolyase was added to a concentration of 0.15 mg/ml for 45 min at 37 ºC. Spheroblasts were collected at 2,000g, 5 min and washed twice in 1 ml of 1.2 M sorbitol, resuspended in 1.2 M sorbitol and 15-25 µl of spheroblasts were applied per well (Teflon-masked multiwell slides, pre-treated with poly-L-lysine solution have been used). Incubation time was 15 min, followed by two washes with PBS-BSA solution (1x PBS with 10 mg/ml BSA, filtered) and blocking with PBS-BSA for 30 min. Primary antibody diluted in PBS-BSA was applied over night. Cells were then washed 4 times with PBS-BSA before incubation with secondary antibody (fluorochrome-coupled) for 30 min at 37 ºC. Cells were washed extensively with PBS-BSA and PBS before cover slips were sealed.

The same microscopy setup as described in 3.2.4.1 has been used.

3.2.5 Surface plasmon resonance

Surface plasmon resonance experiments were performed on a BIAcore-3000 (Biacore, Uppsala, Sweden). Immobilization of a protein A-cc-LRKR fusion protein (with the tetramerforming coiled-coil domain pLI denoted –cc-) to the CM5 Chip (Biacore) was performed using the N-hydroxysuccinimide / N-ethyl-N'-(3-dimethylaminopropyl) carbodiimide hydrochloride (NHS/EDC) method. All steps were performed as described in the user manual. Finally, 650 RU of the tetrameric fusion protein were immobilized. Purified Bmh1 and Bmh2 were dialyzed overnight against 10 mM HEPES, 150 mM NaCl, 50 µM EDTA, 0.005 % (w/v) Tween20, pH 7.4. The flow cells were equilibrated with exactly the same buffer at RT. Measurements took place at a flow-rate of 20 µl/min at 25° C. The reference flow-cell was exposed to the same coupling procedure in the absence of any fusion protein and served as reference for background binding. Concentrations in the range of 11.7 nM to 750 nM of the purified protein have been used. The chip was regenerated in a 1.5 M $MgCl_2$ solution and washed extensively with the equilibration buffer (see above). The binding parameters were analyzed with the BIAevaluate 3.0 software (Biacore) using the 1:1 binding (Langmuir) fitting protocol under the assumption that 14-3-3 proteins were present in the dimeric form. Consistent with this assumption both purified 14-3-3 proteins migrated as dimers when subjected to blue native gel electrophoresis.

3.2.6 *In vitro* COPII budding assay

ER enriched membranes (microsomes) of yeast strains were purified as described in 3.2.2.3. Microsomes were adjusted to equal total protein concentrations by dilution in B88 buffer (concentration used: 10 µg/µl). A typical COPII budding assay was setup as follows:

Microsomes	Cytosol	Sar1	GTPγS / GDP	ATP reg. system	B88
7 µl	1 µl	-	-	-	42 µl
7 µl	1 µl	1 µl	10 µl	10 µl	21 µl

Yeast cytosol (20 µg of total protein per reaction), purified Sar1 (100 ng per reaction), GTPγS (2 mM end concentration) and ATP regeneration system (Baker et al, 1988) were prepared in B88 buffer. Only fresh reagents were used.

Microsomes were incubated for 30 min at 30°C. The budding reaction was stopped by transferring microsomes to ice for 5 min and formed vesicles were separated by low speed centrifugation (5 min at 13,000 rpm at 4°C). After this, vesicles were collected by a high-speed spin (30 min at 35,000 rpm, TLA55 rotor at 4°C). The pellet was resuspended in 30 µl of SDS loading buffer and protein content on sedimented vesicles was analysed by SDS-PAGE and Western blotting.

4. Results

4.1 Purification of untagged 14-3-3 proteins and antibody production

To investigate mechanistic details of the isoform specific role of 14-3-3 proteins in the forward transport of multimeric membrane proteins biochemical methods need to be applied. Quantitative studies of protein-protein interactions require substantial amounts of purified proteins. Biochemical studies, as well as microscopy studies rely on functional antibodies. For this reason, the first aim of this work was to establish a method to purify 14-3-3 proteins, followed by the intention to produce an antibody, that specifically recognises yeast 14-3-3 isoforms Bmh1 and Bmh2.

The previously described binding of 14-3-3 proteins to Arg based motifs raised the idea to use this protein-protein interaction for purification of untagged 14-3-3 proteins instead of affinity tags fused to the protein (see Yuan et al., 2003). Therefore, a construct created by Yuan et al., where the last 36 amino acids of the distal C-terminus of the K_{ATP} channel subunit Kir6.2 (ccKir6.2) were fused to a mutated tetramerizing version of the GCN4 leucine zipper, pLI (see Harbury et al., 1993) and the affinity tag protein A (see Yuan et al., 2003) was immobilised on IgG sepharose. 14-3-3 proteins were over expressed in bacterial cells and the cleared cell lysate was incubated with immobilised ccKir6.2 (see cartoon in Fig. 10). Presentation of the Arg based motif in the Kir6.2 tail in a multimeric fashion strongly increases the binding affinity to 14-3-3 (see Yuan et al., 2003). High salt buffer abolishes the protein-protein interaction and was used for elution. High amounts of untagged 14-3-3 isoforms could be obtained (see Fig. 11 A and B as an example for 14-3-3 Bmh1 and Bmh2). All seven mammalian isoforms as well as both yeast isoforms Bmh1 and Bmh2 could be purified using this strategy.

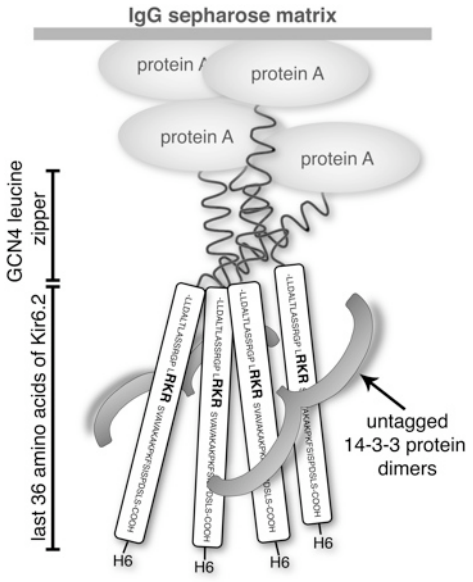

Figure 10: Cartoon of the purification of untagged 14-3-3 proteins from bacterial lysates.

The last 36 amino acids of the distal C-terminus of the K_{ATP} channel subunit Kir6.2 (ccKir6.2) were fused to a mutated version of the GCN4 leucine zipper, pLI (see Harbury et al., 1993) and the affinity tag protein A (see Yuan et al., 2003). The tetrameric presentation of the Arg based motif present in Kir6.2 resulted in a strongly enhanced binding to 14-3-3 proteins and enabled purification of untagged 14-3-3 isoforms.

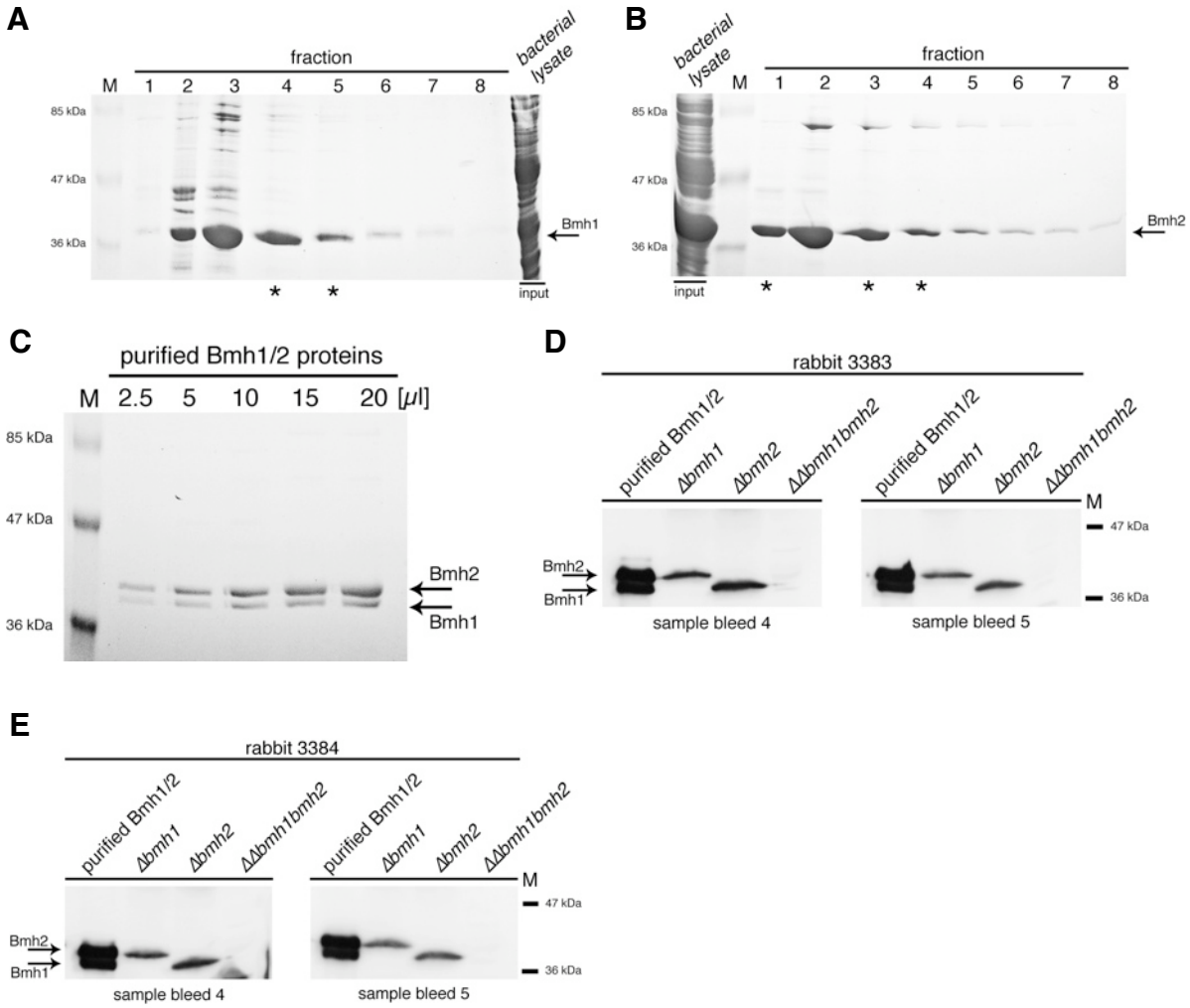

Figure 11: Antibody production employing purified 14-3-3 Bmh1 and Bmh2 proteins.

(A) Typical Coomassie stained SDS-PAGE gel of purified yeast 14-3-3 Bmh1.
1L of bacterial culture was grown to an OD_{600}=0.8 and IPTG induced for 2 h. The bacterial lysate was ultracentrifuged and cleared using a two step ammonium phosphate precipitation. The resulting pellet was resuspended in binding buffer and loaded on the saturated IgG sepharose column containing ccKir6.2.
Elution was performed using high salt (1.5 M $MgCl_2$). Fractions of 1 ml were collected and 10 µl of each fraction were loaded in each lane. The average protein concentration was approx. 1 µg/µl.
Asteriks mark fractions used for antibody raising.

(B) Typical Coomassie stained SDS-PAGE gel of purified yeast 14-3-3 Bmh2 (see (A) for details).

(C) Increasing amounts of purified and pooled 14-3-3 Bmh1 and Bmh2 proteins were loaded on a 10% SDS gel and Coomassie stained.
2.5 µl to 20 µl were taken from protein solution that was used for raising an antibody directed against Bmh1/Bmh2. Total volume of Bmh1/Bmh2 protein solution was 11 ml with a protein concentration of approx. 1 µg/µl.

(D) Test of serum 3383: Both yeast 14-3-3 isoforms could be detected by Western blot analysis of a purified protein mix using sample bleed 4 and 5. A serum dilution of 1:500 was used. 170 ng of Bmh1/Bmh2 protein mix and 5 µl cytosol from single and double knockout strains (150 µg total protein) were loaded in each lane.

(E) Test of serum 3384: Both yeast 14-3-3 isoforms could be detected by Western blot analysis of yeast cytosol by using sample bleed 4 and 5. A serum dilution of 1:500 was used. 170 ng of Bmh1/Bmh2 protein mix and 5 µl cytosol from single and double knockout strains (150 µg total protein) were loaded in each lane.

For the purpose of producing an antibody that recognises yeast 14-3-3 isoforms, purified Bmh1 and Bmh2 were pooled to a total volume of 11 ml with a concentration of approximately 1 µg/µl (see Fig. 11 C). The protein solution was sent out to EUROGENTEC (Belgium) to run an immunisation program in rabbits. The resulting anti-Bmh antiserum was tested in Western blot detection as shown in figure 11 D and E. Sample bleeds 4 and 5 of rabbits 3383 and 3384 were used. Two bands could be detected for the Bmh1/Bmh2 protein mixture. Only the upper Bmh2 band, or the lower Bmh1 band was detected in the according Δ*bmh1* or Δ*bmh2* single knockouts. No band was detected in the double-deletion strain Δ*bmh1*Δ*bmh2*. Hence the antiserum specifically labelled yeast 14-3-3 proteins Bmh1 and Bmh2. The same antiserum was also successfully used in immunofluorescence (see Fig. 21, chapter 4.5).

4.2 Abundance of 14-3-3 Bmh1 and Bmh2 as potential explanation for isoform specificity

As shown in Figure 3 only Bmh1 but not Bmh2 is able to promote forward transport of the tetrameric ccPmp2-reporter protein. Previously, the hypothesis of 14-3-3 proteins masking the COPI retrieval Arg-based motif has been formulated (Yuan et al., 2003). Based on this idea, several hypothesis were tested to explain the differential effect. One of them being the idea, that differences in copy number of the 14-3-3 isoforms create a situation *in vivo* where only one isoform is able to fulfil a productive function because it is present, whereas the other isoform is simply not abundant enough to provide the same degree of masking. Protein copy numbers have been previously suggested for yeast 14-3-3 proteins based on quantitative Western blotting of fusion proteins (Ghaemmaghami et al., 2003): 158,000 molecules per cell for Bmh1 and 47,600 molecules per cell for Bmh2. Since the number of proteins per cell for Bmh1 is more than three times higher than for Bmh2, the positive role of Bmh1 in ccPmp2 forward transport could be explained by differences in abundance. The loss of Bmh1 in a Δ*bmh1* strain could be more drastic than the loss of Bmh2 in a Δ*bmh2* strain.
To answer this question two methods have been tested to quantify 14-3-3 proteins in yeast.

4.2.1 Quantification of Bmh1 and Bmh2 using FACS

Fluorescence-activated cell sorting (FACS) enables screening and sorting of cells expressing proteins tagged with fluorescence markers. A C-terminally GFP tagged version of either Bmh1 or Bmh2 was overexpressed in a yeast wildtype strain using a p416 vector. The idea was to calibrate GFP fluorescence as a reporter of 14-3-3 levels, with the goal of investigating genomically tagged variants in individual knockout strains. For that reason 30,000 cells overexpressing GFP tagged versions of either Bmh1 or Bmh2 were sorted and the median value was determined (see Fig. 12 A-E and 13 A-E). In parallel, 2 mio GFP positive cells were sorted and collected for each isoform and 14-3-3 protein levels were obtained using quantitative Western blot analysis. Using precise amounts of the according purified, untagged 14-3-3 isoform, a standard curve was created and used for calculation of the amount of overexpressed GFP tagged 14-3-3 protein (see Fig. 12 F and 13 F).

Scanning for GFP positive cells resulted in median values for Bmh2-GFP that were twice as high as values for Bmh1-GFP, although protein amounts for the same number of scanned GFP positive cells were very similar (Bmh1: 6.5 ng/1 mio cells, Bmh2: 7.3 ng/1 mio cells). Conclusively, the amount of FACS scanned GFP did not correlate with expressed GFP tagged 14-3-3 proteins. However, one has to mention critically, that the GFP protein amount was out of range in the quantitative Western blot analyses (see Fig. 12 F and 13 F), showing that protein amounts should only be calculated while being in the range of the calibration curve. A disadvantage of the performed FACS measurements becomes clear when comparing the overexpressed Bmh2-GFP bands with the endogenously expressed Bmh2 (see Fig. 13 F). The amount of GFP tagged Bmh2 exceeded the endogenous Bmh2 amount by several times. Overexpression of 14-3-3 proteins however, leads to disorganisation of subcellular compartments (see Fig. 15 A). A controlled expression (by making use of the MET25 promoter in p416) or genomically tagged 14-3-3 proteins in single knockout strains would be a way to eliminate that problem. Still, the disadvantage of having GFP tagged proteins remains. The tag could obscure important parts of the 14-3-3 proteins and interfere with binding to other proteins. Therefore I decided to quantify endogenous levels of Bmh1 and Bmh2 in single knockout strains by quantitative Western blotting only. However, to obtain meaningful results I carefully calibrated the signal and quantified only bands well within the calibration curve (see next paragraph).

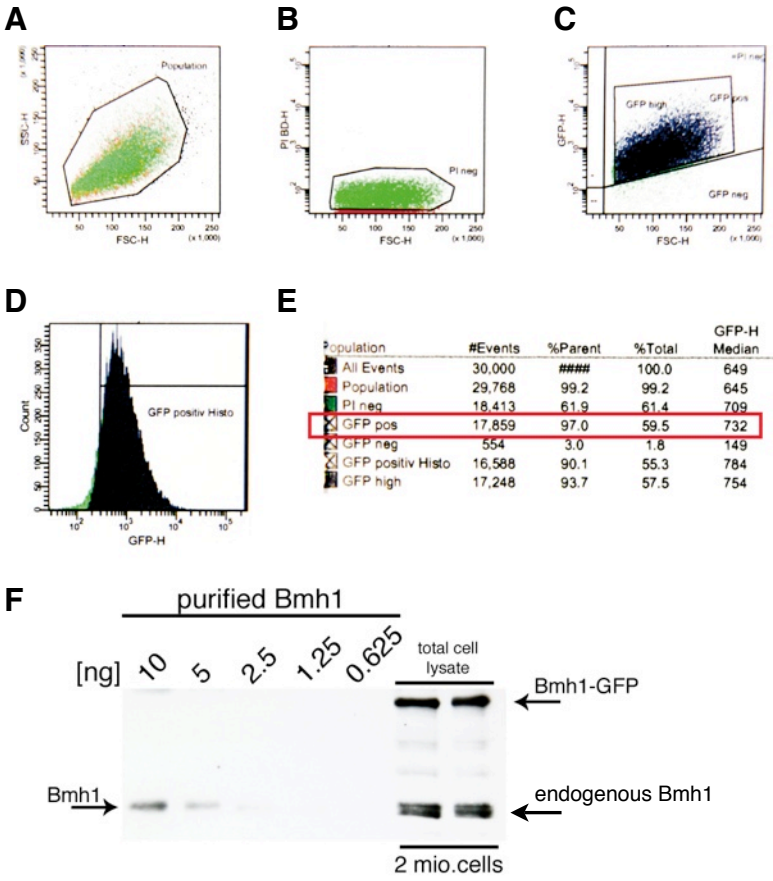

Figure 12: Comparison of FACS and quantitative Western Blot analysis to determine 14-3-3 Bmh1 protein copy numbers per cell.

Determination of GFP intensities for cells overexpressing Bmh1-GFP using FACS.

(A) Graph showing whole cell population of cells overexpressing Bmh1-GFP. X-axis shows forward scatter, which correlated with cell size. Y-axis shows side scatter with correlated with cell shape. Only cells of proper size and shape were selected.

(B) Graph showing selected cell population from (A) stained by PI to mark the nucleus of dead cells. X-axis shows cell size, Y-axis shows positive PI staining.
Only cells that were PI negative were selected.

(C) Graph showing selected cell population from (B). Cells were detected for GFP fluorescence. X-axis shows cell size, Y-axis shows GFP fluorescence.
Only cells that were GFP positive were selected.

(D) Histogramm showing selected cell population from (C). Cells were detected for GFP fluorescence. X-axis shows GFP fluorescence, Y-axis shows number of cells.
Only cells that were GFP positive were selected.

(E) Table summarizing the results for scanning 30,000 cells overexpressing Bmh1-GFP. The median value for GFP positive cells that passed the selected gates (see A, B, C and D) was 732.

(F) 2 mio. cells overexpressing Bmh1-GFP were sorted and collected using the criteria as described in A, B, C and D. Yeast cells were lysed and whole cell lysate was loaded on a SDS-PAGE gel, blotted and detected with anti-Bmh2 antibody. A standard curve was created using precisely defined amounts of purified Bmh1 protein and measuring the integrated signal of the protein bands using ImageJ software. The amount of overexpressed Bmh1-GFP protein was calculated using the information from the standard curve.

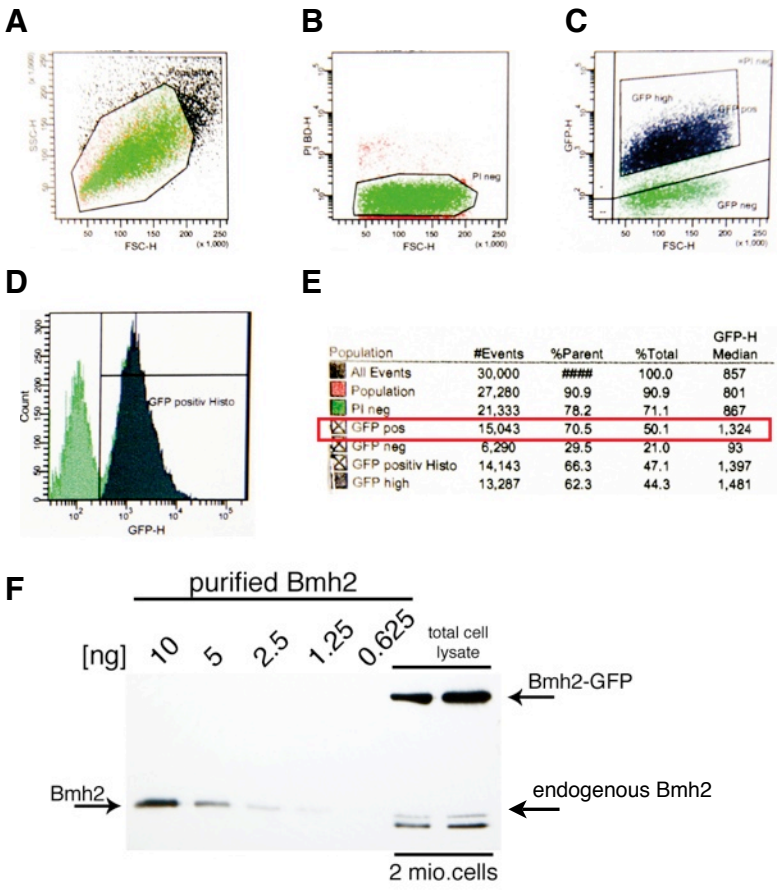

Figure 13: Comparison of FACS and quantitative Western Blot analysis to determine 14-3-3 Bmh2 protein copy numbers per cell.

Determination of GFP intensities for cells overexpressing Bmh2-GFP using FACS.

(A) Graph showing whole cell population of cells overexpressing Bmh2-GFP. X-axis shows forward scatter, which correlated with cell size. Y-axis shows side scatter with correlated with cell shape. Only cells of proper size and shape were selected.

(B), (C) and (D): See description of Figure 12 for more details.

(E) Table summarizing the results for scanning 30,000 cells overexpressing Bmh2-GFP. The median value for GFP positive cells that passed the selected gates (see A, B, C and D) was 1,324.

(F) 2 mio. cells overexpressing Bmh2-GFP were sorted and collected using the criteria as described in A, B, C and D. Yeast cells were lysed and whole cell lysate was loaded on a SDS-PAGE gel, blotted and detected with anti-Bmh2 antibody. A standard curve was created using precisely defined amounts of purified Bmh2 protein and measuring the integrated signal of the protein bands using ImageJ software. The amount of overexpressed Bmh2-GFP protein was calculated using the information from the standard curve.

4.2.2 Quantification of endogenous 14-3-3 proteins

According to Ghaemmaghami and colleagues loss of Bmh1 in the *Δbmh1* strain would reduce total 14-3-3 levels by two-third. However, 14-3-3 proteins are essential and the cell may counter regulate by increased expression of the remaining isoform.

To clarify to what extent the loss of the more abundant isoform Bmh1 reduces total amount of 14-3-3s in the Δ*bmh1* strain and whether the remaining Bmh2 was drastically less abundant, 10^6 yeast cells from either wildtype, Δ*bmh1* or Δ*bmh2* strains were collected by FACS and whole cell lysates were analysed by Western blotting and detected with anti-Bmh2 antiserum (van Heusden et al., 1995). Using defined amounts of purified Bmh1 or Bmh2 a calibration curve was obtained and protein copies per cell could be calculated by analysing the integrated

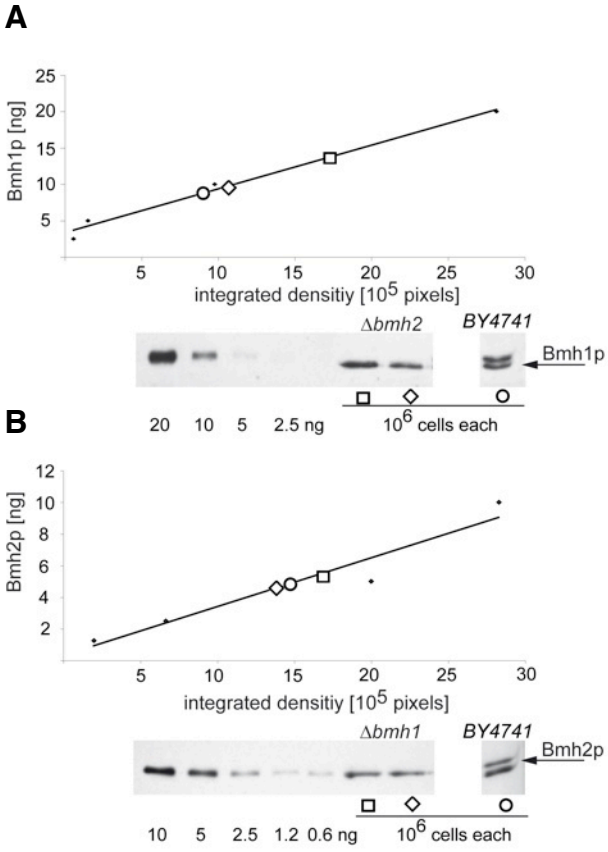

Figure 14: Quantification of endogenous Bmh1 and Bmh2 proteins in single knockout strains.

(A) Quantification of 14-3-3 Bmh1.
10^6 cells expressing only 14-3-3 Bmh1 but not Bmh2 were sorted and collected using the criteria as described in figure 3 (A) and (B). Yeast cells were lysed and whole cell lysate was loaded on a SDS-PAGE gel, blotted and detected with anti-Bmh2 antibody (van Heusden et al., 1995). A standard curve was created using precisely defined amounts of either purified Bmh1 or Bmh2 protein and measuring the integrated signal of the protein bands using ImageJ software. The amount of expressed Bmh1 or Bmh2 protein was calculated using the information from the standard curve.

(B) Quantification of 14-3-3 Bmh2: Details as in (A).

density of the protein bands using image analysis software (see Fig. 14). Measurements resulted in 133,000 (± 16,000; SEM; n=4) copies per cell for Bmh1 and 58,000 (± 19,000; SEM; n=3) copies per cell for Bmh2 in a wildtype strain. Both numbers are very comparable to Ghaemmaghami et al. Interestingly, copy numbers for both isoforms were strongly upregulated in single knockout strains: 214,000 (± 22,000; SEM; n=4, upregulation of 27%)

A

	Bmh1	Bmh2
in EuWTa	168,000 (+/- 37,000)	62,000 (+/- 19,000)
Ghaemmaghami et al.	158,000	47,600
in single KO's	214,000 (+/- 22,000)	86,000 (+/- 1,500)
upregulation	27%	38%

B

14-3-3 dimer	Bmh1/Bmh1	Bmh1/Bmh2	Bmh2/Bmh2
percentage	54%	39%	7%
in EuWTa	62,200	44,400	8,400
in single KO's	107,000	-	43,000
increase in homo dimers	80%	-	412%

Table 3: Yeast 14-3-3 isoforms are upregulated in single knockout strains.

(A) Summary of yeast 14-3-3 protein copies per cell in a wildtype strain (EuWTa) and single 14-3-3 knockout strains. See description of Figure 14 (A) for more detail. Numbers are derived from 5 (in EuWTa) and 4 (in *Δbmh2*) measurements for Bmh1 and 3 (in EuWTa and *Δbmh1*) measurements for Bmh2. Standard error is given in brackets. The resulting difference in copy numbers per cell between wildtype and single knockout strains is given in percent.

(B) Calculation of total number of homo- and hetero-14-3-3 dimers in wildtype and single knockout strains. The number of Bmh2 homodimers increases by 412% compared to wildtype, whereas the number of Bmh1 homodimers increases only by 80%.
Calculations were done according to the following equation (see Steinmeyer et al., 1994): $N_{H1/H2} = n_{H1/H2} / k(1+a)^{k-1}$, with N being the total number of Bmh1 or Bmh2 homo dimers, n being the total number of Bmh1 or Bmh2 subunits, a the ratio of n_{H2}/n_{H1} for Bmh1 homo dimers and n_{H1}/n_{H2} for Bmh2 homo dimers and k the number of subunits (here two).

copies per cell for Bmh1 in the *Δbmh2* strain and 93,000 (±1,900; SEM; n=2, upregulation of 38%) copies per cell for Bmh2 in the *Δbmh1* strain, suggesting a general functional compensation of one isoform for the other (see Table 3 A).

Isoform specific effects of Bmh1 and Bmh2 have been reported in several studies (Gelperin et al., 1995; Roth et al., 1999; Demmel et al., 2008). However, it is unclear whether the demonstrated effects are due to a change in total 14-3-3 copy numbers, or loss of heterodimers, or even increase of specific homodimers. My data allows the estimation of the respective dimer populations in the Δ*bmh1* and Δ*bmh2* single knockout strains as opposed to the wildtype (see Table 3 B). It is worth keeping in mind for the interpretation of further experiments, that Bmh2/Bmh2 homodimers represent a very rare species in wildtype cells (7% of all 14-3-3 dimers), but are more than four-fold abundant in a Δ*bmh1* strain (upregulation 412% in comparison to wildtype). Despite the upregulation of Bmh2/Bmh2

homodimers there was still only ~37% of the total amount of 14-3-3 dimers present in a Δ*bmh1* strain in comparison to wildtype.

Still, the difference in protein copy numbers between Bmh1 and Bmh2 was two-fold. To address the question, if overexpression of Bmh2 will rescue the defect in forward transport of ccPmp2 in the Δ*bmh1* strain, microscopy studies with highly overexpressed Bmh2 in the Δ*bmh1* background have been performed (see Fig. 15). Despite Bmh2 being present at a copy number of approximately 261,000 (± 9,600; SEM; n=8) proteins per cell, no forward transport of the multimeric reporter protein could be observed. In contrast, ccPmp2 strongly accumulated in the ER of the cell. Notably, the morphology of the ER was disturbed as a consequence of Bmh2 overexpression.

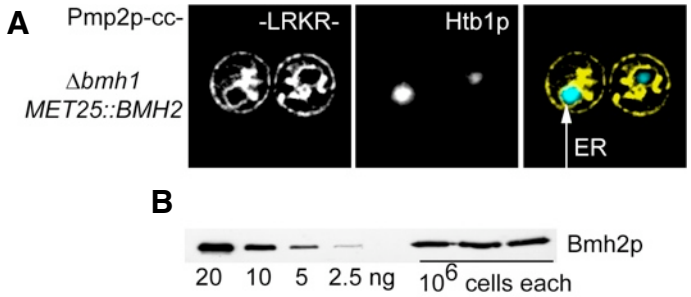

Figure 15: 14-3-3 Bmh2 overexpression does not rescue the defect in forward transport of the *Δbmh1* strain.

(A) Localization of the ccKir6.2 reporter in the *Δbmh1* MET25::BMH2 background.
Fluorescence life cell imaging using a GFP labeled tetrameric Pmp2 reporter protein (ccKir6.2).
The nucleus was marked using a Histone marker, perinuclear ER was highlighted with an arrow.
Despite the overexpression of the Bmh2 isoform the tetrameric ccKir6.2 reporter protein is not able to leave the ER efficiently.
(Microscopy performed by K. Michelsen)

(B) Quantification of 14-3-3 Bmh2 in the *Δbmh1* MET25::BMH2 background.
See text for corresponding statistics. For detailed description see Figure 14 (B).

4.3 Dimerization of 14-3-3 proteins *in vitro*

A major feature of 14-3-3 proteins is their ability to dimerize via highly conserved N-terminal regions (Rittinger et al., 1999) by interactions of their first four alpha helices αA-αD (Xiao et al., 1995, Liu et al., 1995). This allows 14-3-3 proteins to act as scaffolding proteins or to recruit additional proteins (Mrowiec and Schwappach, 2006). In other words, some proposed 14-3-3 mechanisms require dimerization. Since the possibilty to form heterodimers was shown for 14-3-3 isoforms (Jones et al., 1995), I asked if the yeast Bmh1 and Bmh2 isoforms can form stable homodimers in Δ*bmh1* or Δ*bmh2* single knockout strains. Blue Native Gel electrophoresis (BN-PAGE) was applied to answer this question. Since proteins are resolved in their native state, this method can reveal the ratio between proteins being in monomeric state versus proteins be present in multimerized state. Previously purified, untagged 14-3-3

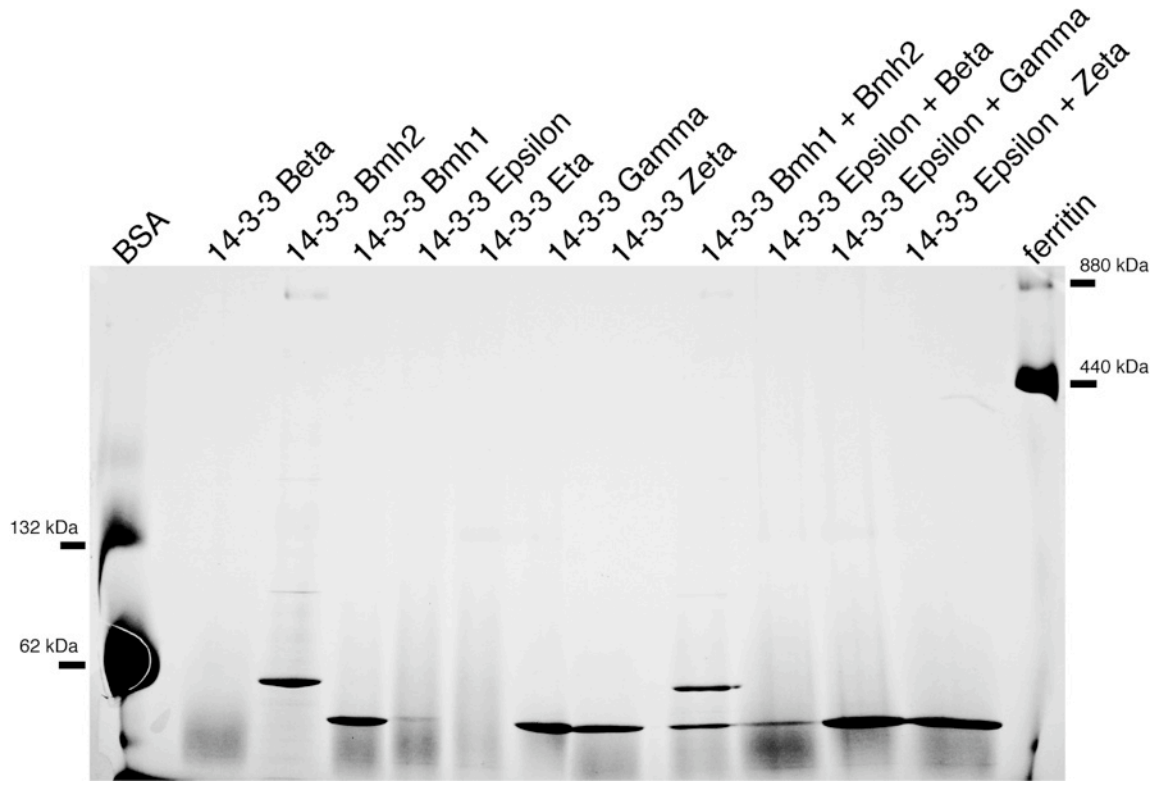

Figure 16: Both 14-3-3 Bmh1 and Bmh2 form homodimers with similar efficiency.

20 µg of untagged 14-3-3 isoforms were seperated by Blue Native polyacrylamide gel electrophoresis. A 5-18% gradient gel was used. All isoforms (except Beta, Epsilon and Eta) show a sharp protein band at the height of ~60 kDa, which fits the size of 14-3-3 dimers.
To check for heterodimerization two different 14-3-3 isoforms were combined in HEPES, pH 7.4 buffer and incubated for 1 h at 4°C. No additional bands could be observed by mixing two different 14-3-3 isoforms.

isoforms were separated on BN-PAGE using a 5-18% gradient gel and Coomassie stained (see Fig. 16). To investigate heterodimerization, different isoforms were mixed and incubated for 1 h at 4 ºC. As shown in Figure 16 all 14-3-3 proteins migrated at a height of approximately 60 kDa, suggesting that all 14-3-3 proteins ran as homodimers (monomer size is ~30 kDa). Mixed 14-3-3 proteins ran at the same height as the putative homodimers. No additional bands could be identified in case of mixing Bmh1 and Bmh2, showing that no exchange of yeast isoforms occurred in the time of 1 h at 4 ºC.

The fact that Bmh1 and Bmh2 form equally stable homodimers as detected by this assay, suggests that it is not the instability of the Bmh2/Bmh2 homodimer that causes defective forward transport in the Δ*bmh1* strain.

4.4 Characterization of binding parameters between yeast 14-3-3s and the tetrameric Kir6.2 tail fusion protein

4.4.1 Quantitative measurements *in vitro*

So far, two possible explanations for the observed isoform specificity (see Fig. 3) could be eliminated. First, overexpression of Bmh2 could not rescue the inability of the tetrameric reporter protein ccPmp2 to leave the ER in a Δ*bmh1* strain. Consequentially, the difference in abundance of yeast 14-3-3 isoforms is not valid as an hypothesis. Secondly, no difference in the ability of Bmh1 and Bmh2 to form dimers could be observed. Suggesting that it is not the lower Bmh2/Bmh2 homodimer stability, that causes the effect. A third hypothesis invokes subtle differences in binding affinity between the tetrameric tail and the respective 14-3-3 isoform. Two different *in vitro* methods have been applied to test for quantitative differences in binding of the yeast 14-3-3 isoforms to the tetrameric reporter protein. Using the protein, that I purified (see chapter 4.1) Isothermal titration calorimetry (ITC) was performed by Karl Duderstadt (UCSF) to obtain binding parameters for Bmh2 to the monomeric and the tetrameric reporter. Since no interaction could be observed for the monomeric tail of Kir6.2 we concluded, that no binding of 14-3-3 occurred. This result underscores the observation that 14-3-3 proteins bind the multimerized Kir6.2 tail with much higher affinity than the monomeric tail (see Fig. 6C in Yuan et al., 2003). In contrast, binding of Bmh2 to the

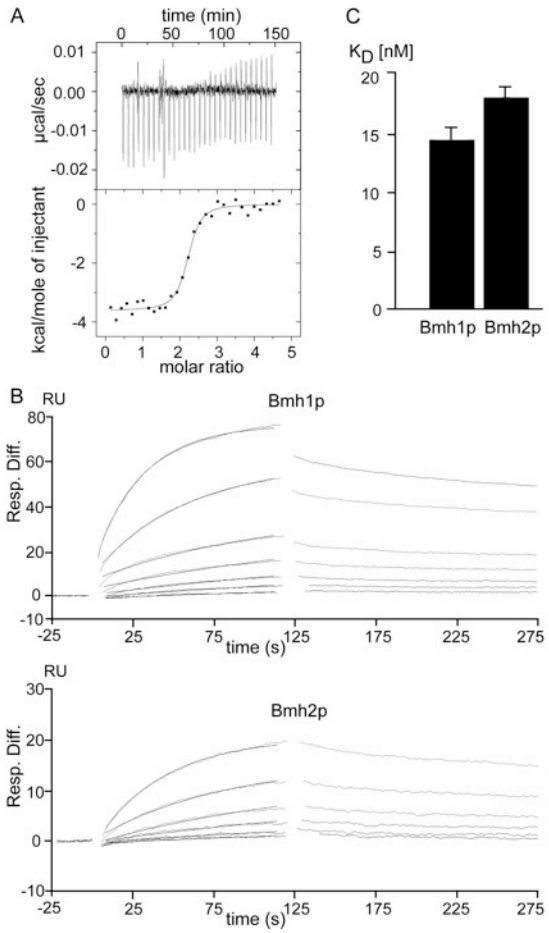

Figure 17: 14-3-3 proteins bind the tetrameric ccKir6.2 tail with similar affinities *in vitro.*

In vitro quantification of binding parameters between yeast 14-3-3 proteins and the tetrameric Kir6.2 tail fusion proteins.

(A) Using isothermal titration calorimetry: Binding curve for the interaction of Bmh2 with the tetrameric Kir6.2 tail (performed by Karl Duderstadt at UCSF).

(B) Using surface plasmon resonance: Binding curves of 14-3-3 Bmh1 and Bmh2 to the tetrameric Kir6.2 tail. 650 RU of the protein A-ccKir6.2 fusion protein were immobilized to the CM5 Chip (Biacore) using the N-hydroxysuccinimide/N-ethyl-N'-(3-dimethyl-aminopropyl) carbodiimide hydrochloride (NHS/EDC) method. Measurements were performed at a flow-rate of 20 µl/min at 25° C. The chip was regenerated with 1.5 M $MgCl_2$ buffer.
Curves for protein concentrations 11.7 nM to 750 nM are shown. X-axis show time, Y-axis show bound protein in Response Units (RU). Association and dissociation phases are displayed.
Data was analyzed with BIAevaluate 3.0 software (Biacore) using a 1:1 binding (Langmuir) fitting protocol.

(C) Summary of binding affinities for both 14-3-3 isoforms to the ccKir6.2 tail. Dissociation constants (K_D values) from (B) are shown as graphs.

tetrameric tail was well detectable (see Fig. 17 A). Fitting the results to a 1:1 binding curve gave a dissociation constant of K_D=6.2 nM. To confirm the results from ITC, the interaction was investigated using surface plasmon resonance (SPR) as a second method. The protein A-ccKir6.2 fusion protein was immobilized on the surface of an CM5 Chip (Biacore) by chemical crosslinking (NHS/EDC method). Defined concentrations of untagged Bmh2 protein (11.7-750 nM) were used to obtain binding curves which could be fitted to a 1:1 (Langmuir) binding model (see Fig. 17 B). The resulting dissociation constant was 17.4 nM (+/- 0.8 nM; SEM). Since both methods delivered K_D in the same order of magnitude, SPR was chosen to measure binding of Bmh1 to the tetrameric Kir6.2 fusion protein. Same concentrations and the same analyses were used to finally obtain a K_D value of 13.8 nM (+/- 1.2 nM; SEM) for the binding of Bmh1 to the tetrameric tail (see Fig. 17 B and C). Comparing the dissociation constants for Bmh1(13.8 nM (+/- 1.2 nM; SEM)) and Bmh2 (17.4 nM (+/- 0.8 nM; SEM)) the differences between both isoforms were too small to account for the differences observed for the localization of the ccPmp2 reporter *in vivo*.

4.4.2 14-3-3 Bmh1 and Bmh2 interact with the multimeric Pmp2-LRKR *in vivo*

No difference in binding affinities of the yeast 14-3-3 isoforms to the tetrameric protein A-ccKir6.2 fusion protein could be detected *in vitro*. To test whether this is also true for the interactions *in vivo*, co-immunoprecipitation experiments have been performed (by K. Michelsen) from yeast cell extract. First of all, monomeric and tetrameric Pmp2-LRKR fusion protein was immunoprecipitated from a yeast wildtype strain and resulting Western blots were detected with an antibody recognising 14-3-3 proteins. Both yeast isoforms could be found to interact with the reporter fusion protein (see Fig. 18 A). As clearly shown in Figure 18 A, much more 14-3-3 proteins could be immunoprecipitated using the multimerized reporter, although the total protein amount used was less. Comparable amounts of reporter fusion protein were immunoprecipitated as shown in the blot detected with anti-6.2 antibody. Quantification of the 14-3-3 bands from three independent experiments resulted in very similar degrees of binding for both 14-3-3 isoforms to the tetrameric reporter (Fig. 18 B black bars) as well as the monomeric reporter fusion protein and underscore the low affinity of both 14-3-3 proteins to the monomeric version (Fig. 18 B grey bars). To furthermore investigate, if Bmh1 and Bmh2 bind the ccPmp2 reporter with similar affinities, co-IPs in the presence of only one isoform were done. Very comparable amounts of either Bmh1 (from Δ*bmh2* strain) or Bmh2 (from Δ*bmh1* strain) were co-immunoprecipitated with the tetrameric reporter (Figure 18 C).

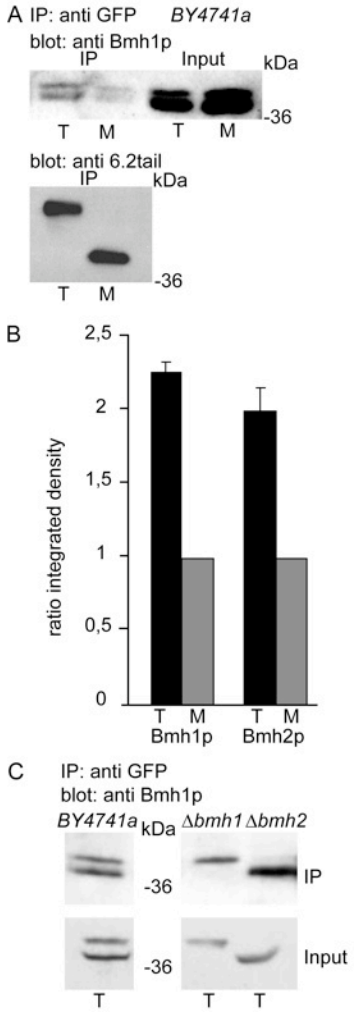

Figure 18: 14-3-3 Bmh1 and Bmh2 proteins recognize the tetrameric Pmp2-cc-LRKR reporter with similar affinities *in vivo.*

(A) Co-immunoprecipitates obtained by immunoprecipitation of the tetrameric (T) or monomeric (M) Pmp2 reporter fused to the tail of Kir6.2. Anti-Bmh blot identifies co-immunoprecipitated 14-3-3 proteins, 2% of the input is shown to demonstrate equal amounts of 14-3-3 proteins in the cellular lysates. Anti-Kir6.2-tail blot controls for comparable enrichment of the two reporter membrane proteins.
(co-IPs performed by K. Michelsen)

(B) Densitometric analysis of three independent experiments of which the blots shown in (A) are representative. Values are normalized to the signals obtained for the monomer.

(C) Co-immunoprecipitates obtained by immunoprecipitation of the tetrameric (T) from lysates of the individual 14-3-3 deletion strains. Anti-Bmh blot identifies the 14-3-3 proteins co-immunoprecipitated with the membrane protein.

Taking quantitative *in vitro* and qualitative *in vivo* experiments together, both yeast isoforms bind the ccPmp2 reporter protein with same affinities *in vitro* and *in vivo*. Consequentially, the observed isoform specificity can not be explained by simple differences in binding.

4.5 Localization of yeast 14-3-3 proteins in the cell

The isoform specific role of yeast 14-3-3 proteins in the forward transport of the ccPmp2 reporter could not be explained by differences in 14-3-3 protein copy numbers, nor by differences in binding affinities to the multimeric reporter protein. To test whether the route of the reporter protein to the cell surface (for the monomeric reporter protein) or the vacuole (for the tetrameric version) involves packaging into COPII vesicles at ER exit sites, I transformed the tetrameric reporter into *sec23-1* strain. This strain normally expresses the COPII component Sec23 under permissive temperature (25 ºC), but switching to the restrictive temperature (30 ºC or 37 ºC) leads to degradation of Sec23. As shown in Figure 19, the tetrameric ccPmp2-LRKR reporter protein localizes to the vacuole in the presence of Sec23

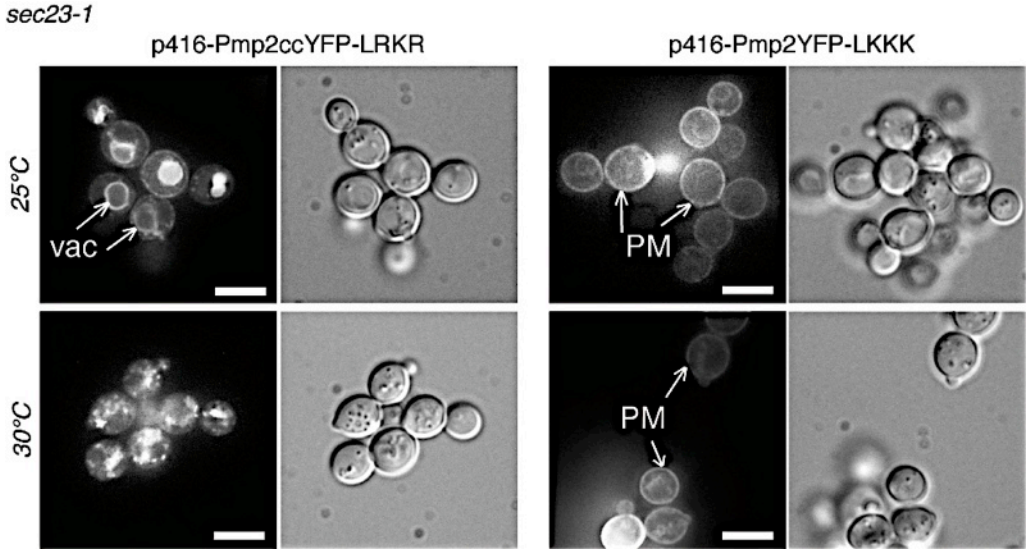

Figure 19: The Pmp2cc-YFP-LRKR reporter travels via COPII vesicles to the vacuole.

Subcellular localization of (1) tetrameric Pmp2 reporter fused to YFP and the LRKR containig tail. (left panel). (2) monomeric Pmp2 reporter fused to YFP and an inactive LKKK mutant of the tail (right panel). This mutant is not recognized by COPI and thus constitutively leaves the ER.
Growth of the temperature sensitive *sec23-1* strain at permissive temperature (25 ºC) , meaning Sec23 presece, leads to export of the tetrameric Pmp2-LRKR reporter to the vacuole (vac) and export of the monomeric Pmp2-LKKK o the plasma membrane (PM). Switching to the restrictive temperature (30 ºC), meaning no Sec23 present, lead to accumulation of the tetrameric Pmp2-LRKR reporter in the ER, whereas the mutated, monomeric version still localized to the plasma membrane (indicating that general protein transport is not massively altered).
Scale bar is 5 μm.

under permissive temperature (Fig. 19, 25 ºC panel). However, switching to the restrictive temperature, meaning Sec23 being degraded, inhibited forward transport of the reporter protein (Fig. 19, 30 ºC panel). To exclude a drastic general effect on all cargo, a monomeric version of the Kir6.2 tail, where the Arg-based LRKR motif has been mutated to LKKK was used (see Fig. 19, right panel). This mutation prevents COPI binding to the tail, thus inhibiting retrograde transport back to the ER. In contrast to the LRKR-containing tetrameric reporter fusion protein, Pmp2YFP-LKKK export to the plasma membrane is not affected by switching to restrictive temperature, suggesting that general trafficking was not harmed (Fig. 19, 30 ºC panel on the right). This result shows that LRKR-reporter trafficking depends on functional COPII transport. Therefore, local availability of one 14-3-3 isoform, but not the other, at ER exit sites could have drastic influence on transport of the reporter protein. For this reason, localization of both yeast 14-3-3 proteins was investigated in the cytosol and in ER-enriched (microsomes) and Golgi-enriched membranes (see Fig. 20). In addition, subcellular localization studies of both isoforms were performed using indirect immunofluorescence (see Fig. 21).

Adjusted amounts of microsomes, cytosolic fractions and Golgi-enriched membranes from wildtype, Δ*bmh1* and Δ*bmh2* single knockout yeast strains were separated using SDS PAGE, blotted and detected with anti-Bmh serum. Both 14-3-3 isoforms are present at all three locations (Fig. 20). Furthermore, the ratio of Bmh1 to Bmh2 was always very comparable, suggesting that either isoform is excluded from specific compartments in the cell and both isoforms are ubiquitously present *in vivo*.

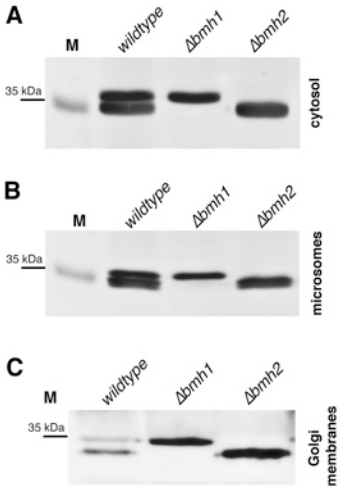

Figure 20: Yeast 14-3-3 isoforms are present in cytosol, in ER enriched membranes and in Golgi membranes in very similar ratios.

Distribution of yeast 14-3-3 isoforms in cellular compartments: (A) Cytosol (5 µl of a 1:10 dilution, 15 µg total protein), (B) ER enriched membranes (10 µl of a 1:10 dilution, 14 µg total protein) and Golgi membranes (25 µl of a 1:5 dilution, 17.5 µg total protein) from yeast wildtype and single knockout strains were seperated on a SDS PAGE gel electrophoresis, blotted and detected using the anti-Bmh serum produced in this work.

Immunofluorescence microscopy was used next to confirm the biochemical results. The big advantage of this method is, that it gives a global overview of protein localization instead of focussing on one specific compartment. The disadvantage is, that the observations are qualitative, whereas biochemical studies can be used to gain quantitative result. Using the

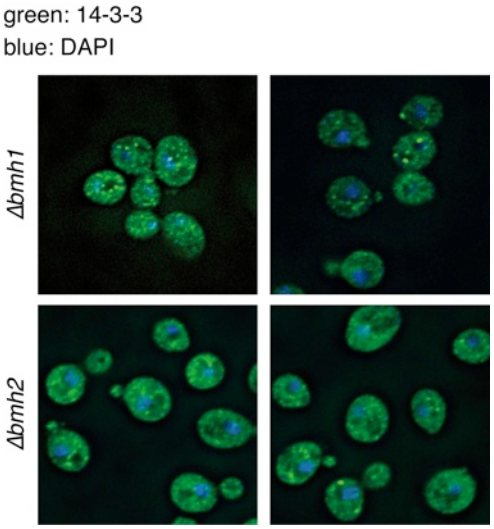

Figure 21: Yeast 14-3-3 isoforms localize differently in the cell.

Subcellular localization of yeast 14-3-3 proteins using immunostaining.

14-3-3 proteins were recognized using an anti-Bmh serum (1:2,000 dilution). Blue channel shows DAPI staining. Scale bar is 5 μm.

14-3-3 Bmh1 (in the *Δbmh2* strain) shows an equally distributed staining pattern. Bmh2 (in the *Δbmh1* strain) appears in some puncta and shows less diffuse staining than Bmh1.

anti-Bmh serum (1:2,000 dilution), that was produced in this study, Bmh1 as well as Bmh2 could be nicely recognized. In contrast to prior biochemical results, immunofluorescence microscopy showed a difference in the localization of Bmh1 and Bmh2. 14-3-3 Bmh1 was found to be distributed very uniformly in the cell, Bmh2 showed a less diffuse staining and appeared in some puncta (see Fig. 21). This result is consistent with data from Demmel et al. They observe a similar pattern for Bmh2 with a 13-myc tag. Unfortunately, the nature of the puncta could not be linked to ER related structures when various antibodies directed against ER and ER-exit-site proteins were employed (data not shown).

In summary, both yeast 14-3-3 proteins show a similar localization pattern in the cell. Both are present in the cytosol, in ER-enriched membranes and in Golgi membranes in comparable levels. However, it can not be excluded, that the punctuated appearance of Bmh2 as seen by immunostaining is linked to a isoform specific role in promoting forward transport of the ccPmp2 reporter.

Furthermore, the difference may not lie in the localization but the function of the two isoforms.

4.6 Search for putative isoform-specific 14-3-3 partners

4.6.1 Stepwise stripping of 14-3-3 proteins from microsomes

14-3-3 proteins can modulate protein-protein interactions in many ways. One possibility is the function of the dimeric 14-3-3s as scaffold proteins (see Mrowiec and Schwappach, 2006). Making use of their dimeric nature, they are able to recruit additional interaction partners via additional binding sites. Since no explanation for the described isoform specificity in promoting forward transport of the ccPmp2 reporter has been found yet, the possibility of additionally recruited and so far unknown isoform-specific interaction partners was investigated next.

Several hundred interactions have been described for 14-3-3 proteins (Pozuelo Rubio et al., 2004). Therefore, it makes sense to limit the interaction range to specific compartments, in this case the ER, to focus on the binding partners which may be involved in export of the

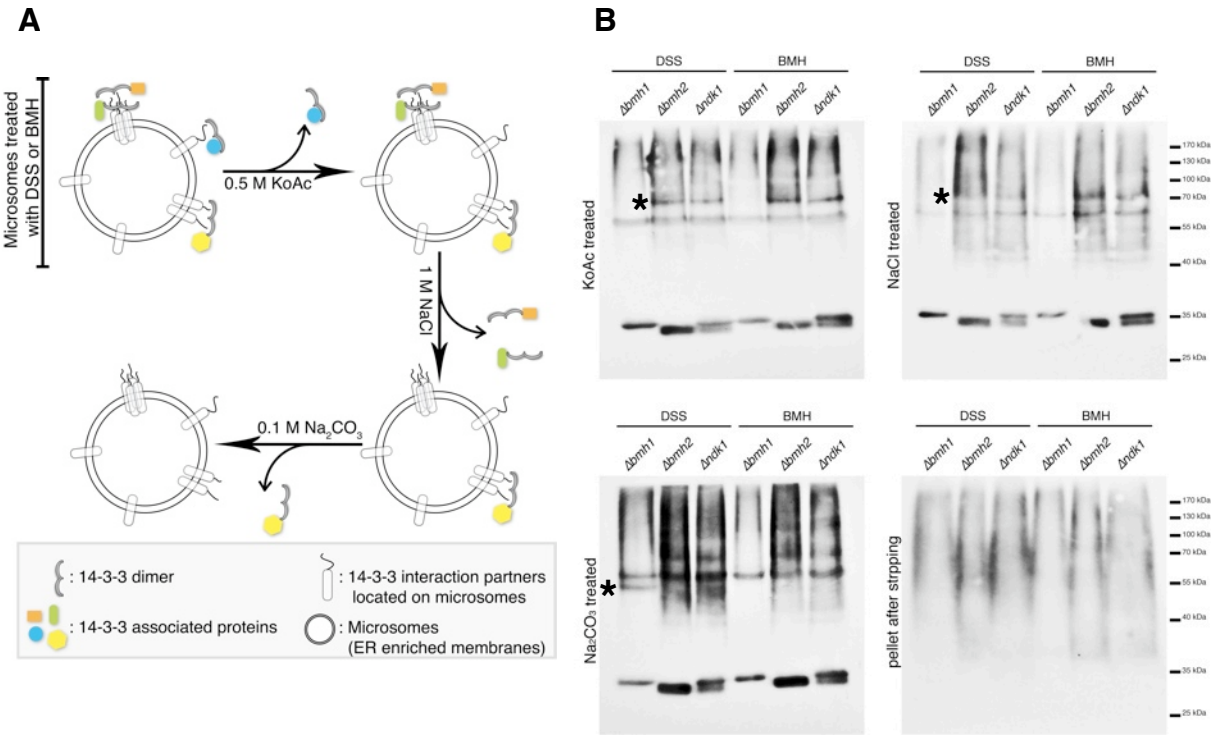

Figure 22: Search for putative isoform-specific 14-3-3 interaction partners by stepwise stripping of 14-3-3 proteins from ER enriched membranes: Three potentially differential bands could be identified.

(A) Cartoon of the procedure.

(B) Adjusted amounts (50 µg of total protein) of ER enriched membranes from *Δbmh1, Δbmh2 and Δndk1* knockout strains were treated with either DSS or BMH crosslink reagent. The samples were then consecutively processed with 0.5 M KoAc, 1 M NaCl and 0.1 M Na_2CO_3 reagents. TCA precipitats were loaded on a SDS PAGE gel, seperated, blotted and detected with an anti-Bmh serum (1:1,000 dilution).
Potentially differential bands are marked by asterisks.

reporter protein. A sequential stripping method was used to concentrate proteins dissociating from ER membranes under a given salt concentration. Microsomes (Wuestehube and Schekman, 1992) from three single knockout strains (Δ*bmh1*, Δ*bmh2* and Δ*ndk1*) were treated with two crosslinking reagents to fix 14-3-3 interactions to its partners. Disuccinimidyl suberate (DSS) crosslinks proteins by reacting with primary amines, bismaleimidohexane (BMH) creates disulphide bonds. After crosslinking, microsomes were incubated in 0.5 M KoAc, followed by treatment with 1 M NaCl and finally with 0.1 M Na_2CO_3 (Fig. 22 A). Proteins which came off after each step were collected and analyzed by SDS PAGE, Western blotting and immunodetection using the anti-Bmh serum. The final membrane pellet was used to check if all 14-3-3 proteins could be stripped from the membrane. A Δ*ndk1* strain was used as a control for both yeast 14-3-3 isoforms being present. As shown in Figure 22 B, three specific bands could be identified. They indicate soluble proteins, that were peripherally associated with the membrane in Δ*bmh2* microsomes (see asterisks in KoAc and NaCl treated gels in Figure 22 B), or with the membrane of Δ*bmh1* microsomes (see asterisks in Na_2CO_3 treated gel in Figure 22 B). All specific bands were only visible with DSS treated microsomes. The efficiency of the crosslink reaction can be judged by the remaining, not crosslinked 14-3-3 bands at the hight of ~30 kDa. Similar amounts of not-crosslinked Bmh1 and Bmh2 proteins could be stripped at all steps, showing, that not all 14-3-3 proteins could be crosslinked to their interaction partners. Either because necessary reaction groups were not available for the crosslink reagents or because a portion of 14-3-3 proteins was simply not protein bound.

4.6.2 Pulldown of putative interaction partners from yeast cytosol

Besides being present on ER membranes, 14-3-3 proteins are also present in the cytosol in high abundance (see Fig. 20 and 21). Most 14-3-3 interactions are thought to be cytosolic, for which reason an additional search for putative partners was performed with yeast cytosol.
14-3-3 Bmh1 or Bmh2 were immobilized using the same column as described in chapter 4.1. Yeast cytosol from a Δ*bmh1*Δ*bmh*2 double deletion strain was used to prevent possible monomer-monomer interactions between 14-3-3 proteins. After incubation and washing, proteins were eluted from the column with increasing concentrations of high salt buffer (from

100 mM to 1.5 M $MgCl_2$) and samples were separated by SDS PAGE gel electrophoresis (see Fig. 23 A). No specific bands for Bmh1 or Bmh2 could be identified in the pulldown (see Fig. 23 B). However, mass spectrometry analysis (performed by A. Bosserhof and T. Ruppert, ZMBH) of an enriched band at the height of ~85 kDa (marked by asterisk in Fig. 23 B) identified the protein as the COPII coat component Sec23. Assuming that our ccPmp2 reporter and the K_{ATP} subunit Kir6.2 leave the ER by COPII vesicles, having identified a component of the machinery as putative interaction partner was motivating. Especially, because an interaction of the yeast 14-3-3 isoforms and Sec23A and Sec23B from HeLa cell extract was previously described in the work of Pozuelo Rubio et al., 2004.

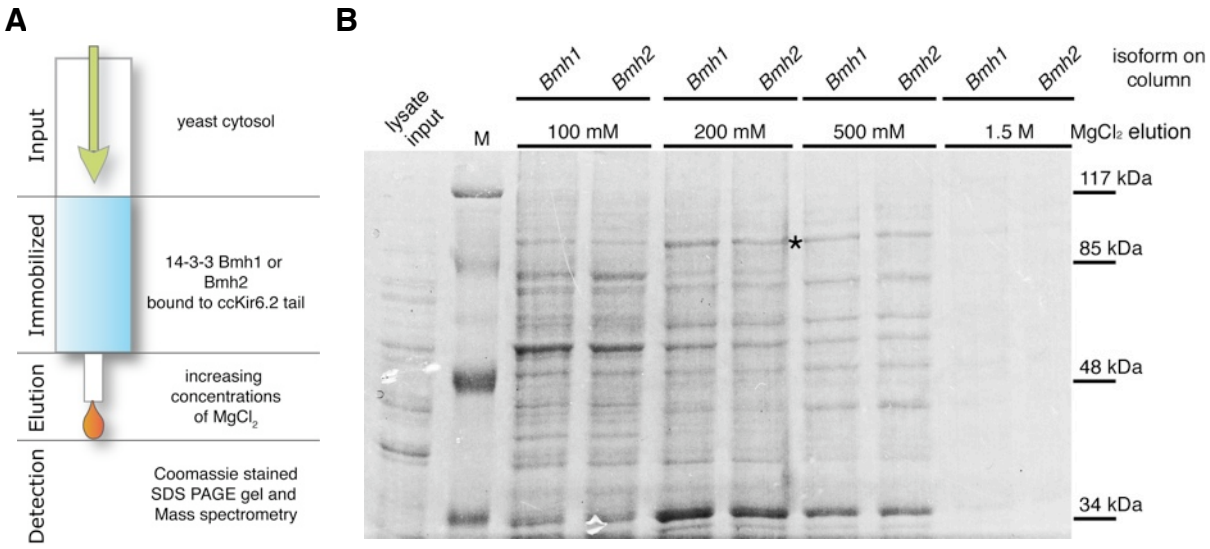

Figure 23: Search for 14-3-3 isoform-specific interaction partners employing purified immobilized Bmh1 and Bmh2: Both yeast 14-3-3 isoforms interact directly or indirectly with Sec23.

(A) Cartoon of the procedure.

(B) Purified 14-3-3 Bmh1 and Bmh2 proteins were immobilized on a IgG column that was saturated with protein A-ccKir6.2 fusion protein. The applied yeast cytosol was from a *Δbmh1Δbmh2* double deletion strain to prevent 14-3-3 monomer to monomer interactions. Yeast proteins were sequentially eluted with 1.5 M $MgCl_2$, seperated by a SDS PAGE gel electrophoresis and Coomassie stained. Asterisk marks a protein band at the height of ~85 kDa, which was identified by mass spectrometry (done by A. Bosserhof and T. Ruppert, ZMBH) as the COPII coat component Sec23.

4.6.3 Role of 14-3-3 - Sec23 interaction in ccPmp2 forward trafficking

14-3-3 proteins interact strongly with phosphorylated motifs which were classified as mode I, mode II and a newly discovered mode III motifs (see Yaffe et al., 1997; Coblitz et al., 2006 and Figure 24 A as a summary). First, it was tested whether the interaction of Bmh1 and

Bmh2 with Sec23 (as described by Pozuelo Rubio et al., 2004) was conserved in yeast. Although no classical interaction motifs could be identified in the yeast homolog, many 14-3-3 interacting proteins bind to variants of the canonical motifs, or even very different motifs (Yaffe et al., 2002). Therefore, the consensus sequence was relaxed and up to three residues preceding the required Proline were allowed. As a result, two highly conserved sequences were identified: A N-terminal sequence (RNSSWSCP) and a C-terminal sequence (RFLLSKLNP). To test if mutation of one or both putative 14-3-3 binding motifs affected trafficking of the multimeric reporter protein, either one or both essential Serines in the motifs were mutated to Asparagines. The mutants were then transformed into a temperature-sensitive *sec23-1* strain. This strain allows to control the stability of the temperature sensitive Sec23 protein by growth temperature. At permissive temperature (20 ºC) wildtype Sec23 protein is expressed, at restrictive temperature (30 ºC or 37 ºC) the wildtype protein is degraded. Expression of the two single mutants (S79N and S726N) as well as the combination of both supported the survival of the *sec23-1* strain at restrictive temperature (Fig. 25). This was particularly important to demonstrate, since the mutation in the C-terminal region could have severely interfered with the essential Sec23-Sar1 interaction and consequentially cell growth (see Bi et al., 2002).

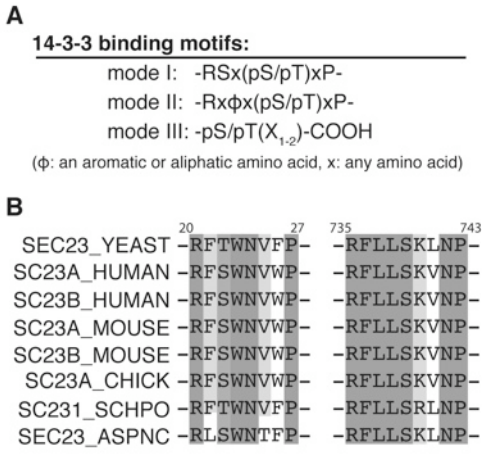

Figure 24: Two putative 14-3-3 binding motifs are highly conserved in Sec23 homologues.

(A) Classical 14-3-3 binding motifs derived from studies addressing the interaction of mammalian 14-3-3 proteins.
All three classical 14-3-3 binding motifs are phosphorylation dependent motifs.
Mode I and mode II binding motifs show Proline two amino acids C-terminal to the phosphorylated Serine or Threonine, mode III shows the phosphorylated Serine or Threonine one or two amino acids to C-terminus of the protein. There seems to be a preference for aromatic or aliphatic side chains in mode II.
Although strongly favoured, the amino acid distribution in the consensus sequences is not required for 14-3-3 binding. Many 14-3-3 binding sites differ from the classical binding motifs.

(B) Alignment of two putative 14-3-3 binding motifs in the N-terminus (RFTWNVFP) and in the highly conserved C-terminus (RFLLSKLNP) of Sec23 proteins.
The most important aspects of the 14-3-3 binding motifs are conserved: Arginine at position 1, Serine or Threonine that can be phosphorylated and Proline at the end of the motif.

But do the mutations specifically interfere with the transport of the tetrameric reporter protein? To answer this question the ccPmp2-YFP reporter was coexpressed with the Sec23

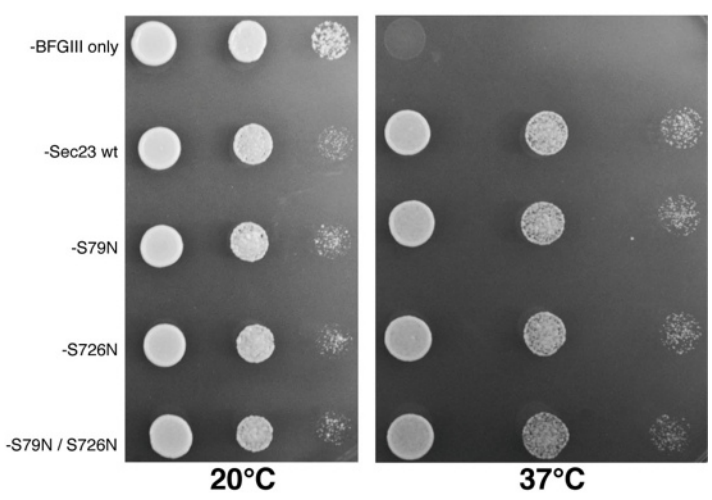

Figure 25: All Sec23 mutants with altered putative 14-3-3 interaction motifs support the survival of a temperature sensitive *sec23-1* strain at the restrictive temperature.

Growth of temperature-sensitive *sec23-1* strain transformed with different *SEC23* mutants. Cells were diluted to an OD_{600}=0.5 and diluted 1:10 and 1:100. 10 µl of each cell concentration was spotted on plates lacking Leucine and grown at permissive temperature (20 ºC) and restrictive temperature (37 ºC) for 3 days. The empty plasmid was used as negative control, a plasmid containing the wildtype *SEC23* was used as positive control.

mutant versions in the *sec23-1* strain and its localization was investigated by life cell imaging (Fig. 26).

In presence of the wildtype Sec23 protein (at 20 ºC) the reporter left the ER very efficiently as shown by the vacuolar staining in all strains (Fig. 26, upper panel). Switching to 30 ºC has a strong effect on all mutant expressing strains. Both strains expressing the single mutants (S79N and S726N) lost their exclusively vacuolar staining and the reporter could be partially

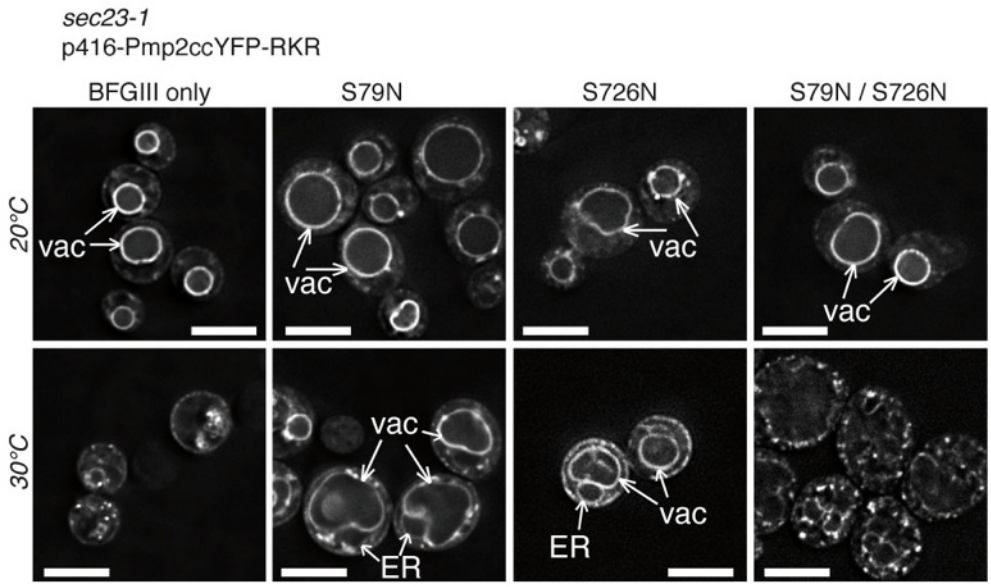

Figure 26: Mutations in the putative 14-3-3 binding sites of yeast Sec23 impair forward transport of the tetrameric Pmp2ccYFP reporter.

Fluorescent images of life cell imaging show the localization of the Pmp2ccYFP reporter in the absence (at 30 ºC - restrictive temperature) or presence (at 20 ºC - permissive temperature) of endogenous Sec23. The empty plasmid (BFGII only) was used as negative control.
Scale bar is 5 µm. Vacuole (vac) and ER (ER) are marked with arrows.

found in the ER as well (Fig. 26, 30 ºC panel for S79N and S726N). The effect seemed to be additive, since combination of both mutants led to total mislocalization of the reporter (see Fig. 26, 30 ºC panel for S79N/S726N).

Taken together, both 14-3-3 Bmh1 and Bmh2 were found to interact with Sec23 from yeast cytosol. Mutations in two putative binding regions in Sec23 supported cell growth but interfered with the transport of the ccPmp2 reporter *in vivo*. Combining both mutations led to strong accumulation of the reporter in bright, punctate structures.

4.6.4 Isoform specificity maps to the 14-3-3 C-termini

Yeast 14-3-3 isoforms Bmh1 and Bmh2 are 81% similar (see alignment in Fig. 27 A). It may therefore be surprising to see isoform specific differences between the two proteins. Main differences can be found in the distal C-termini (Fig. 27 A). To follow the idea that isoform specificity might map to the 14-3-3 C-termini, chimeric proteins were created by exchanging the last 69 amino acids of Bmh1 with the last 75 amino acids of Bmh2 and vice versa. This resulted in two 14-3-3 versions: (1) H1N2C: Bmh1 N-terminus with Bmh2 C-terminus and (2) H2N1C: Bmh2 N-terminus with Bmh1 C-terminus. The chimeric variants were coexpressed with the ccPmp2-YFP reporter protein in the background of a double deletion strain Δ*bmh1*Δ*bmh2*. In this strain Michelsen et al. showed an accumulation of the reporter in the ER due to the lack of 14-3-3 proteins (Michelsen et al., 2006). First, trafficking was checked by expression of the functional Bmh1 isoform as a positive control. As expected, the tetrameric reporter localized exclusively to the vacuole of the cell (see Fig. 27 B, left panel), consistent with its localization in the Δ*bmh2* background. Vacuolar staining was also observed for the 14-3-3 chimera H2N1C (Fig. 27 B, central panel), but not for the chimeric H1N2C variant (Fig. 27 B, right panel). In this case, the reporter localised to the ER only, meaning that replacement of the C-terminal Bmh1 region by the distal Bmh2 C-terminus abolished the positive function of Bmh1 in promoting ER exit of the reporter. Thus, isoform specific behaviour in its effect on ccPmp2 forward trafficking was determined by the 14-3-3 C-termini.

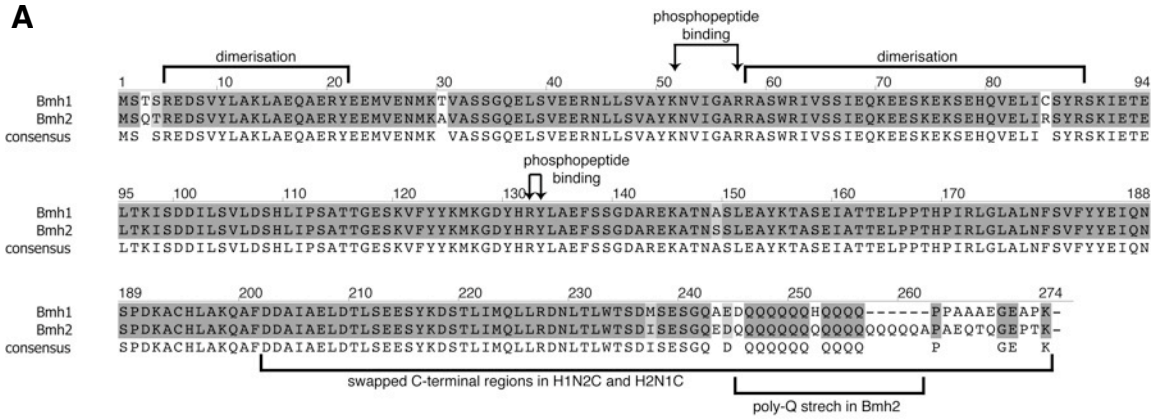

Figure 27: The stimulatory effect of Bmh1 on forward transport of the multimeric reporter protein maps to the C-terminus.

(A) Alignment of yeast 14-3-3 isoforms Bmh1 and Bmh2. Essential regions for 14-3-3 dimerisation, binding of 14-3-3 mode I, II or III binding motifs, the poly-Q stretch in Bmh2 and the C-terminal regions that have been swapped to create chimeric 14-3-3 proteins are highlighted.

(B) Fluorescent images of life cell imaging show the tetrameric Pmp2ccYFP-RKR or -KKK reporter in a Δ*bmh1*Δ*bmh2* double deletion strain expressing the indicated chimeric 14-3-3 variants. Vacuole (vac) and ER (ER) are accentuated by arrows. Scale bar is 5 *μ*m.

4.6.5 C-termini of 14-3-3 Bmh1 and Bmh2 interact with Ndk1

Coming from the findings of the previous chapter, the apparent question was: How can 14-3-3 isoforms achieve different functionality through their small C-terminal ends?

These regions are neither involved in the recognition of phosphorylated binding motifs, nor do they participate in dimer formation (see Fig. 27 A). To test whether they might be involved in recruitment of additional proteins a pulldown experiment with yeast cytosol was performed. In contrast to the pulldown experiment shown in chapter 4.6.2, only GST-tagged Bmh1- or Bmh2-C-termini were immobilised on GSH-agarose. Since the region which forms

the 14-3-3 binding groove is not present in this constructs, the experiment was specifically designed to identify putative binding partners that would recognise one but not the other 14-3-3 C-terminus. This allowed a much more specific search for new putative interaction partners, which do not depend on the binding groove and followed up the idea of simultaneous binding of 14-3-3s to the Arg-based motif of the membrane protein and simultaneous recruitment of additional machinery (by the distal C-terminus). The experimental setup is described in Figure 28 A. First, purified yeast cytosol was used as input, the column was washed and 300 mM $MgCl_2$ in washing buffer was used for elution. No isoform specific bands could be identified after seperation by SDS PAGE and Coomassie

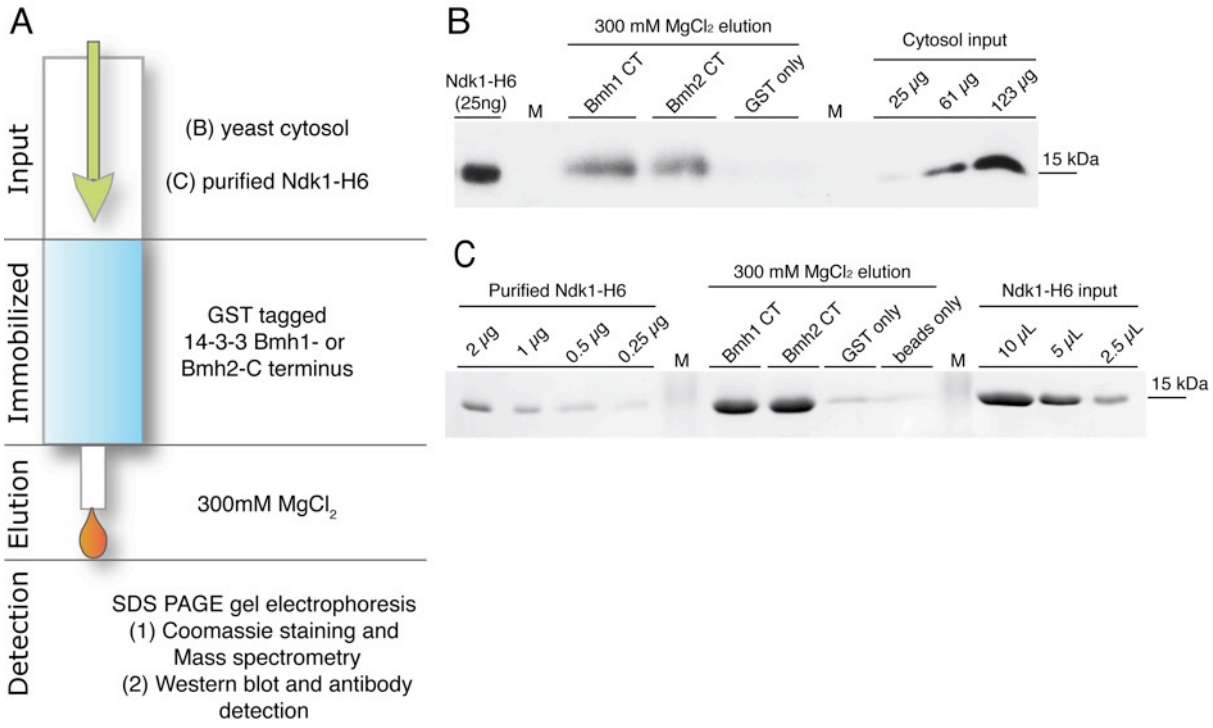

Figure 28: The C-termini of 14-3-3 Bmh1 and Bmh2 interact directly with the nucleoside diphosphate kinase Ndk1.

(A) Cartoon of the procedure.

(B) GST tagged Bmh1- and Bmh2-C termini were immobilized on a GSH-agarose column. The column was incubated with yeast cytosol, washed and eluted with 300 mM $MgCl_2$. Elutions were seperated on a 13.5% SDS PAGE gel and detected with an anti-Ndk1 antibody (1:1,000 dilution). Ndk1 was highly enriched from yeast cytosol. The amount of bound Ndk1 was slightly more in the case when Bmh1 C-terminus was immobilized. No binding was observed without immobilized 14-3-3 C-termini.
Specific Ndk1 detection followed enrichment from yeast cytosol and identification by mass spectrometry (data not shown).

(C) C-termini of yeast 14-3-3 proteins interact directly with Ndk1.
GST tagged Bmh1- and Bmh2-C termini were immobilized on a GSH-agarose column. The column was incubated with purified Ndk1-H6, washed and eluted with 300 mM $MgCl_2$. Elutions were seperated on a 13.5% SDS PAGE gel and detected with an anti-Ndk1 antibody (1:1,000 dilution).
Both 14-3-3 isoforms bind Ndk1 directly. No binding was observed without immobilized 14-3-3 C-termini.

staining. But one protein band at the height of ~15 kDa was highly enriched when the C-termini of Bmh1 and Bmh2 were immobilised (data not shown). The band was absent when only GST was exposed, indicating a specific interaction for the yeast 14-3-3 C-termini. Mass spectrometry analysis (performed by T. Ruppert and A. Bosserhof, ZMBH) identified the band as nucleoside diphosphate kinase (Ndk1). This protein catalyses the transfer of gamma phosphates from nucleoside triphosphates to nucleoside diphosphates (Palmieri et al., 1973; Jong and Ma, 1991; Fukuchi et al., 1993). Interestingly, the human homolog Nm23H2 was shown to play a role in the formation of COPII vesicles in mammalian cells (Kapetanovich et al., 2005). Mass spectrometry results were confirmed by detection of the highly enriched Ndk1 band using an anti-Ndk1 antibody (Pain lab; see Figure 28 B). To test if binding of Ndk1 to the 14-3-3 C-termini was direct, the experiment was repeated with purified, His-tagged Ndk1 protein as input. Again, strong binding of Ndk1 to the 14-3-3 C-termini was observed and the interaction was dependent on the presence of either Bmh1- or Bmh2-C-terminus since no Ndk1 was bound when using immobilised GST or empty beads (see Fig. 28 C).

In summary, both yeast 14-3-3 C-termini interact with the nucleoside diphosphate kinase (Ndk1) by direct binding. The connection of 14-3-3 proteins to Ndk1 furthermore strengthened the notion that there could be a link between Bmh1 and Bmh2 to ER exit via COPII vesicles.

4.7 Role of 14-3-3 proteins in COPII budding

4.7.1 Bmh1 is required for efficient COPII budding

In their work Kapetanovich et al linked the nucleoside diphosphate kinase Nm23H2, a human homolog of the yeast Ndk1 protein, to ER export. They made use of a COPII assembly assay in digitonin-permeabilized cells to identify cytosolic factors involved in ER exit site formation or COPII assembly. They showed that Nm23H2 supports efficient COPII vesicle formation. In my work I found the yeast Ndk1 to interact with the C-termini of 14-3-3 proteins Bmh1 and Bmh2. The interaction was direct and Ndk1 was highly enriched from yeast cytosol. To ask whether 14-3-3 proteins or a complex of 14-3-3 with Ndk1 have a role in COPII vesicle formation as well, an *in vitro* budding assay was performed. For this, ER enriched membranes were purified from wildtype and 14-3-3 single knockout strains and incubated with yeast cytosol in the presence of energy and Sar1 protein (see Figure 29 for details). Energy and Sar1 addition strongly promote COPII vesicle formation (see Lee et al., 2004 for review). Formed vesicles were separated from microsomes by differential centrifugation, collected and analysed by SDS PAGE and immunoblot with antibodies against a COPII coat component (Sec24), ER-Golgi v-SNARES (Sec22, Bos1), a cargo that cycles between the ER and the cis-Golgi (Emp47), the tetrameric ccPmp2 reporter and Bmh1/2. The result for microsomes from wildtype cells (see Figure 30 A) suggested that both 14-3-3 isoforms were present on formed COPII vesicles, as confirmed by the strong accumulation of the COPII coat component Sec24 in the

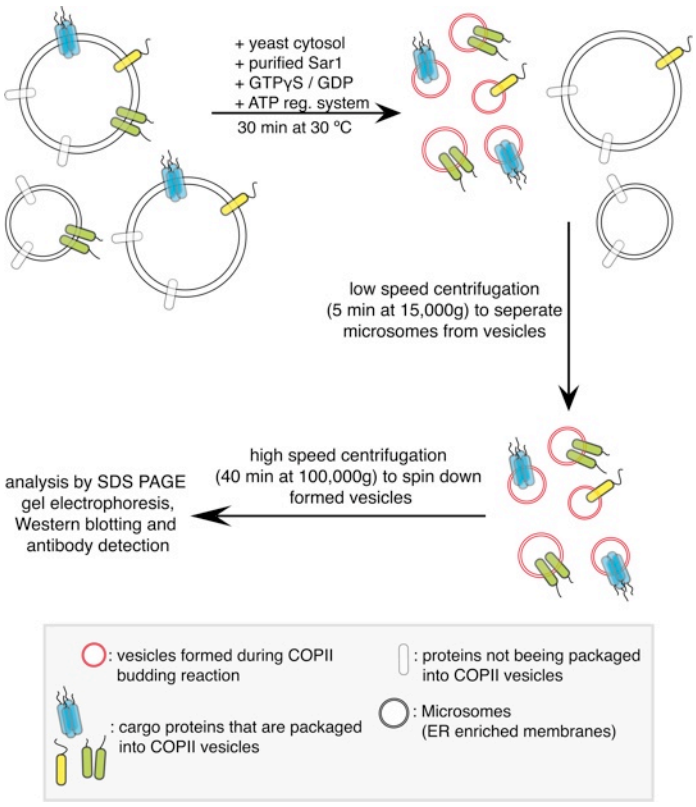

Figure 29: Cartoon of COPII budding assay.

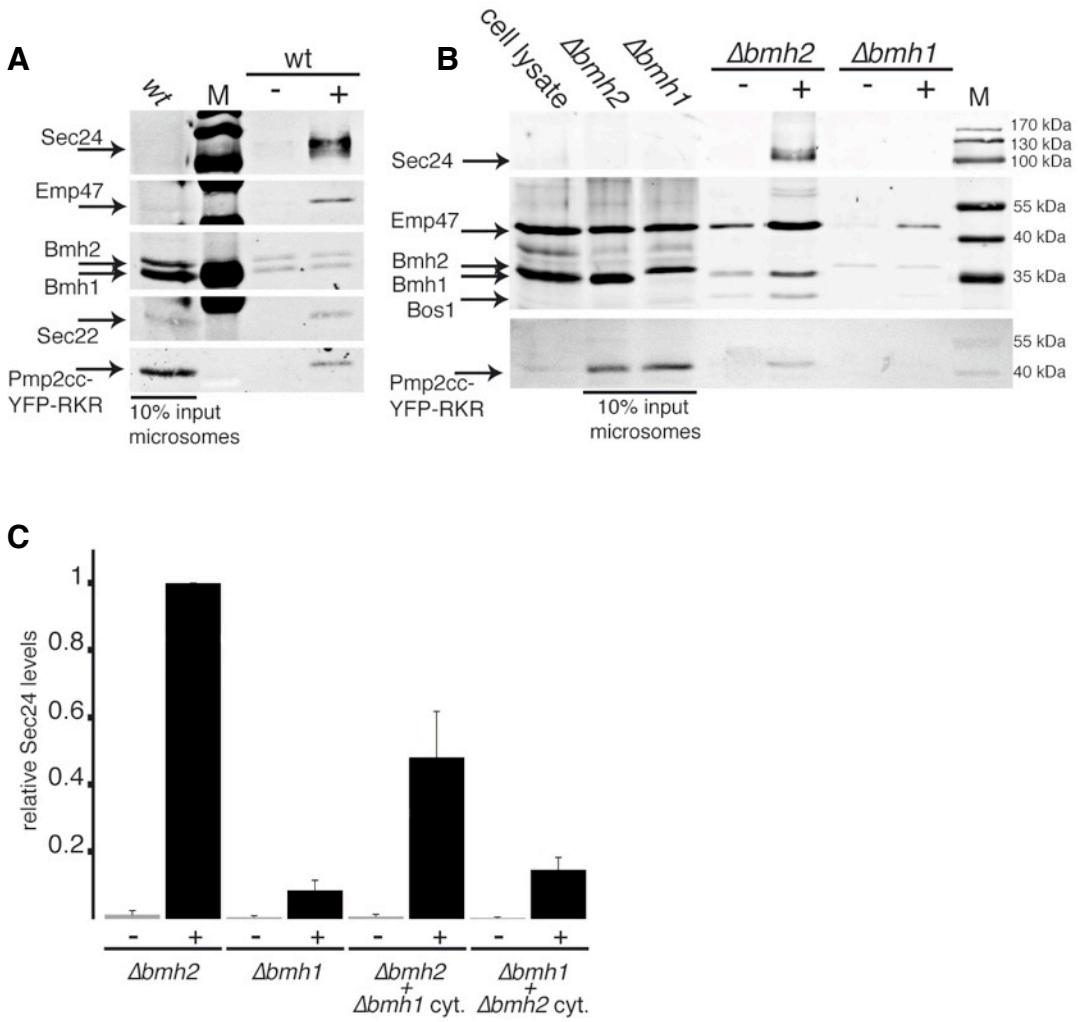

Figure 30: Bmh1 is required for efficient formation of COPII-coated vesicles *in vitro.*

Immunoblots of COPII components and cargo proteins in ER donor membranes and vesicles formed during the budding reaction. Donor membranes were incubated for 30 min at 30 ºC. Formed vesicles were collected from the low spin supernatant of the budding reaction by high speed spin (100,000x g for 40 min).
"-" indicates vesicle formation in the presence of cytosol only, "+" indicates inclusion of cytosol (20 µg of total protein per reaction), purified Sar1 (100 ng of purified protein per reaction), GTPγS (2 mM end concentration in each reaction) and an ATP-regeneration system. The total volume per reaction was 50 µl.
Proteins were separated on a 13.5% SDS PAGE gel, blotted and detected with various antibodies (marked with arrows).

(A) COPII budding of wildtype microsomes and wildtype cytosol.

(B) COPII budding of 14-3-3 single knockout strains.

(C) The effects were quantified from 4 independent experiments (employing three independently prepared batches of microsomes) for the COPII component Sec24 and normalized to the highest signal obtained (*Δbmh2*). Error bar indicates standard error.

same fraction. Both cargo proteins, the reporter protein ccPmp2-YFP as well as Emp47, were efficiently packaged. Performing the budding assay in the absence of Bmh2 did not influence budding efficiency compared to wildtype (Fig. 30 B, Δ*bmh2* lanes). However, lack of Bmh1 lead to strongly reduced packaging (approx. 10 fold reduction; see Δ*bmh1* lanes in Fig. 30 B

and graphs in Fig. 30 C). This is consistent with the results from life cell imaging, where a Δ*bmh1* strain is unable to promote forward transport of the reporter protein from the ER.

The possibility to combine microsomes and cytosol from different knockout strains allowed me to ask whether budding differences depend on Bmh1 presence on the donor membranes, or if cytosolic Bmh1 has an impact on the budding mechanism. Data from several independent experiments was summarised in Figure 30 C. The graph clearly shows, that addition of cytosolic Bmh1 to the budding reaction could not rescue the failure in COPII vesicle formation of the Δ*bmh1* strain. On the other hand, lack of cytosolic Bmh1 decreased budding efficiency by approx. 50% compared to Δ*bmh2*. Still, presence of Bmh1 on the donor membrane seemed to be more relevant than cytosolic Bmh1 (as measured by Sec24 presence on formed COPII vesicles).

Unexpectedly, effects of Bmh1 in COPII budding were not limited to the Pmp2 reporter, but were relevant for packaging of other cargo (here: Emp47) and for the enrichment of coat components, implying that the defect in the Δ*bmh1* strain is general to the process of COPII vesicle formation.

4.7.2 Effects of 14-3-3 Bmh1 on trafficking of cycling cargo

Lack of Bmh1 leads to reduced competitive fitness (Giaever et al., 2002) and the Δ*bmh1* strain showed slower growth than wildtype (data not shown). But nevertheless, this strain is perfectly viable. It seemed hard to believe, that the very strong general effect of Bmh1 on COPII budding influences all COPII cargo proteins. In contrast, it seemed more likely, that only a subclass is affected. Life cell imaging studies were performed to monitor the localisation of three different GFP fusion proteins. First, Pmp2GFP-LRERS, a monomeric Pmp2 reporter exposing a COPI retrieval signal of intermediate efficacy (Michelsen et al., 2006), second, Gef1-GFP, a voltage-gated chloride channel localized to the Golgi (Schwappach et al., 1998) and third, CPY-GFP, a carboxypeptidase Y localised to the vacuole (Westphal et al., 1996).

In contrast to the Pmp2 reporter, Gef1 and CPY do not cycle, due to the lack of the Arg-based motif or other retrieval signals.

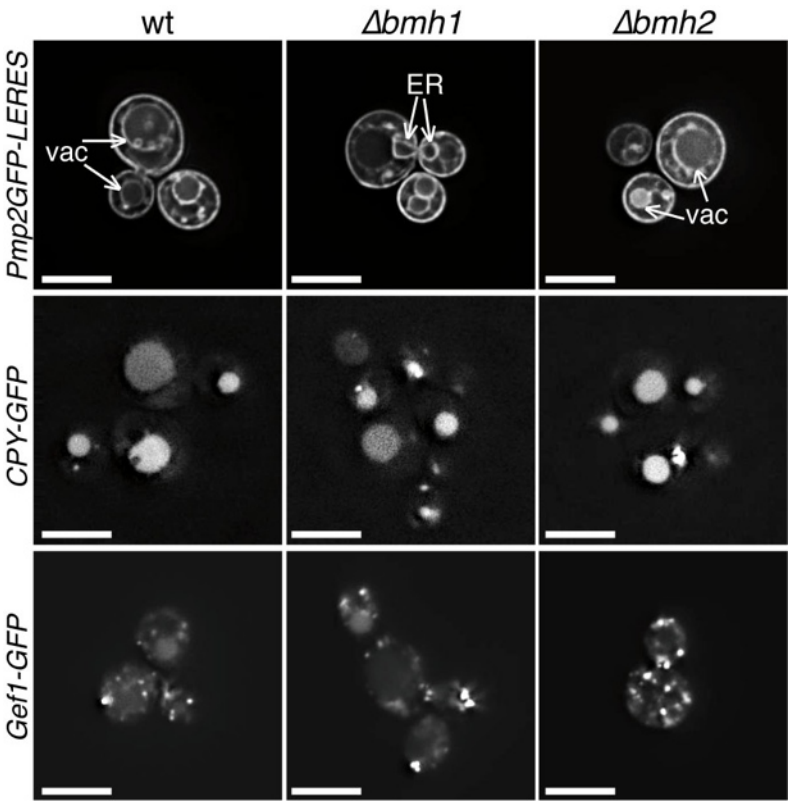

Figure 31: General role of Bmh1 in ER exit of cycling cargo *in vivo.*

An ER retrieval signal renders cargo sensitive to *BMH1* deletion *in vivo*.

Fluorescent images of life cell imaging show the localization of different cargo proteins in the respective 14-3-3 deletion strains. The cycling, monomeric Pmp2 reporter Pmp2GFP-LRERS exposes a COPI retrieval signal of intermediate efficacy (Michelsen et al., 2006). Knock out of Bmh1 (*Δbmh1*) but not Bmh2 (*Δbmh2*) leads to a steady state localization of the reporter in the ER.
Gef1 and CPY do not cycle due to a lack of a ER retrieval signal and are localised to the Golgi (Schwappach et al., 1998) and the vacuole (Westphal et al., 1996). Their localization is not dependent on the presence of either 14-3-3 isoform.
Arrows indicate the vacuole (vac) or the perinuclear ER (ER). Scale bar is 5 μm.

In a wildtype strain, all three proteins localised as expected (see Fig. 31, left panel). Trafficking of neither protein was influenced by the knockout of 14-3-3 Bmh2 (see Fig. 31, right panel). However, in a Δ*bmh1* strain localisation of the Pmp2GFP-LRERS reporter changed from a vacuolar to more ER staining, whereas both non-cycling proteins showed identical staining patterns compared to wildtype (see Fig. 31, panel for Δ*bmh1*). This result restricted the role of Bmh1 *in vivo* to cycling cargo proteins.

4.7.3 A dual role for Bmh1 in COPII packaging

To provide more evidence for the requirement of Bmh1 on the donor membrane for efficient COPII vesicle formation, budding was monitored in more detail by using an antibody against the Kir6.2 subunit to detect packaging of the reporter, an antibody recognising the ER-Golgi v-SNARE Bos1 and the anti-Bmh serum (see Fig. 32). As already summarised (graph in Fig. 30 C) the COPII coat component Sec24 was strongly concentrated on vesicles formed from Bmh1 microsomes and less abundant when Bmh2 microsomes were used (see lanes where cytosol and energy was added, marked with grey background and by arrows). Indicating, that

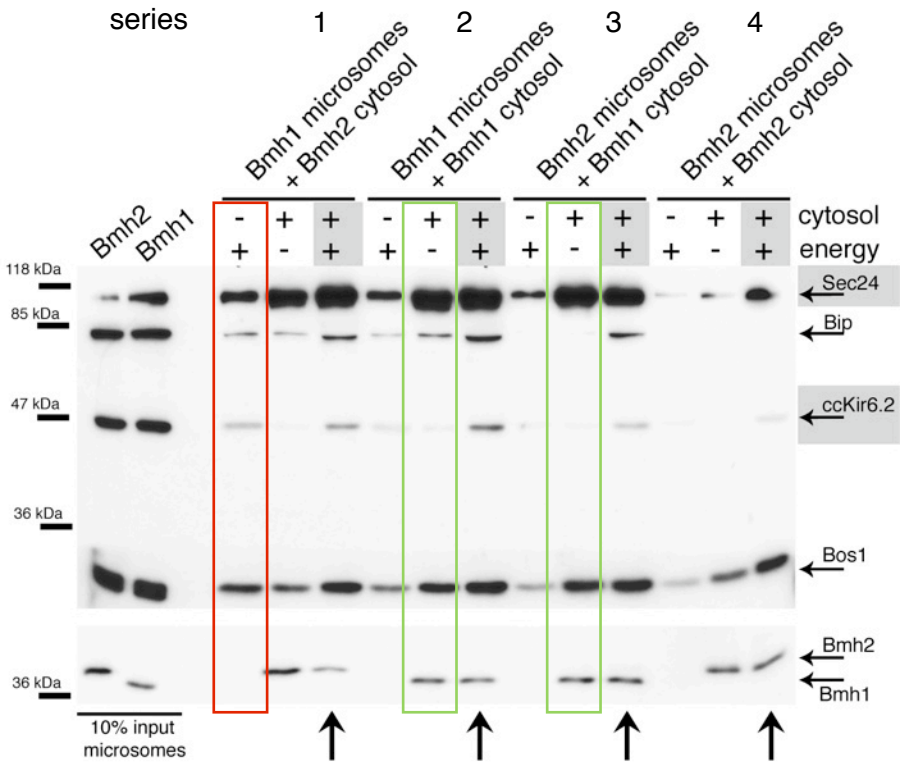

Figure 32: Presence of Bmh1 on the donor membrane is required for stimulation of COPII-coated vesicles formation and reporter packaging *in vitro*.

Immunoblots of COPII components and cargo proteins in ER donor membranes and vesicles formed during the budding reaction.
Purified Sar1 protein was added into all reactions. "+" energy indicates the addition of GTPγS and an ATP regeneration system.
See description of Figure 30 for more detail.
Most important lanes and detected proteins are highlighted by grey background and arrows.

Bmh1 may have a role in recruiting or stabilising COPII component on the vesicles. On the other hand, high amounts of Sec24 and Bos1 were also recruited without energy addition for budding reactions where Bmh1 was added to the cytosol (see Fig. 32, green boxes). Suggesting that Bmh1 may be relevant for recruitment of COPII components from the cytosol. Interestingly, strong stimulation of cargo packaging (see Fig. 32, ccKir6.2 detection) was only achieved with Bmh1 microsomes and Bmh1 cytosol and the addition of cytosol and energy.

Some packaging however, could be observed with Bmh1 microsomes per se as they packaged low amounts of reporter protein when only energy was added. In this case the ratio of packaged cargo to Sec24 was very high, implying that very dense vesicles had been formed (see Fig. 32, red box).

Detection for 14-3-3 proteins showed strong enrichment of Bmh1 and Bmh2 on the vesicles from added cytosol. Although both 14-3-3s were present on donor membranes in significant

amounts, they made only a small proportion of the total 14-3-3s on formed vesicles and were hard to detect at all (see Fig. 32: missing Bmh1 band in series 1 and missing Bmh2 band in series 3).

Can addition of purified Bmh1 to the budding reaction rescue the packaging defect of the Δ*bmh1* strain?

For this purpose Bmh1 and Bmh2 microsomes were incubated with Bmh2 cytosol in the presence (+ Bmh1) or absence (- Bmh1) of purified Bmh1 protein (Fig. 33). Vesicles were analysed by antibodies detecting Sec24, Emp47 (as cargo), Bip (as ER localised protein, not processed by COPII) and the ER-Golgi v-SNARE Sec22 and Bos1 (see Fig. 33). As previously shown, Bmh2 microsomes with Bmh2 cytosol did not promote packaging at all (see Fig. 33, series 4). Microsomes containing Bmh1 allowed formation of some vesicles and some reporter packaging (see Fig. 33, series 2). This was consistent with results from former budding assays (shown in Fig. 32). Addition of Bmh1 in the background of Bmh2 cytosol strongly enhanced the ability of packaging the cargo protein into COPII vesicles (see Fig. 33, lanes marked by grey background and arrows), but it did not enhance Sec24 enrichment to the

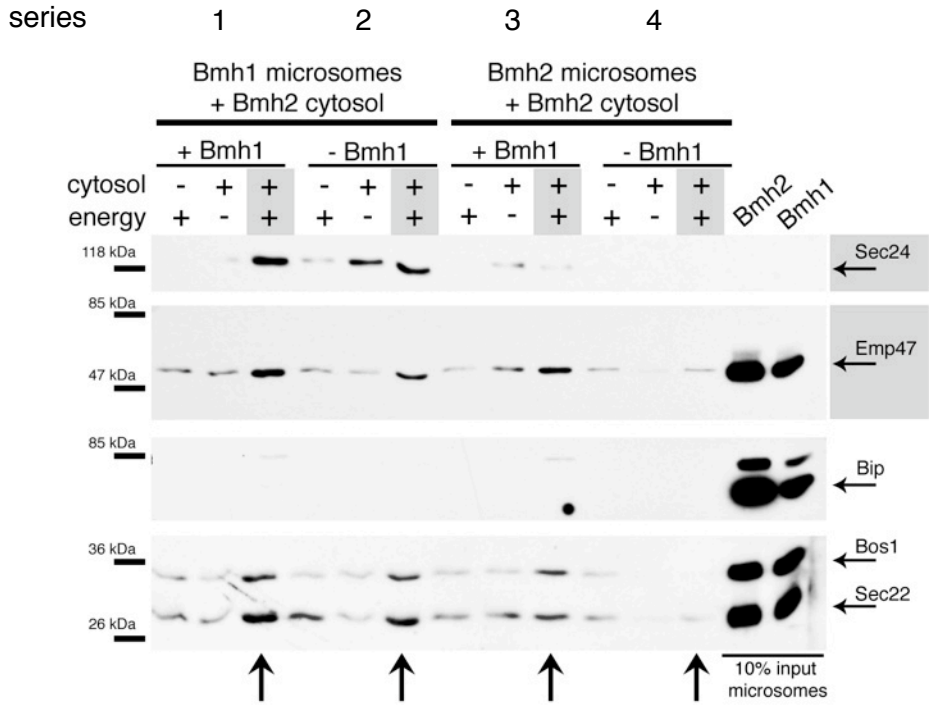

Figure 33: Addition of Bmh1 to the *in vitro* packaging assay can partially rescue the defect of a *Δbmh1* strain.

Immunoblots of COPII components and cargo proteins in ER donor membranes and vesicles formed during the budding reaction.
See description of Figure 30 for more detail.
No cytosolic Bmh1 was present. "+ Bmh1" indicates the addition of purified Bmh1 protein to the budding reaction.
Most important lanes and detected proteins are highlighted by grey background and arrows.

same extent. Only a weak Sec24 protein band could be detected upon Bmh1 addition when only Bmh2 was present in donor membranes and cytosol, although Emp47 was efficiently packaged into vesicles (see Fig. 33, series 3).

Taken together, only Bmh1 promoted COPII budding *in vitro*. Packaging of the reporter protein was already detected when Bmh1 microsomes were incubated with energy and further stimulation was achieved when Bmh1 containing cytosol was added. These findings suggest a dual effect of Bmh1 on COPII budding, which is dependent on whether Bmh1 is membrane bound or cytosolic.

4.7.4 Ndk1 deletion does not affect COPII budding

14-3-3 Bmh1 was shown to promote COPII vesicle formation. Furthermore, Bmh1 and Bmh2 C-termini were found to interact directly with the nucleoside diphosphate kinase (Ndk1) from yeast. The human homolog of Ndk1, Nm23H2, was previously described to have an influence on COPII export from the ER in mammalian cells (Kapetanovich et al., 2005). The resulting question was, if the effects of Nm23H2 are transferable to yeast and if the role of 14-3-3 proteins is linked to Ndk1. In other words: Does Ndk1 participate in the mechanism of COPII vesicle formation?

First, the presence of Ndk1 on ER enriched membranes was confirmed by Western blot detection with a HA-antibody. Therefore, Ndk1 was genomically HA-tagged to improve antibody detection, since the endogenous protein is only present in low copy numbers and was not detectable on membrane fractions using a Ndk1 specific antibody. As shown in Figure 34, endogenous Ndk1-HA was found on ER enriched membranes. However, no 14-3-3 isoform specific membrane association could be identified (see Fig. 34: Ndk1-HA band in Δ*bmh1* and Δ*bmh2* microsomes). No band was visible neither for microsomes from a

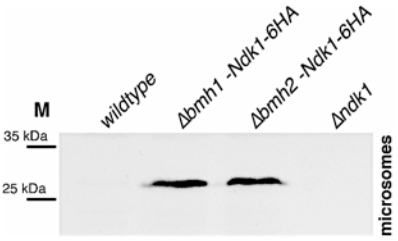

Figure 34: Ndk1 is present on microsomes.

5 µl of ER enriched membranes (total protein concentration 1.25 µg/ µl each) were loaded on a 13.5% SDS gel separated, blotted and detected with anti-HA antibody.
Ndk1 protein was genomically HA-tagged to improve signal-to-noise in Western blot detection. Ndk1 presence on microsomes is not influenced by the lack of either 14-3-3 isoform.

wildtype strain, expressing Ndk1 that was not HA-tagged, nor for microsomes from a strain lacking Ndk1 (Δ*ndk1*).

Ndk1 is best characterised in its function to catalyse the transfer of gamma phosphates from nucleoside triphosphates to nucleoside diphosphates (Jong and Ma, 1991; Fukuchi et al., 1993). This enzymatic activity relies on an intermediate self-phosphorylation step of a central histidine residue in Ndk1. Previous findings revealed that mutating the critical His^{119} residue leads to loss of Ndk1 enzyme activity (Amutha and Pain, 2003). According to Kapetanovich et al the role of Nm23H2 does not require the enzyme activity. The authors speculate that Nm23H2 may have a structural role in ER exit site formation instead. To test this hypothesis *in vitro*, the COPII budding assay was performed in the presence of GDP instead of non-hydrolysable GTPγS. The purpose was to make budding dependent on the enzyme activity of Ndk1 to synthesise GTP from ATP, since GTP is needed for COPII vesicle formation. A wildtype strain was compared to a strain lacking Ndk1 (Δ*ndk1*).

As shown in Figure 35, deletion of Ndk1 did not interfere with COPII budding at all. Addition of energy and Sar1 (see Fig. 35, green box) was sufficient to obtain enrichment of Sec24 and COPII specific SNARES (see Fig. 35, Bet1 and Bos1 detection) on the vesicles and efficient packaging of both reporter proteins (see Fig. 35, Emp47 and ccPmp2 detection). Both, Δ*ndk1* and wildtype strains showed a very similar budding behaviour and were not affected by absence or addition of neither Sar1, Ndk1 nor its mutated version (mut.). There might however be a slight stimulation of reporter packaging by addition of Ndk1 or its mutant

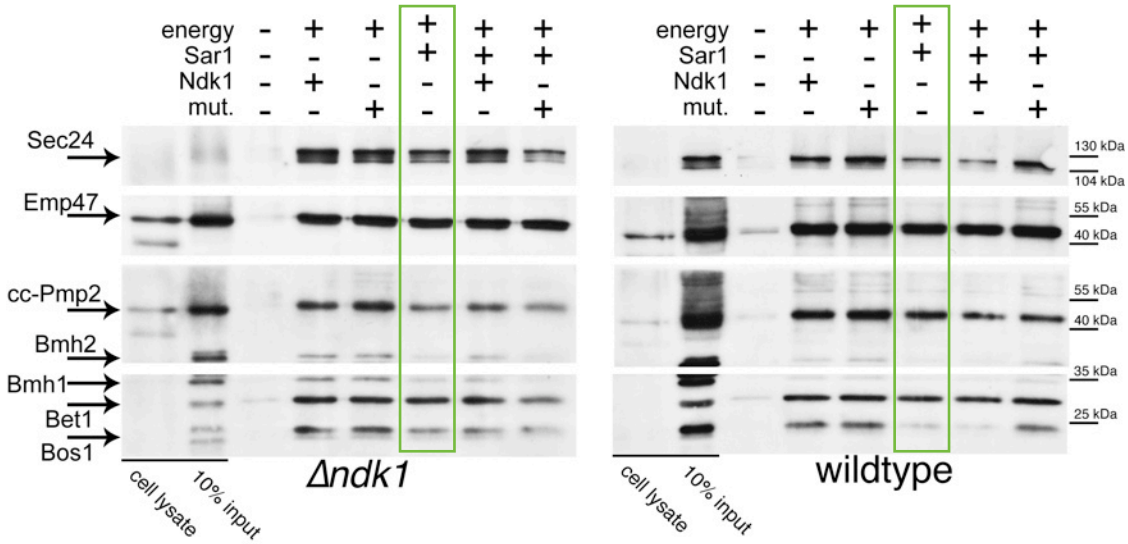

Figure 35: Absence of Ndk1 leads to very efficient COPII budding *in vitro;* No Ndk1 nucleoside diphosphate enzyme activity is needed for efficient COPII budding.

Immunoblots of COPII components and cargo proteins in ER donor membranes and vesicles formed during the budding reaction.
Details as described in Figure 30 except for the usage of GDP instead of GTPγS.

version in the absence of added recombinant Sar1. This seemed very surprising, since Sar1 addition is required for COPII vesicle formation in the *in vitro* budding assay.

4.7.5 Ndk1 and 14-3-3 Bmh1 are required in combination for efficient COPII vesicle formation

Since 14-3-3 Bmh1 showed a strong effect on COPII budding I tested the Δ*ndk1* strain for a comparable effect. As shown in the previous chapter, the knockout had no effect on vesicle formation in the *in vitro* assay. However, the detected interaction between Ndk1 and 14-3-3 proteins encouraged me to investigate the behaviour of double-knockout strains where Ndk1 knockout was combined with either Bmh1 or Bmh2 deletion (resulting in Δ*ndk1*Δ*bmh1* and Δ*ndk1*Δ*bmh2* strains respectively). Again, the in vitro COPII budding assay was performed as described in 4.7.1.

First, budding of the Δ*ndk1* strain was monitored in the presence of GTPγS. Results obtained were consistent with previous results (see Fig. 35). Surprisingly, budding in the absence of Ndk1 and Bmh1, meaning only Bmh2 was present (see Fig. 36 B), was very efficient. This result inverted what had been obtained with the Δ*bmh2* strain, which was incapable of forming COPII vesicles *in vitro* during the timeframe of the experiment (see Fig. 30 B). In the Δ*ndk1*Δ*bmh1* background, no stimulation could be achieved by addition of either Sar1, Ndk1 or the Ndk1 mutant (Fig. 36 B: see constantly efficient recruitment of Sec24, SNARES and cargo). Budding behaviour in the presence of only Bmh1, but not Ndk1 and Bmh2 (Δ*ndk1*Δ*bmh2* strain, Fig. 36 C) diverged completely from the Δ*ndk1*Δ*bmh1* strain in the way, that vesicle formation was dependent on the addition of Ndk1 protein or the enzymatic inactive mutant (see Fig. 36 C: lanes marked with grey background and arrows). Adding only Sar1 into the reaction did not promote budding. On the other hand, addition of only Ndk1 or the mutant was sufficient for efficient budding, thus no added Sar1 was needed.

In summary, I conclude that the positive effect of 14-3-3 Bmh1 on COPII budding depended on the presence of Ndk1, whereas Bmh2 in combination with Ndk1 negatively interfered with vesicle formation. The results also suggest, that Bmh2 alone has a positive effect on budding.

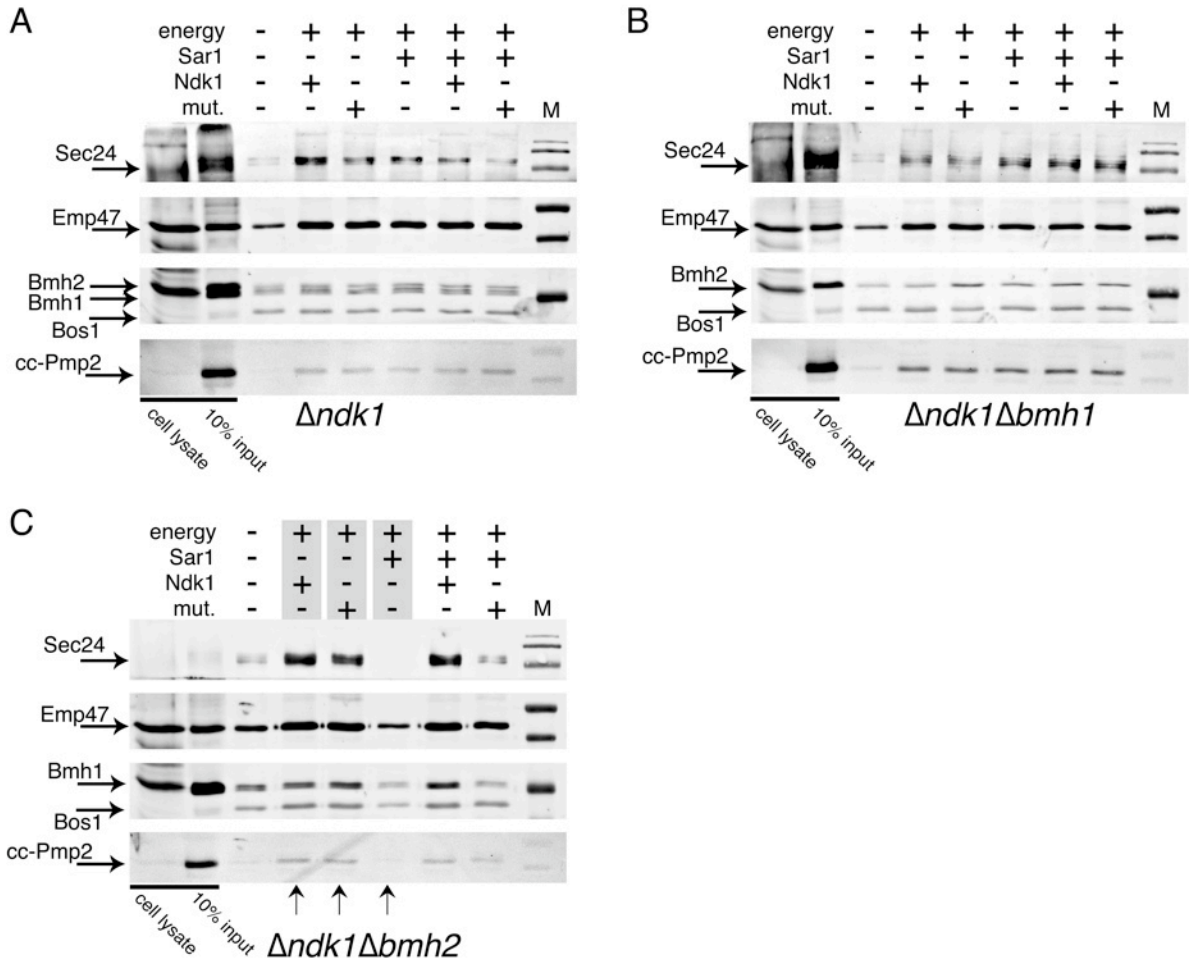

Figure 36: Ndk1 and Bmh1 (but not Bmh2) are required in combination for efficient COPII budding *in vitro.*

Immunoblots of COPII components and cargo proteins in ER donor membranes and vesicles formed during the budding reaction.
Details as described in Figure 30.
Sar1 (100 ng per reaction), Ndk1 and an enzymatic inactive Ndk1 mutant (mut.) (each 15 μg per reaction) were added into the budding reaction (+) or were absent (-).
Most important lanes and detected proteins are highlighted with grey boxes and arrows.

(A) *In vitro* COPII budding assay was performed in a *Δndk1* strain with both 14-3-3 isoforms present.

(B) *In vitro* COPII budding assay was performed in a *Δndk1Δbmh1* strain with only 14-3-3 Bmh2 present.

(C) *In vitro* COPII budding assay was performed in a *Δndk1Δbmh2* strain with only 14-3-3 Bmh1 present.

In the presence of both 14-3-3 isoforms Bmh1 and Bmh2 (*Δndk1*) no stimulation of budding or reporter packaging can be observed by adding Ndk1. Budding and packaging is efficient when Bmh1 and Ndk1 are missing (*Δndk1Δbmh2*). Addition of purified Ndk1 or its enzymatic inactive mutant highly stimulates budding in a strain lacking Bmh2 (*Δndk1Δbmh2*).

4.7.6 Quantification of Sec24 levels on the donor membranes

The surprising differences between both double-deletion Δ*ndk1*Δ*bmh1* and Δ*ndk1*Δ*bmh2* strains and the respective single deletion strains Δ*bmh1* and Δ*bmh2* could be a result of different amounts of COPII components present on the donor membranes. For this purpose, microsomes from six yeast strains, that had been used in this work were analysed and Sec24 levels were compared (see Fig. 37). Analogous to previously obtained results, yeast strains which budded worst (Δ*bmh1* and Δ*ndk1*Δ*bmh2*) had low levels of Sec24 on their donor membranes and strains which were efficient in budding had high amounts of Sec24 present (see Fig. 37 wildtype, Δ*bmh2*, Δ*ndk* and Δ*ndk1*Δ*bmh1*). Thus, the observed isoform specific differences in promoting COPII vesicle formation might be due to differences in abundance of COPII components on ER membranes.

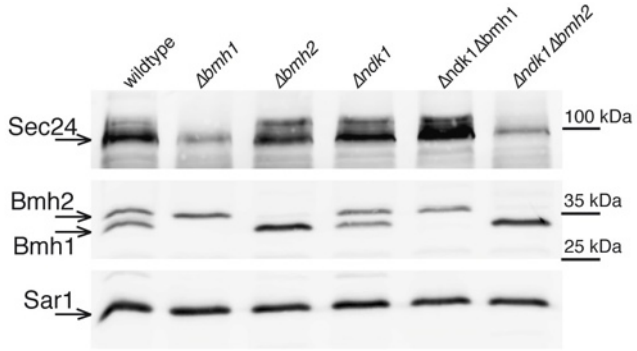

Figure 37: Sec24 is not equally present on ER enriched donor membranes in various knock out strains.

Characterization of ER enriched donor membranes used for *in vitro* COPII budding assays. Microsomes from various strains (adjusted to 14 µg of total protein each) were resolved on a 13.5% SDS PAGE gel, blotted and detected with the indicated antibodies.
The strain lacking Bmh1 (*Δbmh1*) and the strain having Bmh1 but not Ndk1 (*Δndk1Δbmh2*) have strongly decreased levels of Sec24 present on the ER enriched donor membranes.

5. Discussion

14-3-3 proteins have been described to play a crucial role in the trafficking of various membrane proteins. Examples are the $GABA_B$ receptor, K^+ channels TASK-1 and TASK-3, the invariant chain of the MHCII complex and a number of reporter proteins presenting the C-terminus tail of Kir6.2, a subunit of the ATP sensitive potassium channel (K_{ATP}) (see Table 1 for details). All these proteins have in common that they are multimers and expose a COPI-interaction motif in addition to a 14-3-3 recognition site. The increasing number of 14-3-3 interactions with these proteins underscores the importance of 14-3-3s in regulation of multimeric membrane protein trafficking. However, little is known about mechanistic details of the interactions between 14-3-3 isoforms and membrane proteins. Especially the role of 14-3-3 isoform specificity has not been addressed yet.

In my study I made use of a well defined reporter system, where the last 36 amino acids of Kir6.2 were fused to the isoproteolipid Pmp2, a type-I membrane protein in yeast. Usage of the yeast system allowed me to combine biochemical and *in vivo* methods. My work resulted in further insights into the function of 14-3-3 proteins in K_{ATP} trafficking as I could define the step of forward transport at which isoform specific 14-3-3 function occurs and identify the region in the yeast Bmh1 isoform that creates isoform specificity.

The nucleoside diphosphate kinase Ndk1 was found to interact with the Bmh1 and Bmh2 C-termini. The putative roles of 14-3-3s and Ndk1 will be discussed in this chapter.

5.1 The role of 14-3-3 proteins in forward trafficking is isoform specific

As shown by Michelsen and colleagues only Bmh1 but not Bmh2 can promote forward transport of the tetrameric Pmp2 reporter (see Fig. 3). Examples of isoform specificity of 14-3-3 proteins are rare. The human isoform 14-3-3 Sigma was shown to specifically facilitate cytokinesis (Wilker et al., 2005). The authors solved the X-ray crystal structure of the human 14-3-3 Sigma and identified an isoform specific binding site that is involved in specific ligand discrimination of the 14-3-3 Sigma isoform. Mutation of the involved residues

to the sequence that is present in all other isoforms, replaced the specific binding capability of 14-3-3 sigma. Paul et al found 14-3-3 isoforms to be localized differently in plant cells and propose subcellular localization as one way to facilitate isoform specificity (Paul et al., 2005). In yeast, other groups have previously presented results that point towards putative negative effects of Bmh2 in the cell. First, Demmel et al showed that Bmh2 localizes differently than Bmh1 in small puncta. Since they were using a 13-myc tag, that could potentially influence subcellular localization, I decided to repeat this analysis by immunofluorescence microscopy using untagged Bmh1 and Bmh2. Although the differences in staining patterns were not as pronounced, results could be confirmed (see Fig. 21). One can speculate that Bmh2 puncta are small aggregates that result from the interactions of the C-terminal poly-Q stretches of Bmh2 homodimers. The poly-Q stretch is only present in Bmh2 but not Bmh1. Secondly, Roth and colleagues reported that overexpression of the Bmh2 C-terminus is toxic and cells failed to polarize vesicular transport. Moreover, overexpression of Bmh2 caused damage to the ER structure. This was consistent with my observations (see Fig. 15). Finally, Δ*bmh1* cells grew significantly slower than wildtype or Δ*bmh2* cells and their competitive fitness is reduced (Giaever et al., 2002; data not shown). Taking into account, that 14-3-3 proteins are believed to be present and functional only in dimeric form, as homo- and heterodimers, the number of Bmh2 homodimers in the Δ*bmh1* strain increased by 412%, whereas Bmh1 homodimers increased only by 80% in the Δ*bmh2* background (see Table 3 B). Nevertheless, the total number of Bmh2/Bmh2 homodimers in a Δ*bmh1* strain replaces only ~36% of total 14-3-3 dimers in a wildtype strain.

Combining my findings with the information provided by other groups, a dominant negative effect of Bmh2 on the regulation of the forward transport of ccPmp2 could contribute to the observed isoform specificity.

Still, overexpression of Bmh2 in the Δ*bmh1* background could not rescue the loss of Bmh1 (see Fig. 15 A), implying a functional difference between the two isoforms.

Even though immunofluorescence provides a global overview of the localization of a protein within the whole cell, it was particularly difficult for either 14-3-3 isoform to identify compartments in which one, but not the other isoform was localised or enriched. This can be explained by the high expression levels of both proteins and their large cytosolic pool (see Fig. 21). In addition, the small size of yeast cells limits the resolution. Therefore, I

complemented microscopy data with Western blot detection of Bmh1 and Bmh2 in ER- and Golgi-enriched membranes in comparison to cytosolic 14-3-3 abundance (see Fig. 20). It was surprising to see that both isoforms are present on ER and Golgi membranes in high amounts, although no prominent ER staining could be seen in immunostaining. The fact that Bmh1 and Bmh2 from single knockout strains can be ER- and Golgi-membrane localised shows that both homodimers are recruited to compartments that are involved in the secretory pathway. No evidence could be found for differences in homodimer stability using Blue Native gel electrophoresis (BN-PAGE). All 14-3-3 isoforms formed stable homodimers and no exchange of 14-3-3 monomers was observed in the timeframe of the experiment. One has to emphasise critically however, that the experiment was performed at a temperature of 4 ºC for 1 h, so that dissociation of homodimers could probably not occur. It has been furthermore suggested, that the balance between 14-3-3 homo- and heterodimers *in vivo* might be strongly regulated (Yaffe et al., 2002). Meaning, that regulatory factors might be missing in dimerization studies performed *in vitro*.

Another putative explanation for isoform specificity are differences in binding affinities between Bmh1 and Bmh2 and the Kir6.2 tail. Again, *in vitro* and *in vivo* experiments were combined to tackle the problem. Making use of the previously purified, untagged 14-3-3 isoforms (see chapter 4.1) Isothermal calorimetry (ITC) was performed by K. Duderstadt (UCSF) to obtain binding affinities for the none-functional Bmh2 isoform to the Kir6.2-tail (see Fig. 17 A). As expected from previous work done by Yuan et al, where only very weak interaction to monomeric presentation of the Kir6.2-tail could be observed (see Fig. 6C in Yuan et al., 2003), binding affinity to the monomeric version was not detectable by ITC. Using the tetrameric ccKir6.2 tail instead, resulted in detectable interaction and a dissociation constant of K_D=6.2 nM, indicating very strong binding. This result underscores the preferential binding of 14-3-3 proteins to mutimerized presentation of the LRKR-Arg-based motif. In addition to ITC, I applied surface plasmon resonance (SPR) as a second quantitative method to determine dissociation constants for Bmh2 and Bmh1. Both methods complement each other very well. The advantage of SPR in comparison to ITC is that very low amounts of protein can be used and that binding can be directly observed. This allows direct determination of binding kinetics (association (on-) and dissociation (off-) rates) and gives additional information of the binding characteristics. The disadvantage of SPR is the

immobilization of the bait protein onto a planar surface, whereas ITC experiments are performed in buffer solution, without immobilization. Amount of immobilized bait protein, immobilization method and concentration range of ligand protein are crucial parameters to obtain useful results from SPR experiments and were therefore carefully adjusted. For both methods, data analysis was carried out under the assumption that only 14-3-3 dimers were present. This assumption was well verified by previous experiments (see text above).

First, I repeated binding of Bmh2 to the tetrameric tail. The resulting K_D value (17.4 nM) was well in the range of the dissociation constant obtained by ITC, confirming strong binding of Bmh2 to the ccKir6.2 tail. Surprisingly, the K_D value for the functional Bmh1 isoform was very comparable (13.8 nM). Analogous results were obtained *in vivo* through co-immunoprecipitation experiments (see Fig. 18), confirming the correctness and relevance of binding parameters that resulted from *in vitro* binding studies.

In summary, both yeast 14-3-3 isoforms are present on ER- and Golgi-enriched membranes and in the cytosol in similar amounts. No differences in binding affinities to the tetrameric reporter protein could be found *in vitro* and *in vivo* when the two isoforms are compared.

Taking into account, that overexpression of Bmh2 in a Δ*bmh1* strain to the same total level of 14-3-3 proteins as in wildtype did not rescue trafficking deficiency of the Δ*bmh1* strain (see Fig. 15), the hypothesis of simple masking of the LRLR-motif by Bmh1 but not Bmh2 can not be valid. Instead, other mechanisms must be responsible for isoform specific differences between Bmh1 and Bmh2. This will be discussed in the next paragraph.

5.2 Yeast 14-3-3 isoforms interact with a COPII component

Different hypothetical mechanisms for 14-3-3-dependent trafficking to the cell surface have been discussed (see Fig. 4; Mrowiec and Schwappach, 2006). Masking, a mechanism that is valid for a number of proteins including proteins that are involved in Ras and heterotrimeric G-protein signaling, or mitochondrial and nuclear proteins (see Fig. 2 for more examples), however, seems to be an insufficient hypothesis for multimeric membrane proteins. My results clearly demonstrate, that although equally present and binding the reporter with similar affinity, the non-functional Bmh2 isoform can not rescue trafficking defects of the Δ*bmh1* strain. In their recent work on K^+ channels O'Kelly and Goldstein emphasize that masking of

a C-terminal COPI motif alone is not sufficient to promote efficient forward transport of TASK-1. Instead they show that 14-3-3s have to recruit p11, a protein that stimulates ER exit. Since p11 can not bind to the C-terminus of TASK-1 in absence of 14-3-3, they propose a scaffolding function of 14-3-3 in addition to masking a N-terminal COPI motif (O'Kelly and Goldstein, 2008). The same mechanism could be a plausible hypothesis for the observed isoform specific behavior observed for ccPmp2 trafficking in my studies. Since both 14-3-3 proteins were found on ER-enriched and Golgi-enriched membranes (see Fig. 20 B and C), the hypothesis that they possibly recruit coat components or modulators of the early secretory pathway was tested using sequential stripping and pulldown experiments (see chapter 4.6). First, ER enriched membranes were sequentially treated with KoAc, NaCl and Na_2CO_3 to concentrate putative interaction partners of either Bmh1 or Bmh2. To prevent dissociation of putative complexes, microsomes were first crosslinked with DSS and BMH crosslinker. Although two specific bands for Bmh1 (in the Δ*bmh2* strain) and one Bmh2 specific band (in the Δ*bmh1* strain) were identified, not all 14-3-3 proteins could be crosslinked as shown by the prominent 14-3-3 monomer bands in Figure 22. This could be explained by inaccessible reaction groups for the crosslink reagents. Furthermore, Coomassie staining to identify putative membrane associated reaction partners of 14-3-3 proteins was not possible, since no affinity purification step was implemented. Alternative strategies must be performed in the future to identify 14-3-3 complexes on ER membranes: CO-IP experiments would allow specific affinity purification and enrichment of 14-3-3 complexes. To prevent dissociation of complexes, a crosslink treatment can be performed as a first step. Using Blue Native PAGE membrane protein complexes could be investigated in their native state. The advantage of this method is that no crosslinker treatment would be required. However, detergent-based solubilization of ER membranes in the experimental procedure could interfere with 14-3-3 binding to putative interaction partners and facilitate dissociation of those complexes.

Some coat components like the COPII components Sec23/24 and Sec 13/31 are recruited from the cytosol to the membrane. To test whether 14-3-3 proteins bind to cytosolic interaction partners that are possibly involved in trafficking of the Pmp2 reporter, a pulldown approach was chosen. 14-3-3 proteins were bound to the immobilized tetrameric Kir6.2 tail and incubated with yeast cytosol (see chapter 4.6.2). Unfortunately, no isoform specific bands were found. Still, one prominent, enriched band was identified by mass spectrometry as the COPII inner coat component Sec23 (see Fig. 23). This result was complemented by

previously published findings. In a large scale affinity-purification experiment Pozuelo Rubio and colleagues found an interaction of the yeast Bmh1 and Bmh2 isoforms with both Sec23 isoforms (Sec23A and Sec23B) from HeLa cytosol (Pozuelo Rubio et al., 2004). The authors did not test for isoform specific binding though, since both isoforms were immobilized on the Sepharose matrix together. Phosphorylation dependent mode-I, mode-II and mode-III binding motifs are the best described interaction sequences for 14-3-3 proteins (see Fig. 24 A). Besides Sec23A and Sec23B, Pozuelo Rubio et al identified more than 200 interactions partners for 14-3-3 Bmh1 and Bmh2 by eluting with a phosphopeptide that was competing for the binding pockets of 14-3-3s. This results suggests that most interactions involve binding of the phosphorylation dependent motifs. The most important feature of these motifs is the presence of a phosphorylated Serine or Threonine following an Arginine and a Proline residue at the end. None of these motifs is present in the sequence of yeast Sec23. However, many similar or alternative binding motifs have been shown to act as binding sites for 14-3-3s (see Yaffe et al., 2002). Thus, the consensus sequence was relaxed to three residues following the phosphorylated residue. As a consequence two putative motifs were identified in Sec23. Making use of a temperature sensitive *sec23-1* strain, the mutants were expressed under permissive and restrictive temperatures where the temperature-sensitive allele is inactive. Both mutants alone and in combination supported growth of the temperature sensitive strain at the restrictive temperature, indicating that none of the mutants introduced a severe, global defect in comparison to wildtype (see Fig. 25). However, localization of the ccPmp2 reporter was strongly influenced by the mutations (Fig. 26). The effects were additive, so that the reporter was completely mislocalized and could not be found in the vacuole anymore in the double mutant (see Fig. 26, S79N/S726N panel). This result was surprising, because reporter trafficking was crucially affected by the Sec23 mutants, whereas general growth was comparable to a wildtype strain. The finding suggested that the mutated Sec23 sites are specifically involved in trafficking of the Pmp2 reporter, but do not create general trafficking defects. To investigate if loss of Bmh1 is specific for a subgroup of proteins, localization of three different cargo proteins was observed in the Δ*bmh1* strain (Fig. 31). Only cycling cargo was found to be affected by the loss of Bmh1. This provides a possible link between 14-3-3 Bmh1 and COPII coat components and implies the idea, that 14-3-3 proteins have a regulatory role in forward trafficking for this class of recycling proteins and do not influence trafficking in a more general way. So far, regulation of COPII vesicle formation has been

suggested to be controlled by cargo recognition and sequentially increasing GTPase activity (Antonny et al. 2001; Miller et al., 2003; Sato and Nakano, 2007), thus by regulation of the kinetics of vesicle formation. Recent studies on the structure of the COPII coat add a new mechanism of regulation, since they suggest sterical control of vesicle formation through flexible coordination of coat components (see Stagg et al., 2006 and 2008). The findings that outer coat components Sec13/31 interact with inner coat components (Sec23/24-Sar1) and Sec13/31 is arranged to adapt to specific cargo, suggest new roles for regulatory factors.

To further investigate the putative link between trafficking defects specific for cycling cargo in the Δ*bmh1* knockout and trafficking defects with Sec23 mutations, I suggest using live cell imaging for localization studies of GFP-tagged cycling and non-cycling cargo (ccPmp2-RERS reporter versus CPY and Gef1) in the temperature sensitive *sec23-1* strain expressing either one or both Sec23 mutants under restrictive temperature. A pulldown approach with the Sec23 mutants can be used to test if binding of 14-3-3 to Sec23 depends on the presence of the mutated residues. Using either an ATP-regeneration system or λ-phosphatase in the pulldown could answer the question if binding is phosphorylation dependent. Those experiments can be complemented by co-immunoprecipitation experiments to test for *in vivo* interaction of 14-3-3s and Sec23 mutations.

5.3 Small differences in the distal C-termini create isoform specificity

All 14-3-3 proteins share a common structure and very similar sequences. Especially the yeast isoforms are highly similar (see Fig. 27 A). The highest sequence diversity can be found in the 14-3-3 C-termini. Do small differences in the Bmh1 and Bmh2 C-termini correlate with isoform specificity? I swapped the last 69 amino acids of Bmh1 with the last 75 amino acids of Bmh2 and vice versa. The advantage of having a defined isoform specific effect and the fact that only two isoforms are present in yeast made it possible to show, that only the Bmh1 C-terminus is able to promote forward transport (see Fig. 27 B). The result that the chimeric H2N1C isoform did promote forward transport is consistent with the idea that the distal C-terminal parts of yeast 14-3-3 proteins exert their effects independently of dimerization or binding pocket formation and are an independent interaction region. This hypothesis has been

discussed by other groups as well, since it was found that the C-termini are a very flexible region of 14-3-3 proteins (see Obsilova et al., 2008 for review). Roth and colleagues for example showed in yeast that overexpression of the carboxy-terminal region of Bmh2 but not Bmh1 was lethal (Roth et al., 1999). Although the authors do not give an mechanistic explanation, they speculate that binding to additional downstream partners could explain isoform specificity. My observations and these findings gave me reason to perform pulldown experiments with the distal C-termini of Bmh1 and Bmh2 to search for putative, specific binding partners. Again, no isoform specific bands could be identified. However, a small 15 kDa protein was highly enriched from yeast cytosol. Mass spectrometry analysis identified the protein as Ndk1 (nucleoside diphospohate kinase). I was able to confirm the interaction by immunoblotting and showed that it is direct (see Fig. 28). Ndk1 is best described for its enzymatic function in creating GTP from GDP and ATP (Agarwal et al., 1978; Jong and Ma, 1991; Fukuchi et al., 1993). GTP is required to initiate COPI and COPII vesicle formation, therefore Ndk1 seemed a very interesting protein to potentially participate in the regulation of trafficking by controlling local availability of GTP (see Fig. 38 B). In addition, recent work connected the human homolog of Ndk1, Nm23H2, to COPII vesicle formation in mammalian cells (Kapetanovich et al., 2005). The authors identified Nm23H2 from mammalian cytosol in a sequential multi-step purification procedure as a regulator of COPII assembly. They made use of a COPII assembly assay in digitonin-permeabilized cells to show stimulation of ER exit site formation in Nm23H2 presence. Knockdown of Nm23H2 lead to reduced COPII assembly.

For those reasons I decided to follow up the connection between 14-3-3s and Ndk1 and a possible role of the interaction in forward trafficking.

5.4 14-3-3 Bmh1 as regulator of COPII vesicle formation

My findings that yeast 14-3-3 proteins interact with the COPII component Sec23 and my pulldown experiments identifying Ndk1 (that has previously been described to be involved in efficient COPII vesicle formation in mammalian cells) as a putative 14-3-3 binding partner motivated me to investigate the role of yeast 14-3-3s in COPII budding in detail. I made use of an *in vitro* budding assay that has the advantage to uncouple COPII vesicle formation from

other trafficking effects that occur *in vivo*. In contrast to steady state localization studies *in vivo*, the *in vitro* assay allows mechanistic studies in a controlled environment. Together with the possibility to combine ER enriched membranes from different yeast knockout strains with different yeast cytosols, the COPII budding assay turned out to be a powerful tool for mechanistic investigations adressing the role of 14-3-3 and Ndk1 in vesicle formation. Comparison of wildtype, Δ*bmh1* and Δ*bmh2* conditions revealed a big difference in the ability of Bmh1 and Bmh2 to promote COPII budding (Fig. 30 B). Lack of Bmh1 resulted in poor packaging and no detectable Sec24 on budded vesicles. Surprisingly, the strong effect did not only apply to the tetrameric reporter, but also to Emp47, a cargo protein, that has no 14-3-3 binding motif. The second surprising outcome was, that cytosolic Bmh1 could not rescue packaging defects of the Δ*bmh1* strain. On the other hand, lack of Bmh1 in the Δ*bmh1* cytosol reduced Sec24 recruitment by ~50% when Bmh1 was present on the microsomes only (see Fig. 30 C). To further separate both effects, I performed the same budding assays with and without addition of purified Bmh1 (see Fig. 33). Adding purified Bmh1 to a budding assay where only Bmh2 microsomes and Bmh2 cytosol were used, resulted in clearly stimulated packaging. However, no increase in Sec24 recruitment was observed. In contrast, vesicle formation relying on Bmh1 microsomes and Bmh2 cytosol lead to efficiently recruited Sec24 but only poor packaging. In summary, a dual role for Bmh1 was observed in COPII budding experiments. Strong presence of Sec24 on budded COPII vesicles originating from Bmh1 containing donor membranes suggests a membrane associated role of Bmh1 on ER membranes. 14-3-3 Bmh1 may have a role in structural co-ordination of coat components, or in stabilisation of the inner coat. The observed interaction with Sec23 strengthens this hypothesis. In addition, cytosolic Bmh1 could be responsible for the recruitment of regulatory components to ER exit sites. Ndk1, which was shown to interact with the 14-3-3 C-termini was a good candidate to potentially mediate the isoform specific role of Bmh1. Therefore COPII budding assays with ER membranes from the Δ*ndk1* strain were compared to wildtype budding (Fig. 35). Unexpectedly, COPII vesicle formation from a Ndk1 deletion strain was highly efficient and very comparable to wildtype. This finding is controversial when comparing to data by Kapetanovich et al, where knockdown of Nm23H2 lead to reduced ER-exit kinetics of GalNacT2-GFP (Kapetonovich et al., 2005). As the loss of Ndk1 was not crucial for COPII budding, I asked if knockout of Ndk1 and Bmh1 or Bmh2 in combination influences vesicle formation. To further separate the exact functions of the three proteins I

performed the budding reaction under various conditions (see Fig. 36). The first unexpected finding was that Sec24 was strongly present on vesicles and cargo packaging was very efficient in the Δ*ndk1*Δ*bmh1* strain. This result implies a positive role in COPII budding for Bmh2 alone, but a putative negative complex when Bmh2 and Ndk1 are expressed together (compare budding results from Δ*bmh1* strain, Fig. 30 B). The very opposite result was obtained for budding of the Δ*ndk1*Δ*bmh2* strain. No vesicle formation was observed in the presence of Bmh1 alone. Efficient packaging was induced upon addition of Ndk1 or the enzymatically inactive Ndk1 mutant, even without adding purified Sar1 protein (see Fig. 36 C). In conclusion, Bmh1 and Ndk1 act in combination to enhance packaging. Together they seem to form a highly stimulating complex and promote COPII vesicle formation even in the presence of low amounts of cytosolic Sar1 (see cartoon in Figure 38 A).

How can Bmh1-Ndk1 form a promoting complex, if affinity of Bmh1 and Bmh2 C-termini to Ndk1 was shown to be similar? A possible explanation could be differences in *in vitro* binding and *in vivo* binding of 14-3-3s to Ndk1. In my pulldown experiment only the distal C-termini were exposed. Several groups however reported that flexible C-termini can regulate the binding of 14-3-3s to interaction partners *in vivo* (Obsilova et al., 2004, Silhan et al., 2004). The suggested explanation is, that a flexible 14-3-3 C-terminus can autoinhibit the 14-3-3 binding groove. This inhibition is controlled by phosphorylation (Silhan et al., 2004). Truong and colleagues observed a lowered affinity of 14-3-3s to binding partners in presence of their C-termini (Truong et al., 2002). It might be, that 14-3-3 Bmh1 and Bmh2 can perform the

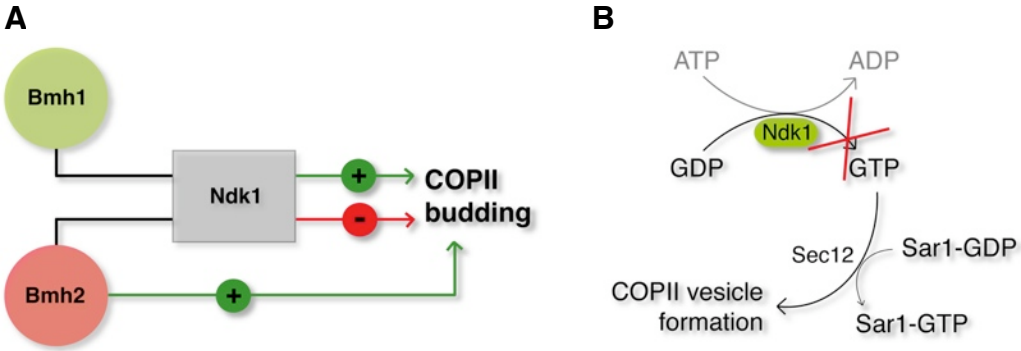

Figure 38:
(A) Model of 14-3-3-Ndk1 influence on COPII vesicle formation.

14-3-3 Bmh1 requires Ndk1 to stimulate COPII budding, whereas Bmh2 in the presence of Ndk1 (membrane bound?) inhibits COPII budding. A *Δndk1Δbmh1* strain was very efficient in COPII vesicle formation, indicating a positive role of Bmh2 in the absence of Ndk1.

(B) Cartoon showing the putative connection between Ndk1 enzyme activity and COPII budding.

The hypothesis that Ndk1 enzyme activity (GTP production) could create a local pool of high GTP concentration and by this promote COPII vesicle formation was excluded by using a catalytically inactive mutant, that was as efficient as the active Ndk1 version in stimulation of COPII budding (see Fig. 36).

same binding to Ndk1 *in vitro*, but their binding-unbinding dynamics *in vivo* are modulated by different C-termini interactions with their binding groove.

Consistent with results presented by Kapetanovich and colleagues, Ndk1 stimulation does not depend on its enzymatic activity, as shown by efficient budding of the Δ*ndk1*Δ*bmh2* strain with addition of the mutant Ndk1 version. This means, that the hypothesis of Ndk1 increasing the local GTP availability for regulation of vesicle budding is not valid (see cartoon in Fig. 38 B).

5.5 Speculations and outlook

14-3-3 proteins were found to act as regulator proteins of COPII vesicle formation. Putative binding sites were identified in Sec23 and mutation of these phosphorylation dependent motifs on Sec23 resulted in mislocalization of the ccPmp2 reporter protein. Although a direct *in vivo* interaction between yeast 14-3-3s and Sec23 has still to be proven, a regulatory role in inner coat assembly and stabilization could be a mechanism by which 14-3-3s promote forward transport in a isoform specific way. This hypothesis is supported by the fact, that the Δ*bmh1* strain shows a strongly reduced presence of Sec24 on ER enriched membranes. Furthermore, membrane bound 14-3-3 Bmh1, but not Bmh2, strongly enhances Sec24 presence on budded vesicles.

Bmh1 needs Ndk1 for its stimulatory function. The fact, that addition of Ndk1 to the budding reaction strongly promotes vesicle formation from Δ*bmh2* microsomes even in the presence of only low amounts of cytosolic Sar1, suggests a structural role for the Bmh1-Ndk1 combination. A similar speculation was also formulated by Kapetanovich and colleagues for the COPII promoting function of the human Ndk1 homolog Nm23H2. Recent findings by Stagg et al present a new idea for COPII regulation in which a flexible hinge region adjusting the geometry of outer coat components Sec13/31 and their binding to Sec23/24-Sar1 could be an interaction surface for various regulatory proteins. Bmh1 in combination with Ndk1 could act in this way. Similar examples have been reported lately, Higashio et al identified Smy2 as a modulator of the Sec23/24 inner coat (Higashio et al., 2008).

The region of yeast 14-3-3 Bmh1 necessary for forward transport stimulation was narrowed down to its C-terminus. Although Bmh1 and Bmh2 C-termini showed similar affinity for

Ndk1 in pulldown experiments, isoform specificity *in vivo* could be explained by regulation of flexible C-termini and 14-3-3 binding groove interactions as discussed above. The idea, that 14-3-3 Bmh1 and Bmh2 differ significantly in their native protein structure is supported by Blue Native PAGE where the 14-3-3 protein bands, which run at the height of a dimer, differ significantly in their running behavior, while the monomers differ only by 1-3 kDa in size (see Fig. 39).

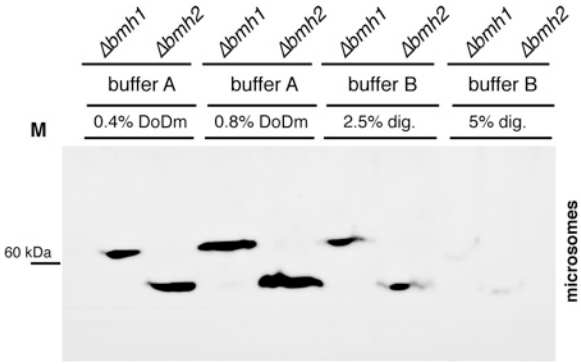

Figure 39: 14-3-3 Bmh1 and Bmh2 are present on microsomes as dimers that differ significantly in their running behavior on Blue Native PAGE gels.

Microsomes of *Δbmh1* and *Δmbh2* strains (200 µg of total protein) were solubilized in buffer A or buffer B (see buffer list for more details) and either Dodecyl β-D maltoside (DoDm) or digitonin (dig.) for 30 min on ice. Then microsomes were separated under native conditions on Blue Native PAGE, blotted and detected with anti-bmh antiserum.
Although Bmh2 and Bmh1 differ only by 1 kDa in size, they show significantly different running behavior under native conditions.
(Experiment performed by E. Arakel.)

Taking the data obtained in my study together, one has to conclude, that simple masking of the Arg-based COPI recognition motif by 14-3-3 proteins is not a sufficient explanation for the observed isoform specificity. Instead, a regulatory function of 14-3-3 proteins in the forward trafficking of K_{ATP} channels at the level of COPII vesicle formation can be proposed. Further investigations of the interaction between 14-3-3s and COPII inner coat components are necessary though. The yeast system remains a powerful tool for further experiments, since it allows the expression of mutated COPII components in temperature sensitive strains, where essential genes are downregulated and offers the possibility to generate ER enriched membranes and cytosol from various knockout strains.

Ndk1 was identified as a putative interaction partner of yeast 14-3-3 proteins that was necessary to stimulate COPII budding *in vitro*. The human homolog of Ndk1 was recently connected to changes in ER morphology (Baughman et al., 2008) through lipid binding. Electron microscopy could be used as an approach to test for Ndk1 induced changes in ER exit site morphology. Temmermann and colleagues presented a new assay based on flow-

cytometry that allows investigation of lipid binding by fluorescently labelled proteins (Temmermann et al., 2009, in press). This method could be adopted to investigate binding of Ndk1 and complexes of Ndk1 and either Bmh1 or Bmh2 to liposomes resembling ER or Golgi membranes in lipid composition.

6. References

1. Agarwal, R. P., Robison, B. & Parks, R. E., Jr. Nucleoside diphosphokinase from human erythrocytes. Methods Enzymol 51, 376-86 (1978).
2. Amutha, B. & Pain, D. Nucleoside diphosphate kinase of Saccharomyces cerevisiae, Ynk1p: localization to the mitochondrial intermembrane space. Biochem J 370, 805-15 (2003).
3. Antonny, B., Madden, D., Hamamoto, S., Orci, L. & Schekman, R. Dynamics of the COPII coat with GTP and stable analogues. Nat Cell Biol 3, 531-7 (2001).
4. Antonny, B. & Schekman, R. ER export: public transportation by the COPII coach. Curr Opin Cell Biol 13, 438-43 (2001).
5. Aridor, M., Bannykh, S. I., Rowe, T. & Balch, W. E. Cargo can modulate COPII vesicle formation from the endoplasmic reticulum. J Biol Chem 274, 4389-99 (1999).
6. Aridor, M. & Balch, W. E. Kinase signaling initiates coat complex II (COPII) recruitment and export from the mammalian endoplasmic reticulum. J Biol Chem 275, 35673-6 (2000).
7. Ashcroft, F. M., Harrison, D. E. & Ashcroft, S. J. Glucose induces closure of single potassium channels in isolated rat pancreatic beta-cells. Nature 312, 446-8 (1984).
8. Ashcroft, F. M. & Rorsman, P. Electrophysiology of the pancreatic beta-cell. Prog Biophys Mol Biol 54, 87-143 (1989).
9. Babenko, A. P., Aguilar-Bryan, L. & Bryan, J. A view of sur/KIR6.X, KATP channels. Annu Rev Physiol 60, 667-87 (1998).
10. Baker, D., Hicke, L., Rexach, M., Schleyer, M. & Schekman, R. Reconstitution of SEC gene product-dependent intercompartmental protein transport. Cell 54, 335-44 (1988).
11. Balch, W. E., McCaffery, J. M., Plutner, H. & Farquhar, M. G. Vesicular stomatitis virus glycoprotein is sorted and concentrated during export from the endoplasmic reticulum. Cell 76, 841-52 (1994).
12. Barlowe, C. & Schekman, R. SEC12 encodes a guanine-nucleotide-exchange factor essential for transport vesicle budding from the ER. Nature 365, 347-9 (1993).

13. Barlowe, C., d'Enfert, C. & Schekman, R. Purification and characterization of SAR1p, a small GTP-binding protein required for transport vesicle formation from the endoplasmic reticulum. J Biol Chem 268, 873-9 (1993).
14. Barlowe, C. et al. COPII: a membrane coat formed by Sec proteins that drive vesicle budding from the endoplasmic reticulum. Cell 77, 895-907 (1994).
15. Baughman, C., Morin-Leisk, J. & Lee, T. Nucleoside diphosphate kinase B (NDKB) scaffolds endoplasmic reticulum membranes in vitro. Exp Cell Res 314, 2702-14 (2008).
16. Bi, X., Corpina, R. A. & Goldberg, J. Structure of the Sec23/24-Sar1 pre-budding complex of the COPII vesicle coat. Nature 419, 271-7 (2002).
17. Bradford, M. M. A rapid and sensitive method for the quantitation of microgram quantities of protein utilizing the principle of protein-dye binding. Anal Biochem 72, 248-54 (1976).
18. Bukau, B., Weissman, J. & Horwich, A. Molecular chaperones and protein quality control. Cell 125, 443-51 (2006).
19. Coblitz, B., Wu, M., Shikano, S. & Li, M. C-terminal binding: an expanded repertoire and function of 14-3-3 proteins. FEBS Lett 580, 1531-5 (2006).
20. Cook, D. L., Satin, L. S., Ashford, M. L. & Hales, C. N. ATP-sensitive K+ channels in pancreatic beta-cells. Spare-channel hypothesis. Diabetes 37, 495-8 (1988).
21. Cosson, P., Lefkir, Y., Demolliere, C. & Letourneur, F. New COP1-binding motifs involved in ER retrieval. Embo J 17, 6863-70 (1998).
22. Demmel, L. et al. Nucleocytoplasmic shuttling of the Golgi phosphatidylinositol 4-kinase Pik1 is regulated by 14-3-3 proteins and coordinates Golgi function with cell growth. Mol Biol Cell 19, 1046-61 (2008).
23. Dhillon, A. S. et al. Cyclic AMP-dependent kinase regulates Raf-1 kinase mainly by phosphorylation of serine 259. Mol Cell Biol 22, 3237-46 (2002).
24. Dougherty, M. K. & Morrison, D. K. Unlocking the code of 14-3-3. J Cell Sci 117, 1875-84 (2004).
25. Ellgaard, L. & Helenius, A. Quality control in the endoplasmic reticulum. Nat Rev Mol Cell Biol 4, 181-91 (2003).

26. Farhan, H., Weiss, M., Tani, K., Kaufman, R. J. & Hauri, H. P. Adaptation of endoplasmic reticulum exit sites to acute and chronic increases in cargo load. Embo J 27, 2043-54 (2008).
27. Farsad, K. & De Camilli, P. Mechanisms of membrane deformation. Curr Opin Cell Biol 15, 372-81 (2003).
28. Fukuchi, T., Nikawa, J., Kimura, N. & Watanabe, K. Isolation, overexpression and disruption of a Saccharomyces cerevisiae YNK gene encoding nucleoside diphosphate kinase. Gene 129, 141-6 (1993).
29. Gelperin, D. et al. 14-3-3 proteins: potential roles in vesicular transport and Ras signaling in Saccharomyces cerevisiae. Proc Natl Acad Sci U S A 92, 11539-43 (1995).
30. Ghaemmaghami, S. et al. Global analysis of protein expression in yeast. Nature 425, 737-41 (2003).
31. Giaever, G. et al. Functional profiling of the Saccharomyces cerevisiae genome. Nature 418, 387-91 (2002).
32. Goldberg, J. Structural basis for activation of ARF GTPase: mechanisms of guanine nucleotide exchange and GTP-myristoyl switching. Cell 95, 237-48 (1998).
33. Gorlich, D. & Rapoport, T. A. Protein translocation into proteoliposomes reconstituted from purified components of the endoplasmic reticulum membrane. Cell 75, 615-30 (1993).
34. Guo, Y. & Linstedt, A. D. COPII-Golgi protein interactions regulate COPII coat assembly and Golgi size. J Cell Biol 174, 53-63 (2006).
35. Harbury, P. B., Zhang, T., Kim, P. S. & Alber, T. A switch between two-, three-, and four-stranded coiled coils in GCN4 leucine zipper mutants. Science 262, 1401-7 (1993).
36. Heusser, K. et al. Scavenging of 14-3-3 proteins reveals their involvement in the cell-surface transport of ATP-sensitive K+ channels. J Cell Sci 119, 4353-63 (2006).
37. Higashio, H., Sato, K. & Nakano, A. Smy2p participates in COPII vesicle formation through the interaction with Sec23p/Sec24p subcomplex. Traffic 9, 79-93 (2008).
38. Hirst, J., Bright, N. A., Rous, B. & Robinson, M. S. Characterization of a fourth adaptor-related protein complex. Mol Biol Cell 10, 2787-802 (1999).

39. Hughes, H. & Stephens, D. J. Assembly, organization, and function of the COPII coat. Histochem Cell Biol 129, 129-51 (2008).
40. Jones, D. H., Ley, S. & Aitken, A. Isoforms of 14-3-3 protein can form homo- and heterodimers in vivo and in vitro: implications for function as adapter proteins. FEBS Lett 368, 55-8 (1995).
41. Jong, A. Y. & Ma, J. J. Saccharomyces cerevisiae nucleoside-diphosphate kinase: purification, characterization, and substrate specificity. Arch Biochem Biophys 291, 241-6 (1991).
42. Kapetanovich, L., Baughman, C. & Lee, T. H. Nm23H2 facilitates coat protein complex II assembly and endoplasmic reticulum export in mammalian cells. Mol Biol Cell 16, 835-48 (2005).
43. Kirchhausen, T. Three ways to make a vesicle. Nat Rev Mol Cell Biol 1, 187-98 (2000).
44. Lawyer, F. C. et al. Isolation, characterization, and expression in Escherichia coli of the DNA polymerase gene from Thermus aquaticus. J Biol Chem 264, 6427-37 (1989).
45. Lee, M. C., Miller, E. A., Goldberg, J., Orci, L. & Schekman, R. Bi-directional protein transport between the ER and Golgi. Annu Rev Cell Dev Biol 20, 87-123 (2004).
46. Lee, M. C. et al. Sar1p N-terminal helix initiates membrane curvature and completes the fission of a COPII vesicle. Cell 122, 605-17 (2005).
47. Letourneur, F. et al. Coatomer is essential for retrieval of dilysine-tagged proteins to the endoplasmic reticulum. Cell 79, 1199-207 (1994).
48. Liu, D. et al. Crystal structure of the zeta isoform of the 14-3-3 protein. Nature 376, 191-4 (1995).
49. Mackintosh, C. Dynamic interactions between 14-3-3 proteins and phosphoproteins regulate diverse cellular processes. Biochem J 381, 329-42 (2004).
50. Mancias, J. D. & Goldberg, J. Exiting the endoplasmic reticulum. Traffic 6, 278-85 (2005).
51. Mancias, J. D. & Goldberg, J. Structural basis of cargo membrane protein discrimination by the human COPII coat machinery. Embo J 27, 2918-28 (2008).
52. Mezzacasa, A. & Helenius, A. The transitional ER defines a boundary for quality control in the secretion of tsO45 VSV glycoprotein. Traffic 3, 833-49 (2002).

53. Michelsen, K., Yuan, H. & Schwappach, B. Hide and run. Arginine-based endoplasmic-reticulum-sorting motifs in the assembly of heteromultimeric membrane proteins. EMBO Rep 6, 717-22 (2005).
54. Michelsen, K. et al. A multimeric membrane protein reveals 14-3-3 isoform specificity in forward transport in yeast. Traffic 7, 903-16 (2006).
55. Michelsen, K. et al. Novel cargo-binding site in the beta and delta subunits of coatomer. J Cell Biol 179, 209-17 (2007).
56. Miki, T., Nagashima, K. & Seino, S. The structure and function of the ATP-sensitive K + channel in insulin-secreting pancreatic beta-cells. J Mol Endocrinol 22, 113-23 (1999).
57. Miller, E. A. et al. Multiple cargo binding sites on the COPII subunit Sec24p ensure capture of diverse membrane proteins into transport vesicles. Cell 114, 497-509 (2003).
58. Moore BW, Perez VJ Specific proteins of the nervous system. Physiological and Biochemical Aspects of Nervous Integration (Carlson, F D ed) 1967;343 ± 359
59. Mrowiec, T. & Schwappach, B. 14-3-3 proteins in membrane protein transport. Biol Chem 387, 1227-36 (2006).
60. Navarre, C., Catty, P., Leterme, S., Dietrich, F. & Goffeau, A. Two distinct genes encode small isoproteolipids affecting plasma membrane H(+)-ATPase activity of Saccharomyces cerevisiae. J Biol Chem 269, 21262-8 (1994).
61. Niu, J. et al. RGS3 interacts with 14-3-3 via the N-terminal region distinct from the RGS (regulator of G-protein signalling) domain. Biochem J 365, 677-84 (2002).
62. Noma, A. ATP-regulated K+ channels in cardiac muscle. Nature 305, 147-8 (1983).
63. O'Kelly, I. & Goldstein, S. A. Forward Transport of K2p3.1: mediation by 14-3-3 and COPI, modulation by p11. Traffic 9, 72-8 (2008).
64. Obsilova, V., Silhan, J., Boura, E., Teisinger, J. & Obsil, T. 14-3-3 proteins: a family of versatile molecular regulators. Physiol Res 57 Suppl 3, S11-21 (2008).
65. Orci, L., Ravazzola, M., Amherdt, M., Brown, D. & Perrelet, A. Transport of horseradish peroxidase from the cell surface to the Golgi in insulin-secreting cells: preferential labelling of cisternae located in an intermediate position in the stack. Embo J 5, 2097-101 (1986).

66. Ory, S., Zhou, M., Conrads, T. P., Veenstra, T. D. & Morrison, D. K. Protein phosphatase 2A positively regulates Ras signaling by dephosphorylating KSR1 and Raf-1 on critical 14-3-3 binding sites. Curr Biol 13, 1356-64 (2003).

67. Palmieri, R. et al. Nucleoside triphosphate-nucleoside diphosphate transphosphorylase (nucleoside diphosphokinase). 3. Subunit structure of the crystalline enzyme from brewers' yeast. J Biol Chem 248, 4486-99 (1973).

68. Paul, A. L., Sehnke, P. C. & Ferl, R. J. Isoform-specific subcellular localization among 14-3-3 proteins in Arabidopsis seems to be driven by client interactions. Mol Biol Cell 16, 1735-43 (2005).

69. Pozuelo Rubio, M. et al. 14-3-3-affinity purification of over 200 human phosphoproteins reveals new links to regulation of cellular metabolism, proliferation and trafficking. Biochem J 379, 395-408 (2004).

70. Rittinger, K. et al. Structural analysis of 14-3-3 phosphopeptide complexes identifies a dual role for the nuclear export signal of 14-3-3 in ligand binding. Mol Cell 4, 153-66 (1999).

71. Roth, D., Birkenfeld, J. & Betz, H. Dominant-negative alleles of 14-3-3 proteins cause defects in actin organization and vesicle targeting in the yeast Saccharomyces cerevisiae. FEBS Lett 460, 411-6 (1999).

72. Saiki, R. K. et al. Primer-directed enzymatic amplification of DNA with a thermostable DNA polymerase. Science 239, 487-91 (1988).

73. Sambrook, J., Fritsch, E. F. und Maniatis, T. (1998). Molecular cloning: A laboratory manual. New York: Cold Spring Harbour Laboratory Press.

74. Saraste, J. & Kuismanen, E. Pre- and post-Golgi vacuoles operate in the transport of Semliki Forest virus membrane glycoproteins to the cell surface. Cell 38, 535-49 (1984).

75. Sato, K. & Nakano, A. Mechanisms of COPII vesicle formation and protein sorting. FEBS Lett 581, 2076-82 (2007).

76. Schwappach, B., Stobrawa, S., Hechenberger, M., Steinmeyer, K. & Jentsch, T. J. Golgi localization and functionally important domains in the NH2 and COOH terminus of the yeast CLC putative chloride channel Gef1p. J Biol Chem 273, 15110-8 (1998).

77. Schwappach, B., Zerangue, N., Jan, Y. N. & Jan, L. Y. Molecular basis for K(ATP) assembly: transmembrane interactions mediate association of a K+ channel with an ABC transporter. Neuron 26, 155-67 (2000).

78. Shikano, S. & Li, M. Membrane receptor trafficking: evidence of proximal and distal zones conferred by two independent endoplasmic reticulum localization signals. Proc Natl Acad Sci U S A 100, 5783-8 (2003).

79. Shikano, S., Coblitz, B., Wu, M. & Li, M. 14-3-3 proteins: regulation of endoplasmic reticulum localization and surface expression of membrane proteins. Trends Cell Biol 16, 370-5 (2006).

80. Silhan, J. et al. 14-3-3 protein C-terminal stretch occupies ligand binding groove and is displaced by phosphopeptide binding. J Biol Chem 279, 49113-9 (2004).

81. Sohn, K. et al. A major transmembrane protein of Golgi-derived COPI-coated vesicles involved in coatomer binding. J Cell Biol 135, 1239-48 (1996).

82. Stagg, S. M. et al. Structure of the Sec13/31 COPII coat cage. Nature 439, 234-8 (2006).

83. Stagg, S. M. et al. Structural basis for cargo regulation of COPII coat assembly. Cell 134, 474-84 (2008).

84. Steinmeyer, K., Lorenz, C., Pusch, M., Koch, M. C. & Jentsch, T. J. Multimeric structure of ClC-1 chloride channel revealed by mutations in dominant myotonia congenita (Thomsen). Embo J 13, 737-43 (1994).

85. Truong, A. B., Masters, S. C., Yang, H. & Fu, H. Role of the 14-3-3 C-terminal loop in ligand interaction. Proteins 49, 321-5 (2002).

86. Tzivion, G. & Avruch, J. 14-3-3 proteins: active cofactors in cellular regulation by serine/threonine phosphorylation. J Biol Chem 277, 3061-4 (2002).

87. Ungewickell, E. & Branton, D. Assembly units of clathrin coats. Nature 289, 420-2 (1981).

88. van Hemert, M. J., Steensma, H. Y. & van Heusden, G. P. 14-3-3 proteins: key regulators of cell division, signalling and apoptosis. Bioessays 23, 936-46 (2001).

89. van Heusden, G. P. et al. The 14-3-3 proteins encoded by the BMH1 and BMH2 genes are essential in the yeast Saccharomyces cerevisiae and can be replaced by a plant homologue. Eur J Biochem 229, 45-53 (1995).

90. van Zeijl, M. J., Testerink, C., Kijne, J. W. & Wang, M. Subcellular differences in post-translational modification of barley 14-3-3 proteins. FEBS Lett 473, 292-6 (2000).
91. Westphal, V., Marcusson, E. G., Winther, J. R., Emr, S. D. & van den Hazel, H. B. Multiple pathways for vacuolar sorting of yeast proteinase A. J Biol Chem 271, 11865-70 (1996).
92. Wilker, E. & Yaffe, M. B. 14-3-3 Proteins--a focus on cancer and human disease. J Mol Cell Cardiol 37, 633-42 (2004).
93. Wilker, E. W., Grant, R. A., Artim, S. C. & Yaffe, M. B. A structural basis for 14-3-3sigma functional specificity. J Biol Chem 280, 18891-8 (2005).
94. Wuestehube, L. J. and Schekman, R. Reconstitution of Transport from Endoplasmatic Reticulum to Golgi Complex using Endoplasmatic-Enriched Membrane Fraction from Yeast. (1992).
95. Xiao, B. et al. Structure of a 14-3-3 protein and implications for coordination of multiple signalling pathways. Nature 376, 188-91 (1995).
96. Yaffe, M. B. et al. The structural basis for 14-3-3:phosphopeptide binding specificity. Cell 91, 961-71 (1997).
97. Yaffe, M. B. How do 14-3-3 proteins work?-- Gatekeeper phosphorylation and the molecular anvil hypothesis. FEBS Lett 513, 53-7 (2002).
98. Yuan, H., Michelsen, K. & Schwappach, B. 14-3-3 dimers probe the assembly status of multimeric membrane proteins. Curr Biol 13, 638-46 (2003).
99. Zerangue, N., Schwappach, B., Jan, Y. N. & Jan, L. Y. A new ER trafficking signal regulates the subunit stoichiometry of plasma membrane K(ATP) channels. Neuron 22, 537-48 (1999).
100. Zuzarte, M. et al. Intracellular traffic of the K+ channels TASK-1 and TASK-3: role of N- and C-terminal sorting signals and interaction with 14-3-3 proteins. J Physiol 587, 929-52 (2009).

Abbreviations

A	ampere
AA	amino acid
ABC	ATP-binding cassette
Amp	Ampicilin
AP	alkaline phosphatase
APS	ammonium persulfate
Arf	ADP ribosylation factor 1
ATP/ADP	adenosine tri/diphosphate
ATPase	adenosine triphosphatase
BiP	immunoglobulin heavy chain-binding protein
BSA	bovine serum albumin
bp	base pair
C-terminus	carboxyl-terminus
CCVs	Clathrin-coated vesicles
cDNA	complementary DNA
CGN	*cis*-Golgi network
COPI/II	coatomer protein I/II
DMSO	dimethyl sulfoxide
DNA	Deoxyribonucleic acid
dNTPs	deoxyribonucleotide triphosphates
dox	doxycycline
DSS	disuccinimidyl suberate
DTT	dithiothreitol
EDTA	ethylenediaminetetraacetic acid
ER	endoplasmic reticulum
ERAD	ER-associated degradation
ERES	ER exit sites
ERGIC	ER-Golgi intermediate compartment (VTC)
et al.	et alii
e.g.	for example

FACS	fluorescence-activated cell sorting
g	gram
GAP	GTPase-activating protein
GDP/GTP	guanosine di/triphosphate
GEF	guanine exchange factor
GFP	green fluorescent protein
Glc	glucose
h	hour
Hepes	N-2-hydroxyoxyethylpiperazine-N'-2-ethane sulfonic acid
HRP	horse radish peroxidase
IPTG	isopropylthio-β-D-galactoside
in vitro	in a controlled environment outside of a living organism
in vivo	inside an organism or living tissue
Kan	Kanamycin
KATP	ATP-sensitive potassium channel
kb	kilo-base pair
kDa	kilo-Dalton
KDEL	Lysine-aspartic acid-glutamic acid-leucine
Kir	inwardly rectifying potassium channel
l	liter
LB	Luria-Bertani
m	milli
M	molar
min	minute
mRNA	messenger RNA
µ	micro
N-	amino-
nm	nanometer
oN	over night
PAGE	Polyacrylamide gel electrophoresis
PBS	Phosphate-buffered Saline
PCR	Polymerase chain reaction

PM	plasma membrane
PMSF	phenylmethylsulfonyl fluoride
RKR / R-based signal	arginine-based ER localization signal
RNA	Ribonucleic acid
rpm	revolutions per minute
RU	Response Unit (BiaCore unit)
S/T	serine/threonine
s	second
SDS	sodium dodecyl sulphate
SDS-PAGE	SDS-polyacrylamide gel electrophoresis
SNARE	SNAP receptor
SUR	sulfonylurea receptor
TBS	Tris-buffered Saline
TEMED	tetrametyhylethylene diamine
tet	tetrocycline
TGN	*trans*-Golgi network
TM	transmembrane segment
TMD	transmembrane domains
Tris	Tris-(hydroxymethyl)aminomethane
U	unit
V	volt
vac	vacuole
VTC	Vesicular-tubular cluster (ERGIC)
v/v	volume per volume
w/v	weight per volume